DESIGN OF CHASSIS, IMPACT ATTENUATOR, SUSPENSION AND AERODYNAMIC SYSTEMS OF A FORMULA SAE CAR

A Thesis

Presented to

the Faculty of the Department of Engineering Technology

University of Houston

In Partial Fulfillment

of the Requirements for the Degree

Master of Science

in Engineering Technology

by

Tittu Paul

May, 2019

DESIGN OF CHASSIS, IMPACT ATTENUATOR, SUSPENSION AND AERODYNAMIC SYSTEMS OF A FORMULA SAE CAR

____

Tittu Paul

Approved:

____

Chair of the Committee

Anthony P. Ambler, Dean,

College of Technology

____

Co-chair of the Committee

Burak Basaran, Instructional Assistant Professor,

Engineering Technology

Committee Members:

____

Navdeep Singh, Instructional Assistant Professor,

Engineering Technology

____

Kamran Alba, Assistant Professor,

Engineering Technology

____

George Zouridakis, Associate Dean of Research, College of Technology

____

Wajiha Shireen, Chair, Engineering Technology

ACKNOWLEDGEMENTS

I would like to express my sincere gratitude to many people for their generous contributions and encouragement throughout the works involved in my thesis. First and foremost, I would like to express my great appreciation to my thesis advisor Dr. Burak Basaran for his technical support, patient guidance and advices. He was always there to motivate me whenever I was struggling with the progress and helped me with the directions. This work would not have been possible without his invaluable supports.

I would also like to thank the members of my thesis committee, Dr. Navdeep Singh and Dr. Kamran Alba for their valuable comments and guidance for helping me to finish my works. Working with Dr. Navdeep Singh as an Instructional Assistant for four semesters was a great learning platform and has immensely helped me with the FEA methods required for my thesis work.

I would like to thank my parents and my sister who are always my motivation and strength and for the sacrifices they made throughout my life. They were always there with a smile during all the struggles I had in life and taught me how to overcome them together. I would also like to thank my valuable friends for being there for me whenever I needed them.

DESIGN OF CHASSIS, IMPACT ATTENUATOR, SUSPENSION AND AERODYNAMIC SYSTEMS OF A FORMULA SAE CAR

An Abstract of a Thesis

Presented to

the Faculty of the Department of Engineering Technology

University of Houston

In Partial Fulfillment

of the Requirements for the Degree

Master of Science

in Engineering Technology

by

Tittu Paul

May, 2019

ABSTRACT

Designing the first car for a Formula SAE team can be very challenging and confusing due to close interconnection between the design process of different subsystems. Once the working car is built, it is comparatively easy for the teams to build next year cars by testing and improving the already existing model. This thesis documents an attempt made to design the chassis, impact attenuator, aerodynamics and suspension systems of the first UH College of Technology Formula SAE car. A systematic design methodology was adopted to tackle the challenge of having many unavailable inputs while designing each subsystem. The effectiveness of various parameters selected during designing each subsystem where validated through testing. Chassis was designed according to the FSAE competition rules with the aim of achieving a specific target torsional stiffness. A standard impact attenuator was analyzed using SOLIDWORKS drop test simulation with different impact absorbing materials for its crashworthiness. An optimized double wishbone suspension was designed at front and rear which was found to be the best option available for Formula SAE cars. For the aerodynamic system, optimized multi element wings were designed as front, rear and side devices using ANSYS FLUENT. An undertray diffuser design was compared to the downforce generation capabilities of a side wing, both within the available space limits, and the side wing was found to be generating more downforce. Loads acting on suspension links were found out by calculating the load transfer expected to happen while cornering, braking and accelerating. Finally, FEA was conducted on the suspension links to determine the minimum tube size requirements for the components.

Table of Contents

LIST OF TABLES

LIST OF FIGURES

NOMENCLATURE

Symbols

K	Chassis Torsional Stiffness
F	Force
l	Length
Δy	Vertical displacement of chassis node
v	velocity
a	Acceleration
p	Pressure
ρ	Density
C_L	Coefficient of Lift
C_D	Coefficient of Drag
Re	Reynold’s number
A	Area
D	Downforce
t_F, t_R	Front and Rear Trackwidth
h	Center of Gravity height
$\emptyset$	Angle of tilt
φ	Roll angle
W	Total static load of the car
W_F, W_R	Front and Rear axle normal weight of the car
W_{FCi}, W_{RCi}	Normal load on front and rear inside tires due to lateral load transfer
W_{FCo}, W_{RCo}	Normal load on front and rear outside tires due to lateral load transfer
ΔW_F, ΔW_R	Front and Rear lateral load transfer
ΔW_B, ΔW_A	Longitudinal load transfer due to braking and acceleration
W_{FB}, W_{RB}	Front and rear tire normal loads due to braking load transfer
W_{FA}, W_{RA}	Front and rear tire normal loads due to acceleration load transfer
W_{CBF}, W_{CBR}	Front and rear tire normal loads due to cornering and braking
W_{CAF}, W_{CAR}	Front and rear tire normal loads due to cornering and acceleration
H	Height from roll axis to CG
A_Y	Lateral Acceleration
$K_{\varphi F}, K_{\varphi R}$	Front and Rear axle Roll stiffness
α	Banking angle
R	Cornering radius
W_C	Weight of the vehicle
c	Distance from front axle to CG
b	Distance from rear axle to CG
L	Wheel base

Z_{RF}, Z_{RR}	Front and Rear roll center height
ω	Ride frequency
K_{RF}, K_{RR}	Front and rear axle ride rates
K_{WF}, K_{WR}	Front and rear wheel center rate
K_T	Tire stiffness
$K_{\varphi SF}, K_{\varphi SR}$	Front and rear spring roll stiffness
$K_{\varphi AF}, K_{\varphi AR}$	Front and rear anti-roll bar stiffness
MR_F, MR_R	Front and Rear motion ratio
K_{SF}, K_{SR}	Front and rear spring rates
C_{CRF}, C_{CRR}	Front and rear critical damping coefficient
C_F, C_R	Front and rear damping coefficients
δ	Angle between suspension arm and horizontal
F_{normal}	Normal force on tires
$F_{lateral}$	lateral force on tires
$F_{G,X}$, $F_{G,Y}$	X and Y components of force acting on lower suspension arm
$F_{E,X}$	X component of force acting on upper suspension arm

Abbreviations

CDS	Collegiate Design Series
FSAE	Formula SAE
SAE	Society of Automobile Engineers
ECU	Electronic Control Unit
FEA	Finite Element Analysis
CFD	Computational Fluid Dynamics
CFRP	Carbon Fiber Reinforced Plastic
SLA	Short-Long Arm
TTC	Tire Test Consortium
IC	Instant Center
FVSA	Front View Swing Arm
CAD	Computer Aided Design
AOA	Angle of Attack
FOS	Factor of Safety
CG	Center of Gravity
SSF	Static Stability Factor

CHAPTER 1: Introduction

1.1 FSAE Competition Overview

1.1.1 About the Competition

Formula SAE (FSAE), also referred as Formula Student, is one among SAE International's Collegiate Design Series (CDS) competitions where undergraduate and graduate students team up to design, build and test a Formula style race car. Teams from different part of the globe competes among themselves in various static and dynamic events. The competition is organized by SAE International in 2 different locations in US, Michigan and Lincoln. The event was first organized in 1981 with 4 participant teams, currently have 120 teams (in Michigan competition alone) competing from across the world. The competition has also expanded globally with events being conducted in more than 20 countries by various societies. The main objective for the teams is to design and construct a single seater formula style race car by utilizing their engineering design and management skills. The car will be evaluated in various design, construction, performance and cost judging events. Formula SAE is considered to be one among the world’s best design competitions as it provides students a great platform to apply the classroom knowledge to develop a very complex machine. FSAE Michigan is usually conducted on May, whereas FSAE Lincoln is conducted on June. The registration for both events is open from October to November of the previous year.

1.1.2 General Design Objectives

The teams are provided with a hypothetical problem to design and construct a formula style car intended for non- professional weekend racing, which should be having high performance at less cost. The car should illustrate high performance in acceleration, braking and should have good handling and sufficient durability. The car should satisfy a series of rules provided by the organizing agency which is intended to ensure safety and to promote problem solving skills. Weight reduction is one of the primary objectives throughout the design process as it is directly linked to the performance of other sub-systems of the car. The amount of fuel conception which is evaluated during Endurance event, is closely related to the weight of the car. If the car weighs too much, the engine will burn more fuel to overcome the inertia of the car hence increasing fuel consumption. The performance of the car in dynamic events are mainly governed by how well the car performs in the corners. The ability of the car to cover the corners faster will be crucial for ensuring maximum points from the dynamic events. This is directly related to the amount of grip (lateral force) generated by the tires in corners and the utilization and management of the aerodynamic forces called as lift and drag. Grip generating mechanism is taken care during the suspension design process and is also closely related to the amount of downforce (negative lift) generated from the aerodynamic devices. Factors such as aesthetics, ergonomics, simplicity in design and manufacturability also plays important role in the overall evaluation of the car.

1.1.3 Vehicle Evaluation Process

The vehicle is evaluated in a series of events by experts from the automobile, motorsports, aerospace and other industries. The judging events are classified into Static and Dynamic events. In static events, the overall design is evaluated and in dynamic events the overall performance of the car is evaluated. The maximum points allocated for each individual event according to Formula SAE 2019 rule book is shown in table 1.1.

Table 1.1 FSAE vehicle evaluation points' distribution.

STATIC EVENTS	
Presentation	75 points
Cost	100 points
Design	150 points
Total	**325 points**

DYNAMIC EVENTS	
Acceleration	100 points
Skid Pad	75 points
Autocross	125 points
Efficiency	100 points
Endurance	275 points
Total	**675 points**

a) Presentation Event

During presentation event, the teams are expected to convince the judges acting as the investors of the teams' product, by delivering a detailed business, production, logistical and technical case to support their product. The teams should be able to justify their design and manufacturing philosophies adopted for their product. Evaluation of the presentations are done based on the quality of the content, how the details are organized, proper conveying of idea, use of visual aids and how well the teams respond to the questions.

b) *Cost Event*

Cost event judges the teams on how well they have managed to reduce the overall cost without compromising the performance of the vehicle. It considers the ability of the team to manage the expenses within the budget, and techniques used to improve productivity. Cost event consists of submitting the cost report and event day discussion. Cost report will be having a list of parts of the vehicle and all the costs associated with it. Parts should be classified separately as ‘made’ or ‘bought’. Supporting documents like engineering drawings/manufacturing pictures may be required to prove if a component is listed as ‘made’. During the event day discussion, the teams are required to present their vehicle along with the cost report. The judges will examine if the cost report details the actual vehicle components correctly, the manufacturability of the vehicle, and examine any supporting documents.

c) *Design Event*

Design event judging focusses on the teams’ ability to use engineering principles in efficient and innovative ways to benefit the vehicle in achieving overall performance and cost reduction. A design report and a spec sheet should be submitted by the teams prior to the competition. A design report should include a short description of the team’s vehicle, its specific features, the analysis and testing processes used and vehicle drawings. Judging in design Event is done based on the engineering thought put behind the vehicle design, analyzed from the design report and spec sheet submitted, vehicle inspection and team discussion.

d) Acceleration Event

Acceleration event is intended to judge the straight-line acceleration of the vehicle. The vehicle should travel the 75 m long straight-line course in least time to achieve maximum points. Acceleration event doesn't really evaluate the tire cornering ability and the aerodynamic downforce is not doesn't help acceleration event. The factors which really matters in acceleration event is the transmission system and reduced car weight.

e) Skid Pad Event

Skid Pad event analyses predominantly the cornering ability of the vehicle. The course pattern resembles a figure of eight as shown in figure 1.1.

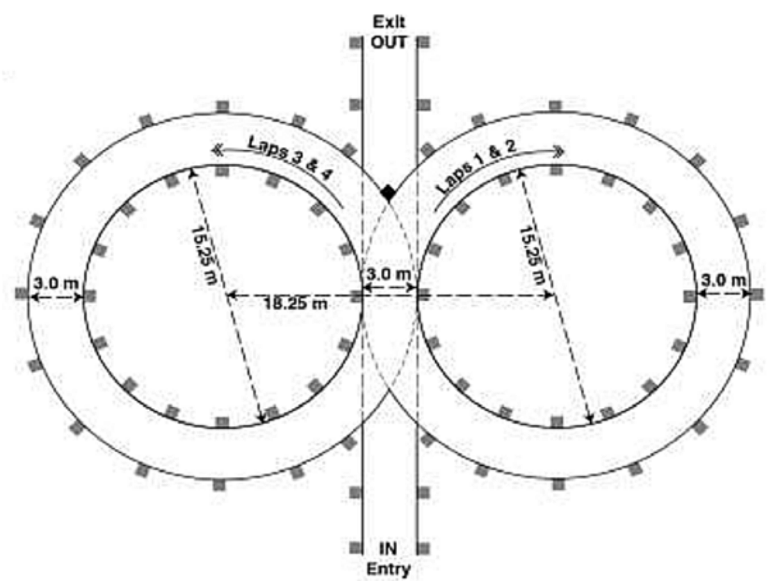

Figure 1.1 FSAE Skid Pad event course [1].

The vehicle will travel through two circular paths, thereby undergoing constant radius cornering. If the cornering performance of the vehicle is good, it will generate large tire grip (lateral force), allowing the vehicle to travel the corner at higher velocity and thereby finishing in less time. The main features of the vehicle which come under scrutiny in skid pad event are the suspension design and aerodynamic downforce generation.

f) Autocross Event

Autocross event will test both straight line acceleration and cornering ability of the vehicle. The course will be approximately 0.80 km long consisting of straights, constant turns with diameters ranging from 23 m to 45 m, hairpin turns with a minimum diameter of 9 m, and other miscellaneous profiles. Since Autocross event is a combination of both acceleration event and skid pad events, all the major features of the vehicle play equal importance in Autocross event. The vehicle should be having good power transmission, less weight and should also generate good grip while cornering.

g) Efficiency Event

Fuel consumption is the evaluation criteria for the efficiency event. It measures the distance travelled by the vehicle with a known amount fuel. The efficiency is measured from the endurance event as the distance travelled with the known maximum fuel is measured to analyze the vehicle efficiency. The two fuels allowed to use for the competition are Gasoline/Petrol and E85. The major factors affecting the fuel efficiency are the transmission system, power generation system and the weight of the vehicle.

h) Endurance Event

Endurance event examines the durability and reliability of the vehicle. The vehicle is supposed to travel over a closed course of approximately 22 km long. Similar to Autocross event, the course will be consisting of constant turns with diameters ranging from 30 m to 54 m, hairpin turns with a minimum diameter of 9 m, and other miscellaneous profiles. Since the vehicle is expected to run for such long distance without any break, endurance event will evaluate every aspect of the vehicle from driving skills to proper functioning of each component. Endurance event holds the maximum points for an individual event throughout the competition, with 275 points. Most of the first-time teams set the main objective as finishing endurance event since finishing the endurance event itself will give the team a respectable position in the overall event.

1.2 FSAE Car Component Systems

1.2.1 Chassis Subsystem

Chassis subsystem includes all the components that holds the vehicle together and it has functions of providing structural stability and strength to the vehicle. The skeleton of a Formula SAE car is made up of either a steel space chassis or a composite monocoque. The main functions of a space chassis/monocoque are to provide an overall structure to the vehicle, provide enough strength/rigidity to the car and to act as a medium to provide mounting points for other components of the car. Even though space chassis and monocoques perform same tasks, many established teams are opting for CFRP monocoques as it reduces the chassis weight considerably along with providing very high stiffness.

1.2.2 Suspension Subsystem

Suspension system acts as an intermediary between the rest of the vehicle and the road, whose main function is to facilitate efficient transfer of power generated by the engine to the road through the tires. Suspension system components include tire, wheel, hub, upright, suspension links, spring, damper and other associated components. Steering system is closely related to the suspension system and its main function is to provide the vehicle directional stability. Steering system components include steering wheel, steering rack and pinion, tie rods and other associated components.

1.2.3 Aerodynamic Subsystem

Aerodynamic subsystem includes wings, undertrays and similar components which helps to utilize the aerodynamic forces generated due to the air flow around the car for the benefit of the vehicle. In formula SAE, wings are mounted on the rear, front or on the sides and its proper optimization would result in providing the vehicle with additional stability mostly while cornering. The objective while designing a wing is to find the optimum airfoil configuration which would provide maximum downforce with minimum drag penalty. This downforce will be transmitted to the suspension through the chassis and will directly influence the lateral force (grip) generated in the tires. The tire grip is directly related to the normal force acting on the tire as shown in figure 1.2.

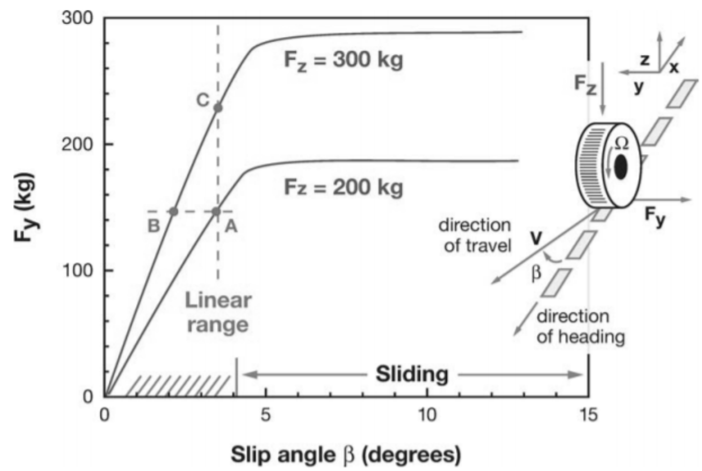

Figure 1.2 Relationship between normal tire load and lateral force [2].

One way to do this by increasing the weight of the body. Since this will cause consuming more power to overcome the inertia, this is the worst idea in race cars. That is where aerodynamics helps, since it provides downforce by making use of the inlet air velocity without adding much to the weight. Earlier, teams did not consider the influence of aerodynamic devices in Formula SAE due to low speeds achieved by the cars. During the last decade, almost every team has identified the positive effects of having optimized aerodynamic devices in reducing the lap times by few seconds, which can impact the overall performance of the car considerably.

1.2.4 Powertrain Subsystem

Powertrain subsystem includes the engine which generate the power, air intake systems, and associated devices used to transmit the power to the wheels. Engines should be four stroke with maximum allowable displacement less than or equal to 710cc. Most of the teams make use of Motorcycle engine with displacement less than specified. Some teams are more advanced in the subject and have manufactured their own engines with specific advantages. Also, the rules state that there should be an air restrictor placed in the intake system to limit the amount of air breathed by engine and thereby controlling the maximum power generated. Waste heat regeneration is still possible in FSAE cars, leading to the use of turbochargers and superchargers by many teams. Teams are required to build associated parts such as air intake and exhaust systems for their specific engine. Powertrain subsystem also includes power transmission systems including differentials, fuel tank, radiators and other associated devices.

1.2.5 Electrical Subsystem

Electrical subsystem includes the electrical/electronic devices used in the vehicle for different purposes. It includes battery, various sensors, driver assistance systems, engine tuning systems and other monitoring and control devices. Teams who are beginners in the competition can start with very basic electrical devices such as a battery system and essential devices for paddle shift if needed. Later they can include advanced systems for various sensors, monitoring and control devices and can incorporate an ECU (Electronic Control Unit) to control all the electrical systems more efficiently.

1.3 Design Process Overview

1.3.1 Thesis objectives

As discussed in the previous sections, FSAE serves as a great learning platform for undergraduate and graduate students in various universities across the globe. Teams along with getting hands on experience of various classroom theories, can also develop and test novel ideas and innovations in various engineering fields. This project is an extensive study on the processes involved in the design of an FSAE car. From literature review, it is understood that there isn’t an exact guide for beginners in FSAE which incorporates the overall design process involved in building an FSAE car. The main objective for this research is to design few of the key subsystems of an FSAE car, chassis, impact attenuator, suspension components and the aerodynamic system. Design of chassis will include the selection of the type of chassis from space chassis or monocoque, structural design considering all the chassis design rule and FEA of the chassis to analyze if the chassis will possess enough stiffness as identified during target definitions. Suspension design will involve selection of suspension type, tires, wheels, suspension kinematics design, force analysis on the suspension components during extreme vehicle maneuvers and other associated stages. Design of aerodynamic systems design involves selection of required aerodynamic devices, selection of airfoil for wings, finding optimal arrangement of airfoils to generate maximum downforce with minimal drag losses and finding theoretical maximum downforces generated by wings or other aerodynamic devices along with their expected weights. It also includes selections or assumptions of various other components which are necessary during the design process of chassis, suspension and aerodynamic systems. Finally, the thesis will conclude by providing insights on how these systems could be improved in the future cars and the way forward from there.

1.3.2 Design Methodology

Building an FSAE car for the first time can be very challenging for teams. As for any other competition sports, resources on latest designing and building techniques are very hard to obtain. There are few good text books which explains how individual systems could be designed for race cars in general. But in reality, they are actually not individual systems, they are rather interconnected systems. For instance, one cannot design a proper suspension system without knowing the overall parameters of the car such as weight, center of gravity location etc. But the overall car details cannot be accurately found out without having a suspension design as well since it is an integral system for the overall car. These challenges can be found in most of the phases of the design. So, it is very important to learn about all the systems and how they are interconnected, before proceeding to the actual design of an individual system. Hence, most important phase in the actual design process is learning about individual systems, knowing what all parameters are needed for the design, and establish the order in which the overall design process should be carried out.

Various subsections of a FSAE vehicle are described in the previous section. As stated before, firstly, various input parameters required for design of the subsections are identified.

a) Chassis Design

Initial chassis design with outer dimensions are mainly done based on various rules stated in FSAE rule book for chassis design. Chassis rules are mainly for driver safety and ergonomics reasons. The cockpit design is done considering the built of a 95th percentile male driver, which can be found in the competition rule book [1]. The rear section of the chassis should provide enough space for mounting the selected engine, differential and other related devices. Along with the selected track width and wheel base, this would give a primitive structure for the chassis. Further addition or trimming of the chassis will be based mainly on the suspension pickup points. Suspension pickup points will be obtained only after designing the suspension itself. Final changes to the chassis are done in order to make it stiff enough as per the target stiffness. That is, once developing a primitive chassis considering the design rules, 95th percentile driver built and engine dimensions, the design should move on to suspension kinematics. Suspension kinematics will give the suspension pick up points, making the designer to develop an advanced version of the chassis. This chassis is optimized to achieve a target stiffness.

b) Suspension Design

Suspension design begins with the selection of few important parameters such as the tires, wheels, brake caliper, ride height etc. Target suspension parameters are identified mainly from literature reviews, that include but not limited to roll center heights, Instantaneous center locations, Kingpin inclinations, Scrub radius, Camber angle, Caster angle and other related parameters. Once these selections are made, suspension geometry design can be done in order to achieve the targets. Suspension geometry design is followed by force analysis to identify maximum forces encountered by various suspension components during cornering, braking and acceleration conditions. Spring and damper parameters are also found out during this stage. Once the forces are identified, the suspension components are optimized for failure modes. Now regarding the design process flow, suspension geometry can be designed using the initial suspension parameter selection and the primitive chassis design. For force analysis, all the loads acting on the vehicle should be known. This includes the total car weight and the aerodynamic downforce. Hence the aerodynamic design should be carried out after suspension geometry design followed by a full assembly of the car with the finished chassis, the body works, impact attenuator, wings/other aerodynamic devices, engine, differentials, suspension, steering system, driver, battery, pedal box and other components with considerable weight. Since this thesis does not include design of steering system, differentials, pedal box etc., some rough models are created with their expected weight from literature review are used to finish the assembly. The objective of creating an assembly at this stage is to find a fairly accurate weight and center of gravity location of the vehicle. Using all these, the remaining suspension design can be completed.

c) *Aerodynamics Design*

First phase in the design of aerodynamic components is to identify the space available in the vehicle to incorporate any aerodynamic device. This is dependent on parameters such as wheel base, track width, chassis dimensions and is also governed by the competition rules. Once the usable space is identified, further design decisions are made on the type of aerodynamic devices to be incorporated into the vehicle. In most Formula SAE cars, aerodynamic devices primary consists of a rear wing, a front wing and any side devices to make use of the ground effects. Wing design starts with selecting an airfoil that is best suited for Formula SAE applications. This is followed by finding best airfoil arrangement which, in the available space, can generate large amount of downforce with minimum drag losses using tools such as Computational Fluid Dynamics (CFD) and/or wind tunnel testing and/or track testing. The aerodynamic forces should also balance to provide stability to the car in aerodynamic effects. This thesis also covers load analysis to find the construction of the wings to withstand the maximum downforce generated by the wings and also to find out the weight of the wings. Hence, as far as the design process flow of aerodynamic design, once the allowable space is identified, can proceed to the whole aerodynamic design.

To summarize, the overall process flow finalized for the design is shown in figure 1.3.

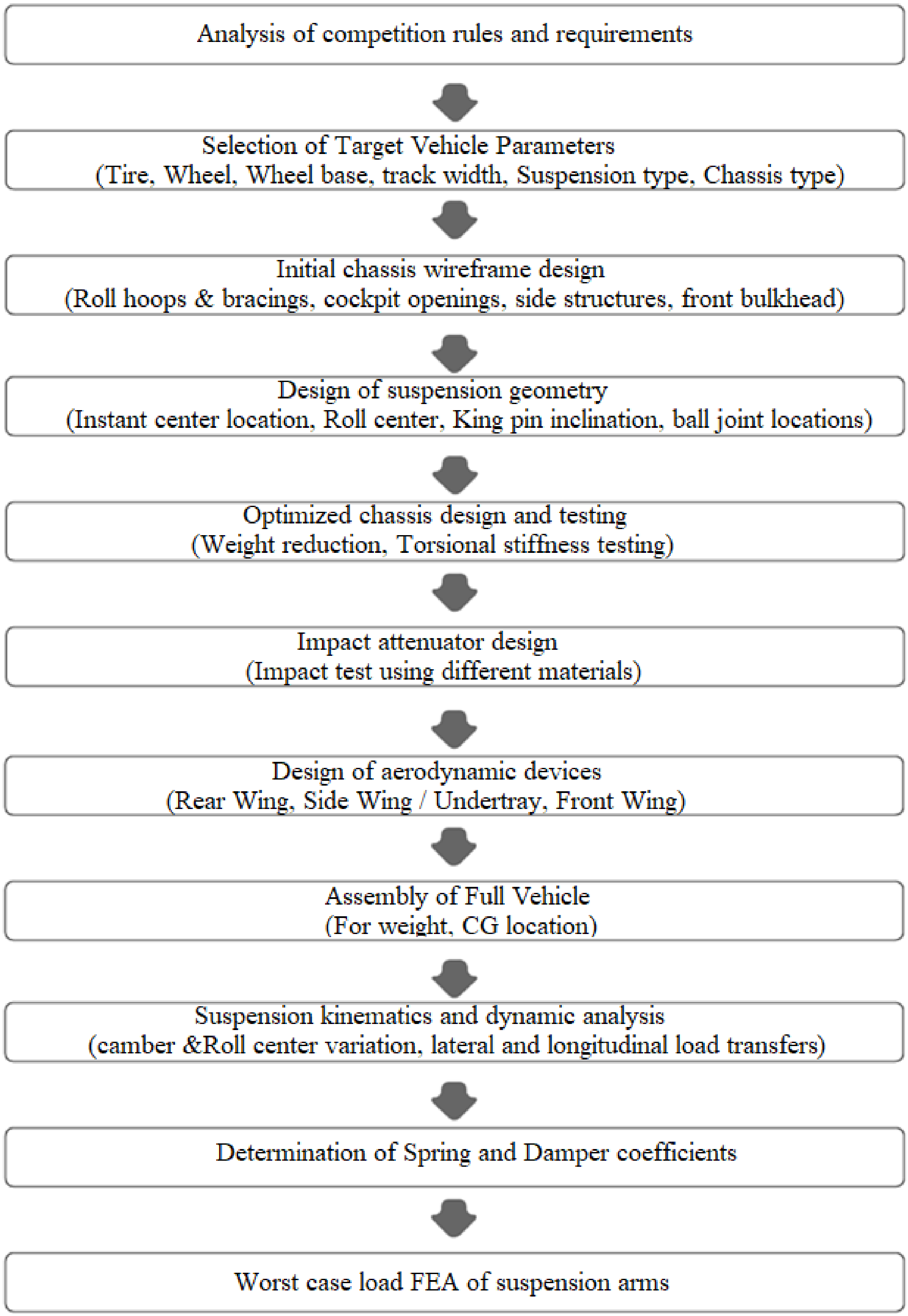

Figure 1.3 Design process flow chart.

CHAPTER 2: Design of Initial parameters

2.1 Study on Features of Best Performing FSAE Cars

For beginners in Formula SAE competitions, the first main resource for developing a proper understanding of the competition, the car, and the design requirements is studying and assessing the sources available for the cars with best performance history. Again, as Formula SAE is primarily a competition sport, one could not expect the good teams to publish the details of their cars to the public. Hence, the aspiring teams have to rely on understanding the available features of the cars and study the science behind those features. A good source the author found for analyzing and comparing features of various cars is the event guide published every year by the organizing committee, the latest being published on 2018 [3]. This contains the main features of all the competing cars and is taken as a reference for various decisions and selections made in this design. The following section will analyze such features and trends in some of the best performing cars.

Considering the competition history results of last 10 years, Universität Stuttgart has been clearly the most successful car. One of the main features of Universität Stuttgart team and other best performing teams is shifting to composite monocoque (usually CFRP) instead of steel space chassis. This reduces the overall weight and provides very high stiffness. Weight reduction is one of the key areas where the best performing team puts focus on. Universität Stuttgart team also lightens the Yamaha R6 engine selected to further weight reduction and slim packaging. Universität Stuttgart team also list optimized aerodynamics as a unique feature. Implementation of optimized aerodynamic devices has been another main feature of almost all good teams for the last decade. Graz Technical University team also focusses on weight reduction by incorporating composite monocoque, along with a CFRP impact attenuator which is more lightweight. Graz Technical University has one of the lightest cars weighing just 514 lbs compared to Universität Stuttgart team at 561 lbs. Cornell University focusses on maintaining exceptional power to weight ratio and incorporates a turbocharger to Honda CBR600RR engine. Turbochargers are used by many universities to enhance the power output by making better use of the waste heat generated. University of Wisconsin – Madison team makes use of materials such as CFRP, aluminum, titanium, magnesium, Inconel and alloy steel for the construction. Another strategy used by this team is using a light weight 450 cc single cylinder engine, with a turbocharger. Using a smaller engine will definitely reduce the overall weight at the expense of some power. Again, it all depends on teams to take decisions on the power they want for the vehicle to win the overall competition. One thing to keep in mind here is Formula SAE is not just a racing competition, but ultimately a design competition. They also boast of a very light weight car weighing around 520 lbs. Carleton University has been one of the top performing teams which has achieved success with steel space chassis when many teams have adopted composite monocoques. They run a 450 cc single cylinder engine which reduces weight and also makes use of 3D printing for many of their components.

There are some common features noticed in many good teams. One of them is adopting 10 inch tires in order to reduce rotational inertia and also lowering the center of gravity. Previously (some teams presently too) teams used to have 13 inch tires in order to get more design freedom for suspension and braking systems since it provides more space to work with. Also, the range and availability of 10 inch tires have increased recently which also inspired teams to use them instead of 13 inch tires. Another common pattern seen in tire selection is regarding the make, as very large majority uses Hoosiers and a few teams opts Goodyear or Continental. In Hoosier tires, another choice made by the teams is the tire compound. Teams uses either R25B or LC0 as their tire material for Hoosier tires. Both are rated as soft rubbers as per Hoosier and LC0 is a new version mainly aimed for Formula SAE competitions. Another common feature is regarding the selection of suspension type. All teams in Formula SAE teams uses SLA (Short-Long Arm) Double Wishbone suspension also known as A-arm suspension. The reason for selecting this suspension type over others will be discussed in detail in the suspension design section.

2.2 Selection of Target Vehicle Parameters

2.2.1 Tire and Wheel Selection

A Formula SAE car is designed focusing on its good cornering performance. While straight line acceleration of a car mainly depends on its power generation, transmission and weight, cornering performance depends more on the vehicle dynamics, suspension and tire performance. Again, whatever power is generated by the car, is converted to the vehicle motion though the four tires of the car. In other words, it is the four contact patches of the tires which acts as an interface to transfer the power generated by the engine to the ground, producing traction. Hence one of the primary selections to be made while designing a race car should be the tire and a suitable wheel. The further design process is greatly influenced by the selection of tires.

As discussed in the previous section, other than 4-5 teams competed out of 120 teams in Michigan in 2018, every team uses Hoosier 10 inch tires. The teams rely on various tire testing data for tire selection and one of the major sources for race car tire test data is the one provided by Formula SAE Tire Test Consortium (FSAE TTC). Tires are one of the complex components in a race car to understand. Tire generates a variety of forces in order to handle the vertical loads as well as the forces generated during cornering, braking or acceleration. It also generates forces which are used for stabilizing and controlling the vehicle during maneuvers and external disturbances. The mechanism of generation of these forces are quite complex to explain. Also, the behavior of the tires will be much different at various tires pressures, temperature and velocity. FSAE TTC was formed by a group of FSAE teams with an aim to provide teams with high quality tire test data. Currently there are over 575 member universities from around the world in the FSAE TTC [4]. They conduct test on selected number of tires each time and provide them to member universities. These data can be used by universities to understand how the tire behaves at different operating conditions and thereby extracting maximum out of the tires. Since, while doing this thesis research, a team is not formed in University of Houston, College of Technology, the FSAE tire test data is not available during the design process. But, it will be a very useful tool while suspension design and tuning of the vehicle. The design presented in this thesis is making use of Hoosier 6.0/18.0-10 LC0 tires which is a 10 inch tire. From the 2018 team specifications report, it is found that this is the most widely used tire with the tire compound being soft and specifically manufactured for FSAE competitions. Tire specifications are shown in the table 2.1.

Table 2.1 Hoosier 6.0/18.0-10 LC0 tire data.

Tire Size	Tread Pattern	Tread Width	Approximate Diameter	Recommended Wheel Width	Wheel Width	Tire Compound
6.0/18.0-10	Slick	6.0 in	18.0 in	6-7 in	7 in	LC0

Wheel selection is done with respect to the recommended wheel specifications for the selected tire. For the selected 10 inch Hoosier 6.0/18.0-10 tire, the recommended wheel width is 6-7 inch. A 6 inch Keizer wheel is selected to use in the design of suspension and other related systems, which is one of the widely used wheels in FSAE competitions. The wheel comes with a variety of backspacing options (variable ‘F’ in the drawing shown below) available. The highest possible backspacing of 5 inch is selected for the wheel to get more space inside the wheels to work when designing the suspension system. The wheel specifications are shown in the table 2.2

Table 2.2 Keizer 10i (10x6) wheel dimensions.

Wheel	**Width**	**Backspacing (dimension 'F')**
Keizer 10i (10x6)	10 in x 6 in	5.00 in

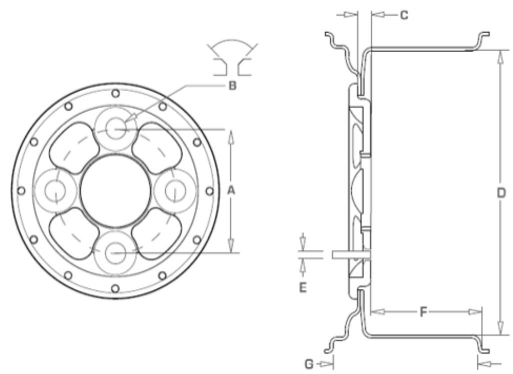

Figure 2.1 Keizer 10i wheel manufacturer drawing [43].

2.2.2 Wheel base and Track width

Wheel base is the distance between the front and rear axles of a vehicle, whereas Track width is the distance between the wheel centers of right and left wheels.

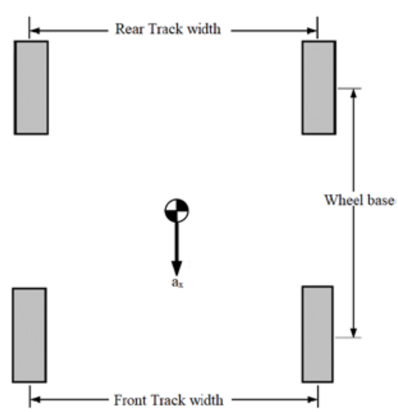

Figure 2.2 Representation of vehicle track width and wheel base.

Competition rule book has specified the minimum wheelbase required for an FSAE car, which is 1525 mm or 60 inches. The rule regarding vehicle track width is that the smaller track width of the vehicle should not be less than 75% of the larger track width either it is front or rear. Increasing the track width will reduce the weight transfer between the wheels while cornering. This means that the tire load will be more evenly distributed and hence it will increase the cornering power. But for race cars where reduction of aerodynamic drag is important, an increased track width is detrimental, as it will make the car wider. Increasing the width of the car will eventually result in increased vehicle weight too. Also, it is not necessary to have similar track widths at the front and rear [5]. Usually, rear wheel drive race cars will have larger track width at the front in order to generate more traction at the rear tires by reducing the rear wheel rolling at corner exits [6]. Wheel base affects the longitudinal weight transfer. Similar to the effects on cornering ability when having a larger track width, having a larger wheel base is also beneficial for the cornering performance. But, the wheel base should not be too large as it will increase the overall length of the vehicle and thereby increasing the weight of the vehicle. Also, vehicles with smaller wheel base will be easy to control while cornering due to the smaller size of the vehicle.

Hence selection of track widths and wheel base should be done by finding a compromise among the benefits of having a larger or smaller track widths and wheel base. Gaffney and Salinas (1997) states that the beginners in race car design should study the track widths and wheel base of other cars in the competition as a beginning point [5]. The dimensional details of the latest competing cars can be found in the ‘Event Guide’ published by the FSAE organizers every year. The event guide published with the details of the 2018 cars is taken as a reference for determining the track width and wheel base for the designing process in this project [3]. Finally, a wheel base of 63 inches (1600 mm), front track width of 48 inches (1220 mm) and rear track width of 46.5 inches (1180 mm) is selected for this project.

2.2.3 Suspension Type Selection

Selection of suspension type to be used in the design is done after careful study of various types of suspensions used in cars along with the specific suspension requirements in an FSAE car. There are five types of suspensions found in car – Beam axle, Swing axle, Trailing link, Strut, Double A-arm suspensions. In Beam axle suspensions, a rigid axle is used to connect both the wheels at front and rear. This is not an independent suspension type and hence it is not possible to control the movement of both the wheels independently. Presently they are used on some heavy load trucks and tractor- trailer trucks since they provide high strength and rigidity. But they have disadvantages of having heavy unsprung weight, space requirements and rough rides.

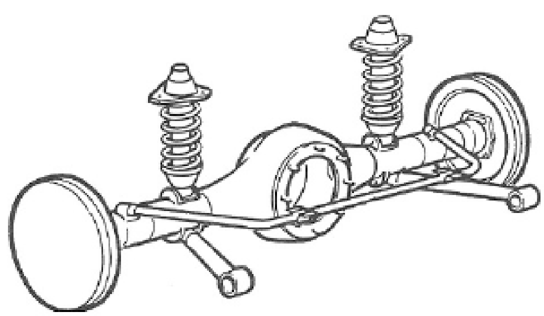

Figure 2.3 Beam axle suspension with coil springs [7].

Swing axle suspensions are one of the first types of independent suspensions in which the independent axles on left and right sides are connected to a pivot near the center of the car.

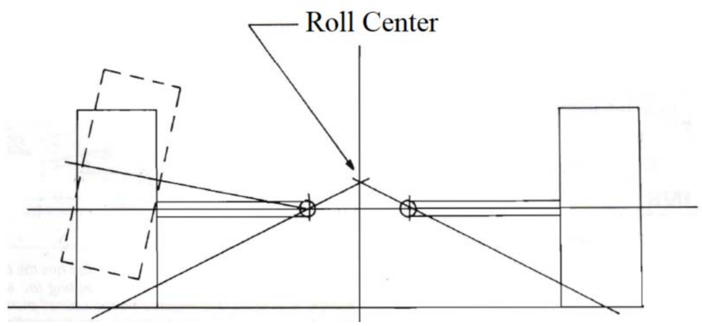

Figure 2.4 Swing axle suspension [8].

Swing axle suspensions have high roll center and short swing arm length. This combination can cause unpredictable handling of the vehicle which is very undesirable in race cars.

In trailing link suspensions, two trailing arms are used to support the steering knuckle. Hence the wheels mot only moves upward during bumps, but they also move backward. They offered better ride quality and packaging, still has many disadvantages mainly if used in high performance cars. The trailing link design can cause bending of the links when high cornering load acts on them which makes them undesirable for race cars.

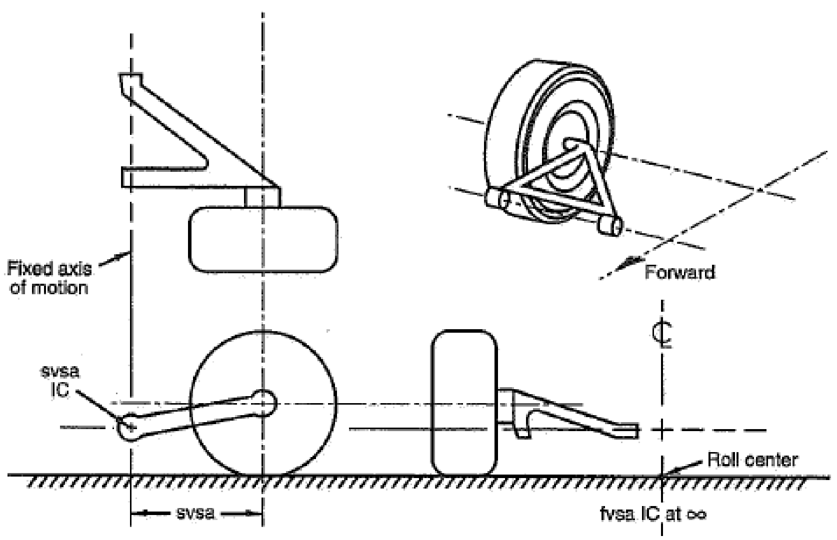

Figure 2.5 Trailing link suspension [6].

Struts or commonly MacPherson struts are one of the most commonly used suspension systems in production cars. The Spring/damper unit or strut is mounted on the A-arm close to the knuckle.

One of the main reasons why it is not commonly used in race cars is that it is not possible to install wider tires when using struts without increasing scrub radius. Also, the camber gain is very less with struts and hence the outside tire will lose its camber during cornering. Struts are used in cars which look for cheap suspensions with compromise on handling.

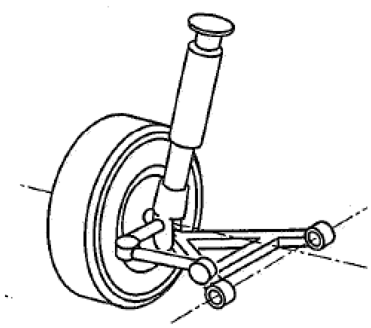

Figure 2.6 MacPherson strut suspension [6].

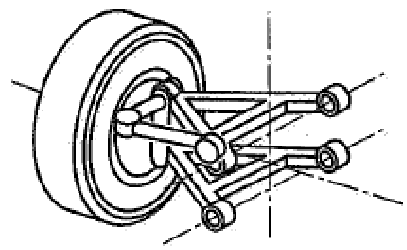

Figure 2.7 Double A-Arm suspension [6].

Double A- arm also known as Double Wishbone, as the name indicates, has two A arms of which one end is mounted to the wheel knuckle and the other end connected to the chassis. This is the most widely used suspension which demands for an independent suspension with the best handling properties. There are both equal length A- arms and unequal length A-arms depending upon the the legth of top and bottom arms. For equal length A-arms the equal length arms will be mounted parallel to the ground, hence the FVSA is infinitely long and the the roll center will be located at the ground level. These disadvanteges can be rectified by using an unequal length A-arm, in which it is possible to achieve any FVSA length and roll center heights depending upon what the dsigner is looking for. This flexibility available with unequal length A-arms make it the best option for using as a race car suspension. Almost all formula type race cars use unequal length A-arms with shorter upper arm and longer lower arm. Hence unequal length Double A-arm suspensions is selected as the suspension to be designed in this project.

2.2.4 Chassis Type Selection

FSAE teams use mainly two types of chassis- Spaceframe or Composite hybrid Monocoque. Spaceframe are built by welding steel tubes together to form the overall shape with required stiffness. Advantage of using a spaceframe chassis is the relative simplicity of the manufacturing process, readily available raw materials, low cost etc. The main disadvantage of using spaceframe chassis is the relatively low stiffness to weight ratio.

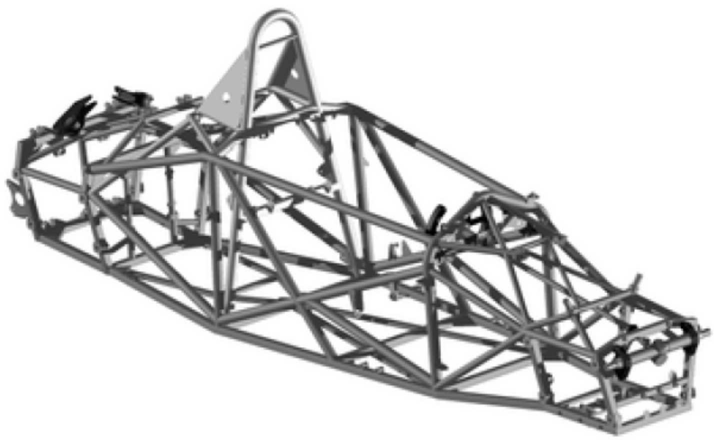

Figure 2.8 Spaceframe chassis [9].

Monocoques are single piece structures mainly made of composite materials. It serves both as the structural member and as the body for the vehicle. Most commonly CFRP are used in the manufacturing of composite monocoques. Hence the overall weight of the chassis and the vehicle can be less without compromising the chassis stiffness.

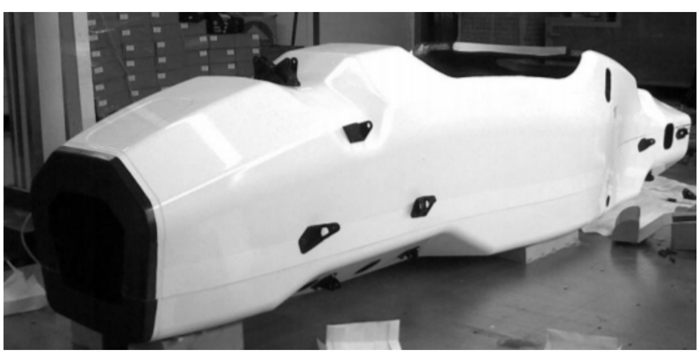

Figure 2.9 Monocoque chassis [10].

Many experienced teams use Composite hybrid Monocoques which is a combination of both a composite monocoque and a rear spaceframe. The composite monocoque structure at the front provides high torsional stiffness at very less weight and the rear spaceframe has advantages of easy construction and access to the engine. Composite CFRP monocoques used in FSAE can yield a torsional stiffness of approximately 3000-7000 lbs ft/degree[11].

Figure 2.10 Hybrid monocoque chassis [10].

Comparing the both types of chassis along with discussion with different people experienced in FSAE competitions, it is decided to move forward with a spaceframe chassis. This is after considering the lower cost and simpler manufacturing methods involved in a spaceframe construction for a first-year team. Even though CFRP monocoques can easily attain a torsional stiffness of more than 3000 lbs ft/deg, it is understood that this is a very high torsional stiffness required for an FSAE car. A spaceframe chassis with a torsional stiffness of approximately 1500 lbs ft/deg to 2000 lbs ft/deg is expected to deliver a good overall performance and handling [12]. Hence, a spaceframe chassis with a torsional stiffness of approximately 2000 lbs ft/deg with a weight less than 60 lbs is decided to be the target parameters of the chassis to be designed in this project.

CHAPTER 3: Component Design

3.1 Initial Chassis Wireframe Design

3.1.1 Chassis Design Rules

As per the Formula SAE rule book, chassis is a structural assembly intended to support all the other components of the vehicle. The general chassis requirement is to protect the driver's head and hand from contacting the ground in case of vehicle rollover. The driver's feet and leg should be inside the chassis structure at any instance. There should be some critical structures in the chassis assembly collectively known as the primary structure. Primal structure includes Main Hoop, Front Hoop, Roll Hoop Braces and supports, Side Impact Structure, Front Bulkhead, Front Bulkhead support and any chassis members, guides, or supports that transfer load from the Driver Restraint System. Main roll hoop is located behind the driver seat and front roll hoop is located above the driver's legs. Roll hoops are structurally supported by roll hoop bracings. Side impact zone of the chassis is located between the front and main roll hoops extending to a height of 350 mm above the ground. The planar structure at the front of the chassis protecting the driver's leg is known as front bulkhead.

The primary chassis is developed such that it has the whole primary structure also making sure that other chassis rules are also satisfied. The two-dimensional template shown in figure 2.11 used to represent the 95^{th} percentile male is used as the main reference used to obtain the minimum required dimensions to accommodate a driver.

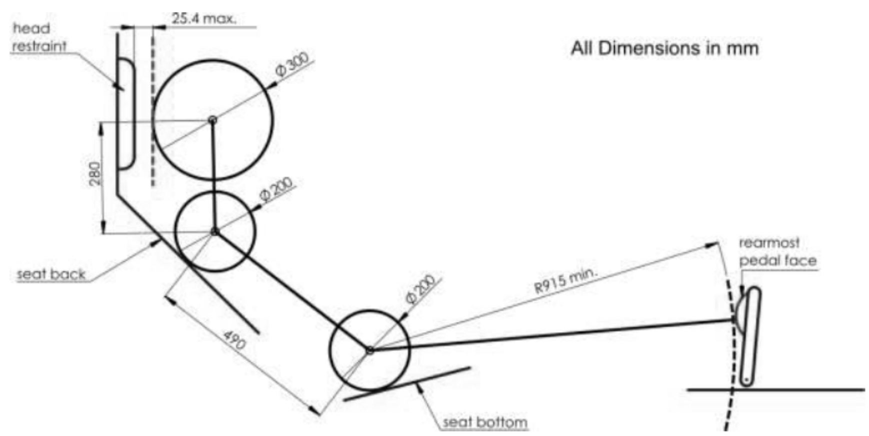

Figure 2.11 95th percentile male dimensions' template [1].

Roll hoops must be designed as per the provided rules for front and main roll hoops. The minimum height for the roll hoops is determined according to the position of the helmet when seated normally. There should be a minimum of 50 mm distance from the top of the helmet to a line drawn connecting top of front and main hoops as shown in figure 2.12. Also, there should be a minimum distance of 50 mm from the top of the helmet to a line drawn connecting top of the main hoop and the lower end of main hoop bracing. If bracing is extending forwards, the rear of the helmet should not be further rearwards than the main hoop rear surface.

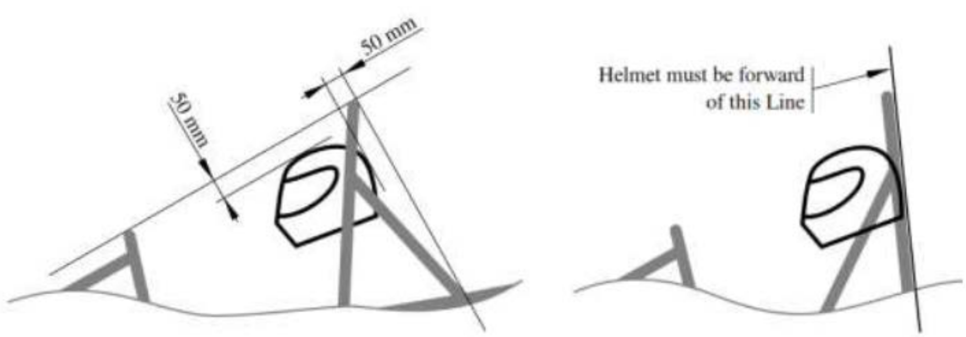

Figure 2.12 Roll hoop and bracing design requirements [1].

The roll hoops must be supported by roll hoop bracings for structural stability during an incident of rollover. Hoops must be supported by two bracings, one on each side of the hoops. Main hoop bracing must be attached at a distance not greater than 160 mm measured from the top of the main hoop and front hoop bracing must be attached at a distance not greater than 50 mm measured from the top of the front hoop.

The front bulkhead must be supported using a minimum of three chassis members on each side of the car- an upper member, a lower member and a diagonal brace for triangulation to the front roll hoop. The location of the upper bracing must be less than 50 mm from the top of the bulkhead on the bulkhead side and within a zone of 100 mm above and 50 mm below the upper side impact member on the roll hoop side.

There should be at least 3 chassis members on both sides of the vehicle to act as the side impact structure. There should be an upper member at a distance between 300-350 mm from the ground connecting the front and main hoops. Lower member should connect the bottom ends of the front and main hoops and the diagonal member should connect the upper and lower side impact members

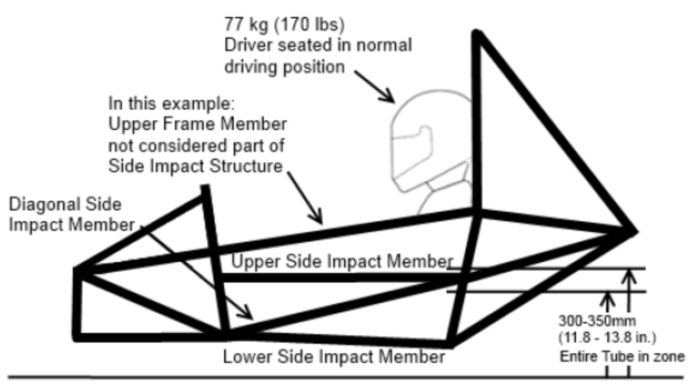

Figure 2.13 Side impact structure requirements [1].

Remaining dimensions of the structure is obtained by the rules provided for the cockpit of the car. The template shown in figure 2.14 should pass through the cockpit, inserted through the opening between the roll hoops from the top parallel to the ground. Internal cross section of the cockpit is mainly decided by the internal cross section provided in figure 2.14. During inspection, the given template must pass through the cockpit until 100 mm rearwards to the location of pedal, when help vertically.

It is also required to have a head restraint to prevent any rearward movement of the head with a head restraint padding of minimum 38 mm thickness and 15 cm width.

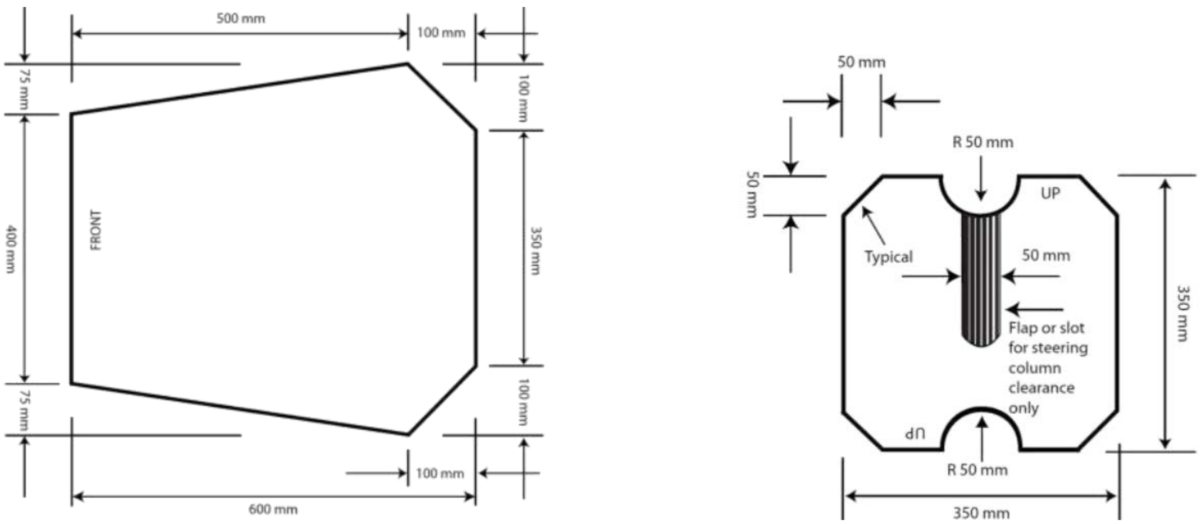

(a) (b)

Figure 2.14 Cockpit opening requirement templates (a) Top view (b) Side view [1].

3.1.2 Initial Wireframe Design

Initial wireframe design is done based on the available parameters obtained from the chassis design rules. The purpose of initial wireframe design is to get started with a rough model with all the primary members as instructed by the rules. The CAD models in this design were mostly developed using SOLIDWORKS and the same is used to develop the initial wireframe as shown in figure 2.15. Initial wireframe consists of roll hoops (main and front), roll hoop bracings, front bulkhead and supports and side impact structures. The rear end of the initial wireframe is designed considering the rough estimated dimensions of Honda CBR600RR engine, which is one of the most commonly used engines in FSAE competition. Again, this is a very primitive design for the chassis, including only the mandatory primary structure members. This initial wireframe will make the next steps in the design process easier.

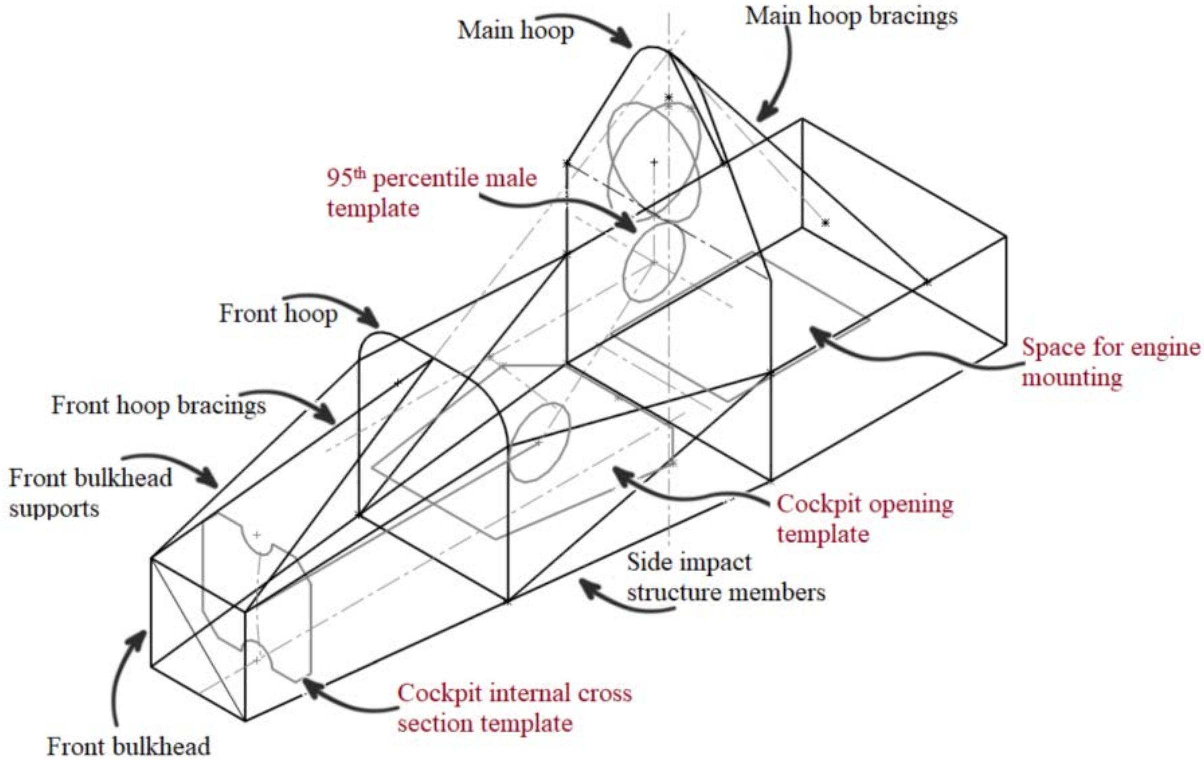

Figure 2.15 Chassis wireframe initial design.

3.2 Design of Suspension Geometry

3.2.1 Selection of Suspension Parameters

3.2.1.1 Front View Swing Arm length

Front View Swing Arm (FVSA) length is the distance from the wheel center to the front view instant center. Instant center (IC) is the imaginary pivot point about which the wheel is going to move during body rolls in cornering. In other words, it is the intersection point of extension of the center lines of the upper and lower control arms. A suitable FVSA length should be selected before proceeding to design the suspension geometry since it is the main parameter which controls the orientation and length of the suspension control arms. If the swing arm length is large, the wheel travel will be smooth, but it will result in less camber gain and vice versa. Adams (1993) recommends a swing arm length of between 100-150 inches as a good compromise between the benefits of long and short swing arms [8]. A front view swing arm length of 100 inches is selected for the design as per the above considerations.

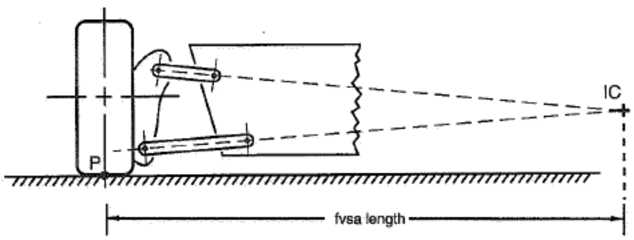

Figure 2.16 Front View Swing Arm length [6].

3.2.1.2 King Pin Inclination and Scrub Radius

King pin inclination is the angle between the line connecting upper and lower ball joints and the normal to the ground. Kingpin inclination along with the location of the ball joints with respect to the wheel center determines scrub radius. Scrub radius is the distance between the point of contact of the line connecting the ball joints and the ground to the wheel center. Scrub radius should be kept as small as possible since the scrub radius determines the amount of twisting forces excreted on the steering wheel. In other words, as the scrub radius decreases, the forces needed to be acted on the steering wheel to turn the tire decreases. King pin inclination should be selected such that the scrub radius is kept to minimum. A king pin inclination of 6^0 is found to be the best compromise for this design considering the other parameters. This yielded a scrub radius of 0.72 inches which is considered to be a low value in FSAE cars.

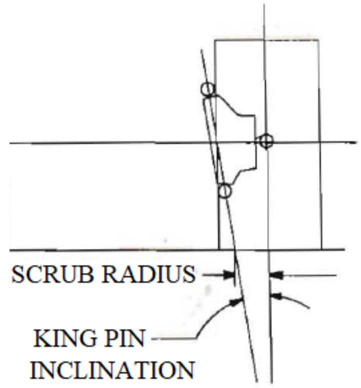

Figure 2.17 King Pin Inclination and Scrub Radius [8].

3.2.1.3 Roll center Height

Roll center of a vehicle in front view is the imaginary point about which the whole vehicle rolls while cornering. Roll center is the intersection point of a line drawn from the center of tire contact patch and the IC and the normal through the center of gravity. Roll center height is the height of roll center above the ground. This depends on the suspension geometry design. There can be different roll center heights for the front and rear suspensions. The line connecting the front and the rear roll centers is called the roll axle.

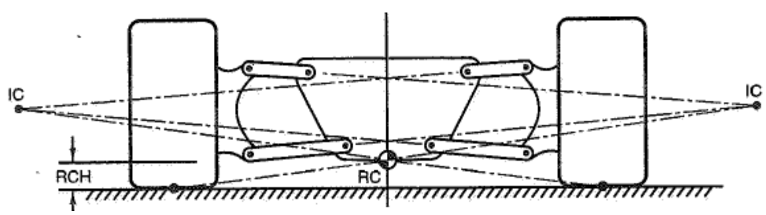

Figure 2.18 Roll center Height [6].

The amount of body roll will depend on the distance between the center of gravity and the roll center since the weight is acted through the center of gravity and a roll moment is created according to this distance. Adams (1993) states that a roll center height is between 1 inch and 3 inch above the ground for most successful cars [8]. In order to keep the design roll center height to be in the range, it is better to select a required roll center first and then design the geometry according to that. Along with the above suggestion and research on roll center heights used by different teams, roll center height of 2 inches at the front and 2.5 inches at the rear is selected.

3.2.2 Front and Rear Suspension Geometry Design

The design of suspension geometry can be now done using the above selected parameters and the initial chassis wireframe designed. Selection of a brake rotor is also needed to be done before proceeding to the design since it decides the space left inside the wheels for locating the ball joints in the wheel end. A few different types of brake rotors commonly used by FSAE teams were analyzed and ISR 22-048-OA is selected for design calculations due to its lowest rotor thickness (2.4 inches or 61 mm). The other details of ISR 22-048-OA rotors are provided in Appendix A. Race car Vehicle Dynamics by Milliken, Chapter 17.5 describes a method to design the suspension geometry [6]. This is taken as the reference for the suspension geometry design in this project. The steps involved in the suspension geometry design is discussed below.

a. In the already designed initial wireframe, draw the front tires according to the front track width selected (48 inches or 1220 mm).
b. Draw lines representing wheel back spacing and brake rotor thickness to locate the possible locations of upper and lower ball joints. Here the wheel back spacing is 5 inches from the inside of the tire, means 1 inch from outside of the tire and the brake rotor thickness is 2.4 inches. Hence the location of lower ball joint is decided to be at a distance of 4.25 inches leaving a gap of 0.85 inches between the rotor and the ball joint.

c. Locate the upper ball joint according to the King pin inclination and the scrub radius required. The selected upper ball joint makes a King pin inclination of 6^0 and scrub radius of 0.72 inches.

d. Locate the predefined roll center at 2 inches high from the ground through the centerline of the vehicle (Assuming that weight will be evenly distributed among left and right sides of the vehicle and hence center of gravity remains at the vehicle center)

e. Draw a line connecting the center of the tire contact line and the roll center. Draw a line at a distance of preselected FVSA length (100 inches in this design). The intersecting point of these two lines is the Instant center.

f. Draw points connecting the upper and lower ball joints to the Instant Center. The A- arms should lie on these two lines since the arms rotate about the Instant center during wheel travel.

g. Now the chassis side ball joint locations can be determined using the previously drawn two lines and the initial wireframe designed. Find the point of intersection of the two lines on the plane of suspension mounting on the chassis.

The same method is followed while designing the rear suspension. The differences would be the difference in roll center height, which is 2.5 inches at the rear and the rear track width which is 46.5 inches or 1180 mm. Apart from that, the steps followed is the same as discussed above.

The resultant front and rear suspension geometries is shown in figure 2.19. Dimensions are in inches.

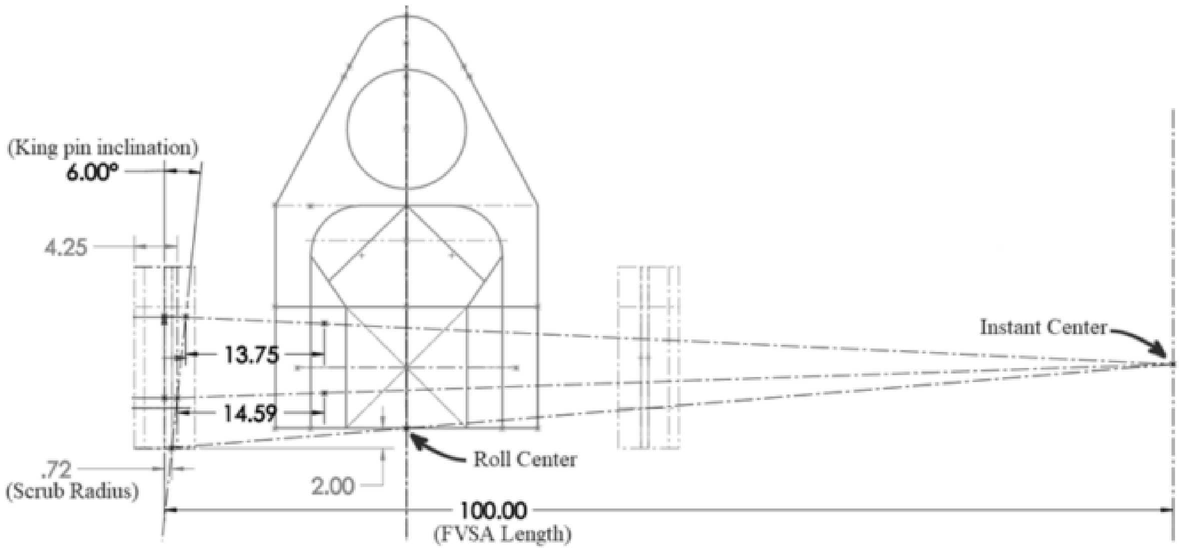

(a)

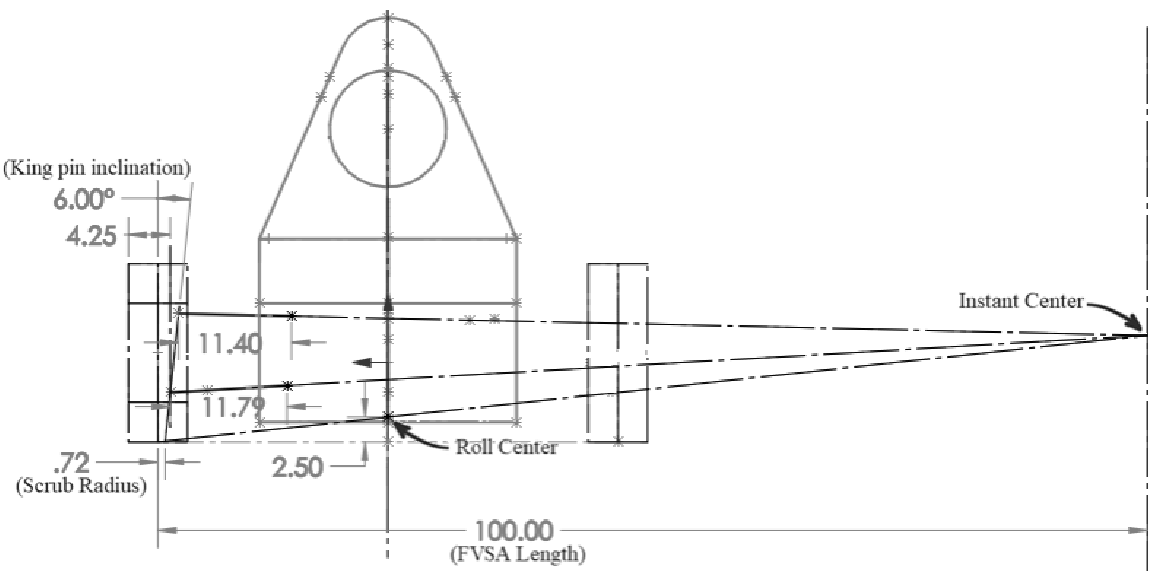

(b)Figure 2.19 Front and rear Suspension geometry design (a) Front suspension (b) Rear suspension.

3.3 Optimized Chassis Design and Testing

3.3.1 Final chassis design process

Once the suspension pickup points are known after suspension geometry design, modifications can be made to the existing initial wireframe to accommodate suspension points. The initial wireframe was modified by removing structures that are not required after adding the nodes at suspension pick up points. Also, the rule book mandates the used of specific tube sizes for construction of different chassis members when steel tubes are used as shown in table 2.3. SOLIDWORKS weldments are used to assign these profiles to the already created chassis wireframe. Now the target for the next phase of chassis design was to attain the target torsional stiffness of above 2000 lbs ft /deg with a total weight less than 60 lbs. SOLIDWORKS simulation with beam elements was used to do FEA on different chassis models created by modifying the already developed base model. Different chassis models were made by varying the tube dimensions used, selecting between square and round tubes wherever permissible, adding/ removing extra structural members.

Table 2.3 Chassis steel tubing minimum dimensions [1].

Minimum Dimensions – Steel Tubing	
Application	**Outside Diameter and Wall Thickness**
Main Hoop, Front Hoop, Shoulder Harness Mounting Bar	Round 1.0 inch x 0.095 inch (Round 25.0 mm x 2.50 mm)
Side Impact Structure, Front Bulkhead, Roll Hoop Bracing, Driver Restraint Harness Attachment (other than Shoulder Harness Mounting Bar)	Round 1.0 inch x 0.065 inch (Round 25.0 mm x 1.75 mm) Square 1.0 inch x 1.0 inch x 0.047 inch (Square 25.0 mm x 25.0 mm x 1.20 mm)
Front Bulkhead Support, Main Hoop Bracing Supports, Shoulder Harness Mounting Bar Bracing	Round 1.0 inch x 0.047 inch (Round 25.0 mm x 1.5 mm)
Bent Upper Side Impact Member	Round 1.375 inch x 0.047 inch (Round 35.0 mm x 1.2 mm)

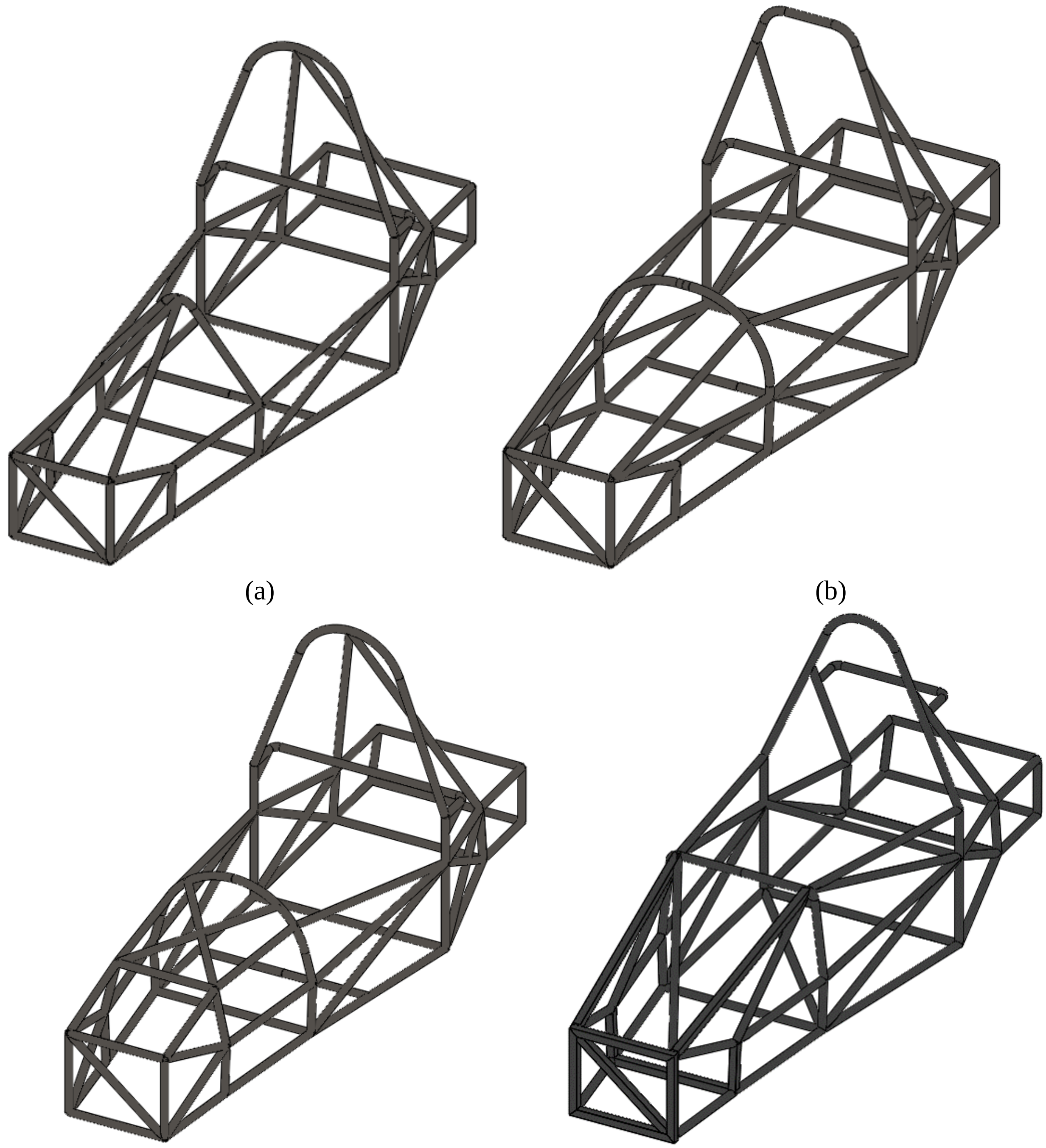

(a) (b) (c) (d)

Figure 2.20 Chassis spaceframe design versions (a) Version 1 (b) Version 2 (c) Version 3 (d) Version 4.

After conducting Finite Element Analysis on all the chassis versions, version 4 is selected since it satisfies both the targets for torsional stiffness and weight.

3.3.2 Material selection

Before proceeding to Finite Element Analysis, the material needed to be used for the chassis should be determined. Steel tubes are recommended by the FSAE rules unless any material with higher strength is available. With increase in strength, usually cost will also go up. Almost all the teams relying on spaceframe chassis uses steel tubes for the construction. FSAE rules states that any steel material used for chassis construction should have a Young's modulus of at least 200 GPa (29.0 x 10^3 ksi), Yield strength of at least 305 MPa (44.2 ksi) and Ultimate strength of at least 365 MPa (52.9 ksi). Availability of the steel tubes with the selected material was also considered as an important constraint. An extensive research was done on the material offerings for steel tubes with the dimensions given in table xx from various manufacturers. Also, the materials commonly used by different FSAE teams were also considered while taking a decision. With all these considerations, the available materials found out were 4130 Alloy steel (Chromoly), and 1018 / 1026 Carbon steels [13]. A comparison was made among these three to select the best suited steel for the chassis.

Table 2.4 Comparison of structural properties of selected steel tubes for chassis.

Material	**Density**	**Young's modulus**	**Yield strength**	**Ultimate strength**
4130 Chromoly	7.85 g/cc or 0.284 lb/in^3	205 GPa or 29.7 x 10^3 ksi	435 MPa or 63.1 ksi	670 MPa or 97.2 ksi
1018 Carbon Steel	7.87 g/cc or 0.284 lb/in^3	205 GPa or 29.7 x 10^3 ksi	370 MPa or 53.7 ksi	440 MPa or 63.8 ksi
1026 Carbon Steel	7.86 g/cc or 0.284 lb/in^3	205 GPa or 29.7 x 10^3 ksi	415 MPa or 60.2 ksi	490 MPa or 71.1 ksi

Comparing the Young's modulus, Yield strength and Ultimate strength of the three steels, it can be seen that all of them satisfies the minimum requirements for those parameters. Also, the density of all three are very similar. Hence the selection can be based on which one performs better since selecting any one of them doesn't have any effect on the weight of the structure. Comparing the values 4130 chromoly is clearly better in terms of the strength values. Also, most of the FASE teams using spaceframe chassis makes use of 4130 chromoly steel due to its high strength to weight ratio, and great weldability.

3.3.3 Chassis Finite Element Analysis

Finalizing the design of chassis can be done by analyzing the chassis models for attaining the required stiffness. Teams utilize both Finite Element Analysis and physical testing to determine the performance of their chassis developed. Finite element Analysis can be a great tool to determine the chassis performance and finalizing the chassis design in a simulation driven product design approach. For testing a chassis model, it is important to know the different modes of loading subjected to an automobile chassis. Then, the chassis should be tested for these conditions using Finite Element Analysis. In an automotive chassis, the main modes of deformation are found out to be Longitudinal torsion, Vertical bending, Lateral Bending and Horizontal Lozenging [14]. Torsional stiffness is considered to be the most important determinant of the chassis performance. If the chassis had good amount of torsional stiffness, then it will naturally have enough stiffness against all other three loading types [12]. Hence, the Longitudinal torsion testing was done on different chassis models to determine the best performing chassis. As stated earlier, the target torsional stiffness for the chassis is 2000 lbs ft/deg.

The main load acting on a race car chassis is the torsional load due to the cornering forces. This will be the load with highest magnitude when compared to other loads acting on it. Torsional stiffness of a chassis can be analyzed using a simple model of fixing one end of the chassis and applying a torque on the other end [12]. In an FSAE spaceframe chassis, this can be done by fixing the rear suspension pickup nodes and applying equal and opposite loads on the front suspension pickup points on the left and right sides. This model is used in this project to analyze the torsional stiffness of the chassis models. SOLIDWORKS simulation is used to carry out Finite Element Analysis on the chassis models with use of beam elements, which is best suited for tubular spaceframes. The fixtures are applied to the rear end suspension pickup points and forces are applied as remote loads at the center of the knuckle as shown in figure 2.26 (The figure shows version 4; forces and fixtures are applied in the same way for all the other chassis versions).

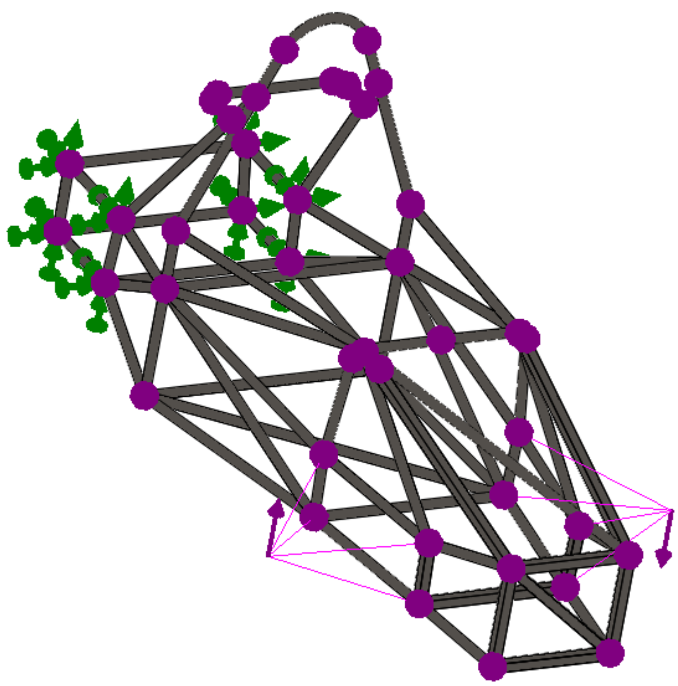

Figure 2.26 Chassis FEA model with loads and constraints.

The torsional stiffness is calculated as shown below. The maximum vertical displacement on both sides of the chassis are measure as Δy_1 and Δy_2 respectively.

$$K = \frac{FL}{\tan^{-1}\left[\frac{(\Delta y_1 + \Delta y_2)}{2L}\right]}$$

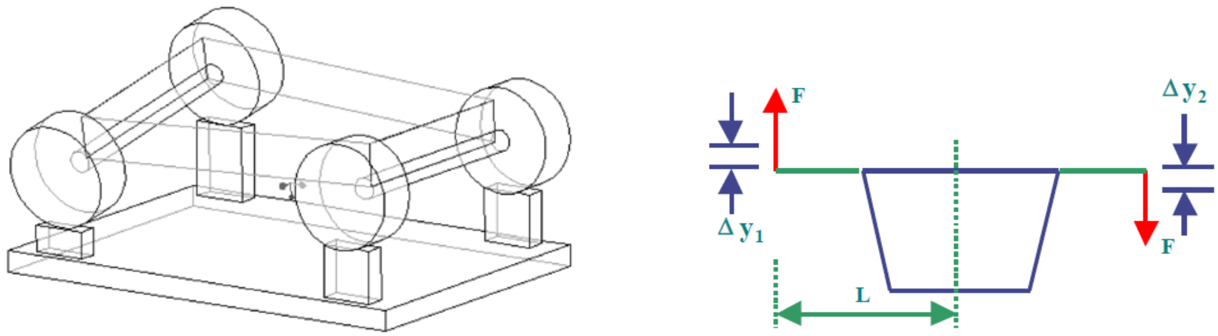

Figure 2.22 Chassis torsional stiffness calculation methodology [12].

The results of analysis done on the four chassis models are shown in figure 2.23 and table 2.5

Table 2.5 FEA results of different chassis versions tested.

Chassis Version	Weight (lbs)	Load (lbs)	L (inches)	Δy_1 (inches)	Δy_2(inches)
Version 1	56	100	22.32	0.060	0.061
Version 2	62	100	22.32	0.055	0.054
Version 3	62	100	22.32	0.050	0.050
Version 4	58	100	22.32	0.033	0.030

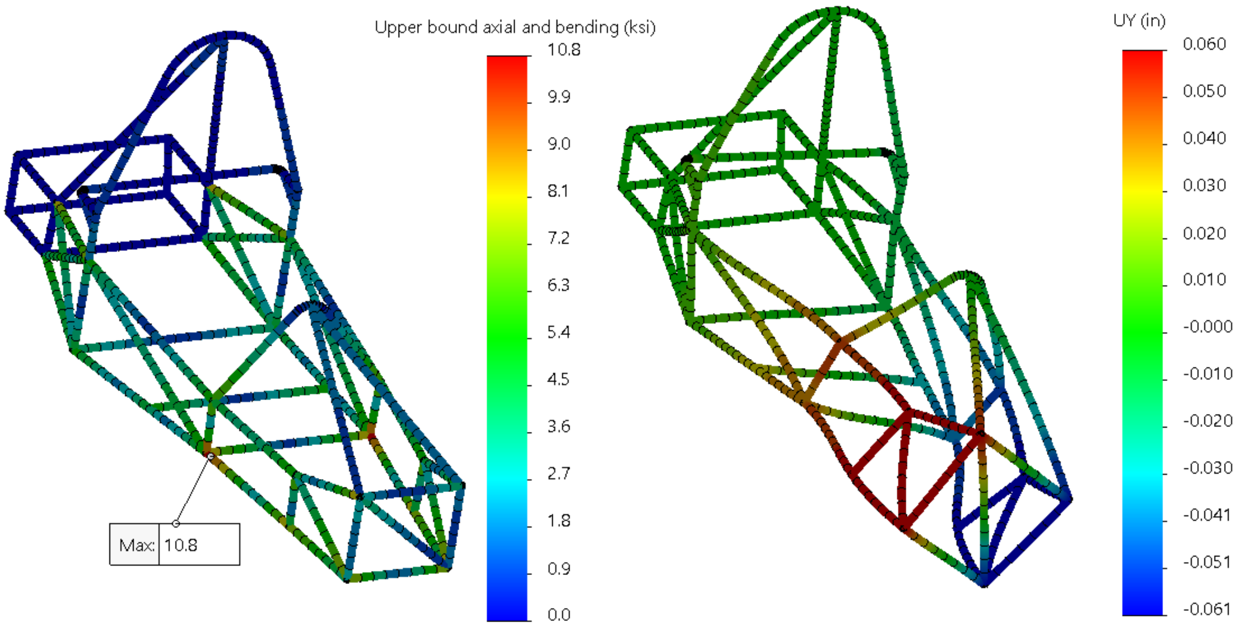
Upper bound axial and bending (ksi)
10.8
9.9
9.0
8.1
7.2
6.3
5.4
4.5
3.6
2.7
1.8
0.9
0.0
Max: 10.8
UY (in)
0.060
0.050
0.040
0.030
0.020
0.010
-0.000
-0.010
-0.020
-0.030
-0.041
-0.051
-0.061

(a)

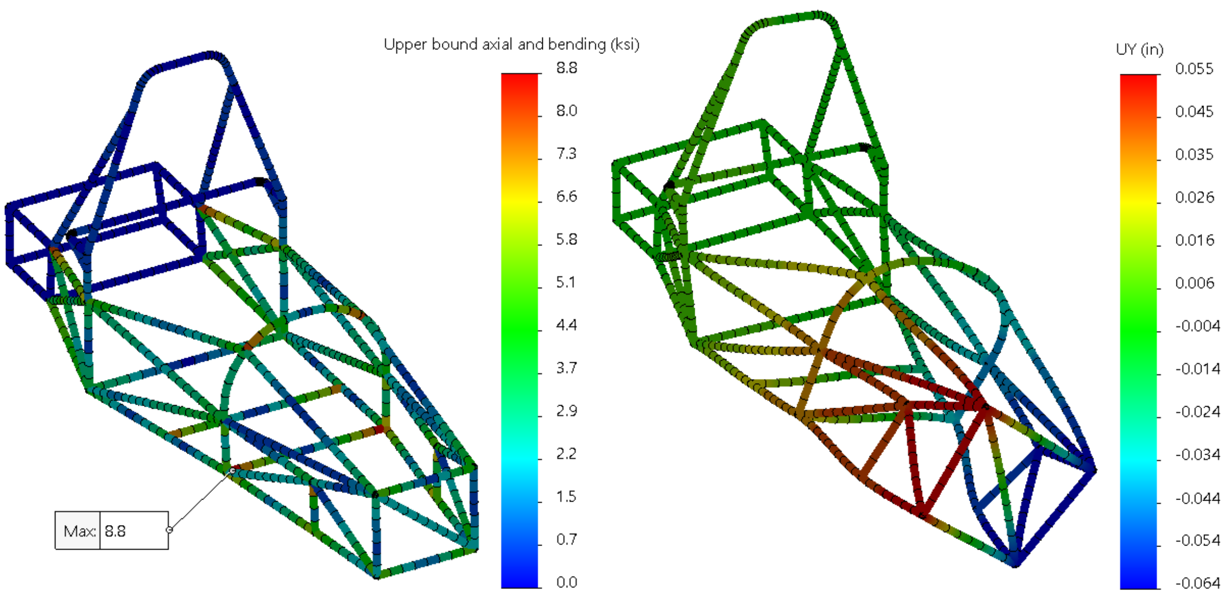
Upper bound axial and bending (ksi)
8.8
8.0
7.3
6.6
5.8
5.1
4.4
3.7
2.9
2.2
1.5
0.7
0.0
Max: 8.8
UY (in)
0.055
0.045
0.035
0.026
0.016
0.006
-0.004
-0.014
-0.024
-0.034
-0.044
-0.054
-0.064

(b)

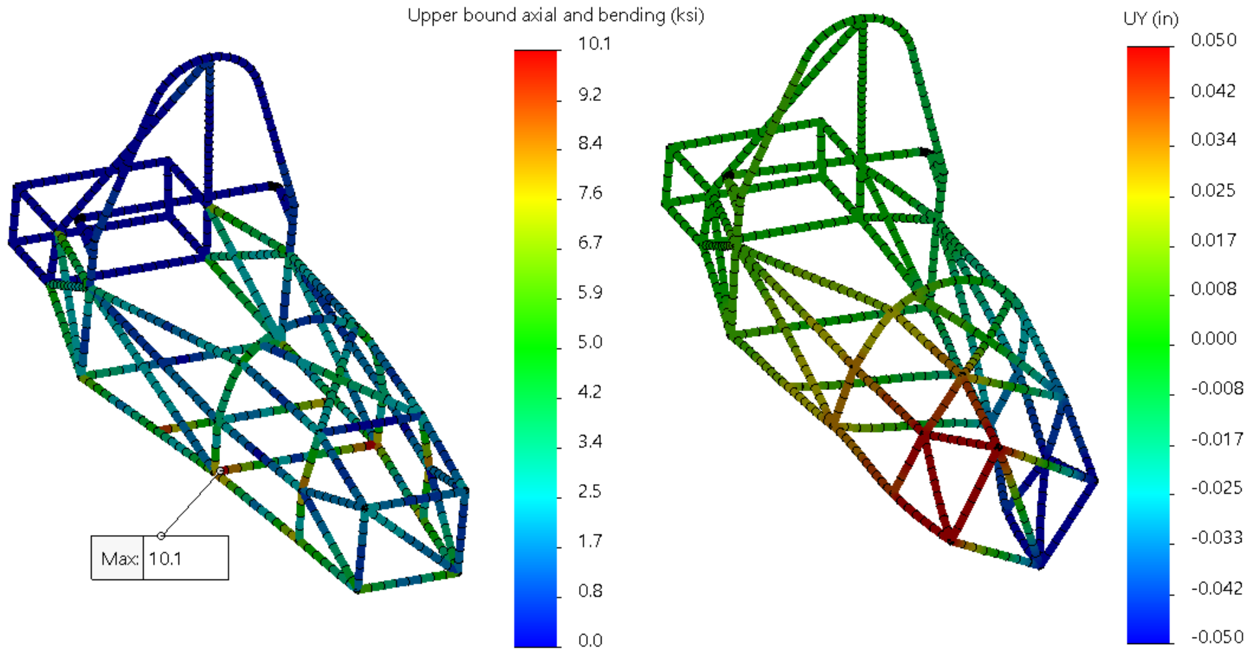

(c)

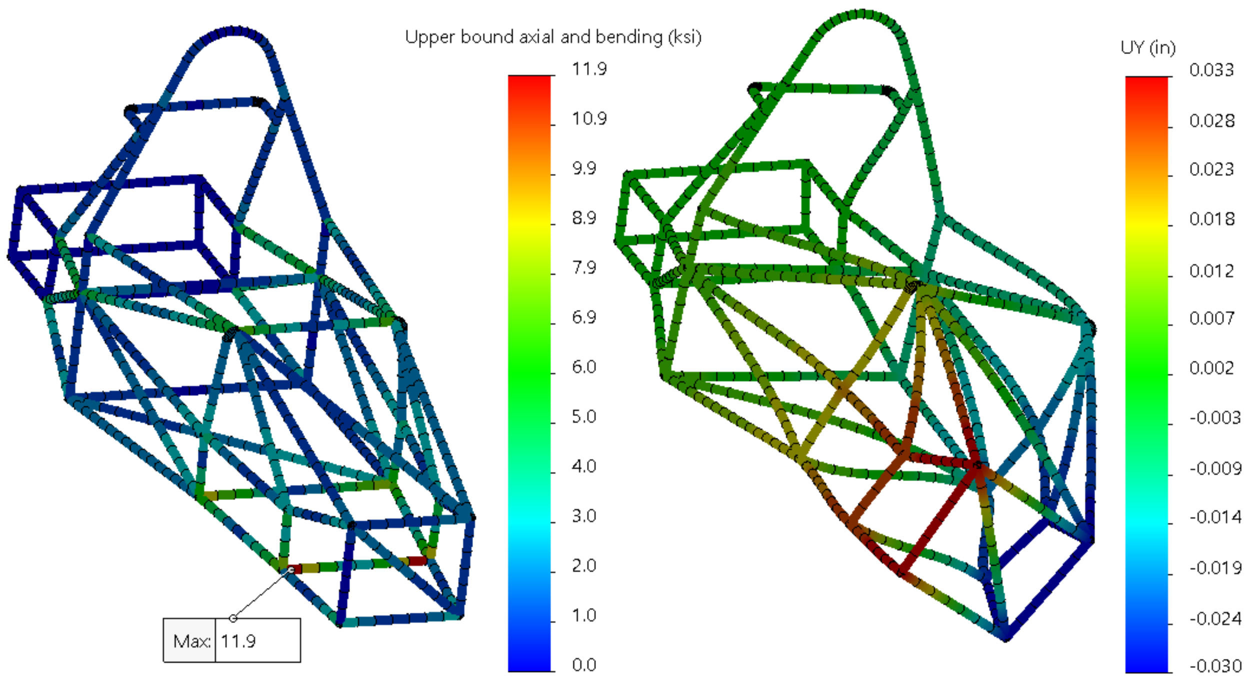

(d)

Figure 2.23 Chassis spaceframe FEA results for torsional stiffness (a) Version 1 (b) Version 2 (c) Version 3 (d) Version 4.

Now once the vertical displacements are known, the torsional stiffness can be calculated as below.

Torsional stiffness of chassis version 1 is given by

$$K_{V1} = \frac{100\ lbs * 22.32\ in}{\tan^{-1}\left[\frac{(0.060\ in + 0.061\ in)}{2 * 22.32\ in}\right]}$$

$$= 14372\ lbs\ in/deg \quad = 1198\ lbs\ ft/deg$$

Torsional stiffness of chassis version 2 is given by

$$K_{V2} = \frac{100\ lbs * 22.32\ in}{\tan^{-1}\left[\frac{(0.055\ in + 0.064\ in)}{2 * 22.32\ in}\right]}$$

$$= 14613\ lbs\ in/deg \quad = 1218\ lbs\ ft/deg$$

Torsional stiffness of chassis version 3 is given by

$$K_{V3} = \frac{100\ lbs * 22.32\ in}{\tan^{-1}\left[\frac{(0.050\ in + 0.050\ in)}{2 * 22.32\ in}\right]}$$

$$= 17390\ lbs\ in/deg \quad = 1449\ lbs\ ft/deg$$

Torsional stiffness of chassis version 4 is given by

$$K_{V4} = \frac{100\ lbs * 22.32\ in}{\tan^{-1}\left[\frac{(0.033\ in + 0.030\ in)}{2 * 22.32\ in}\right]}$$

$$= 27603\ lbs\ in/deg \quad = 2300\ lbs\ ft/deg$$

Comparing the results obtained from the chassis analysis, version 4 was found to be satisfying the target torsional stiffness (>2000 lbs ft/deg) with a torsional stiffness of 2300 lbs ft/deg and weight (<60lbs) with a weight of 58 lbs. Hence this chassis design was finalized for this design.

3.4 Impact Attenuator Design

Impact attenuator is a device mounted at the front of the bulkhead to protect the vehicle during an instance of front on collision. It is made to be deformable and should act as an energy absorbing device. Teams can use the approved standard design of Impact Attenuator which is published in FSAE online website [1] or can design it by their own. This project will be considering that standard impact attenuator design and will be conducting simulations with various energy absorbing materials to compare their performance using an impact simulation tool. Test should be conducted to analyze the performance of the impact attenuator during the impact conditions specified in the impact attenuator rules as shown in the next section.

3.4.1 Impact Attenuator Rules

- Impact attenuator must have a minimum of 200 mm length, 100 mm height and 200 mm width.
- Impact attenuator should be mounted to securely to the front bulkhead through an Anti-Intrusion plate having a minimum thickness of 1.5 mm (0.060 in) if solid steel and 4.0 mm (0.157 in) if solid aluminum plate is used.
- Impact attenuator should cause a vehicle of total mass 300 kg to decelerate at 20 g average and a peak of 40 g when the impact velocity is 7.0 m/s.

3.4.2 Impact Attenuator Modelling

This project will be considering the standard impact attenuator design provided in the FSAE online website which is shown in figure 2.24

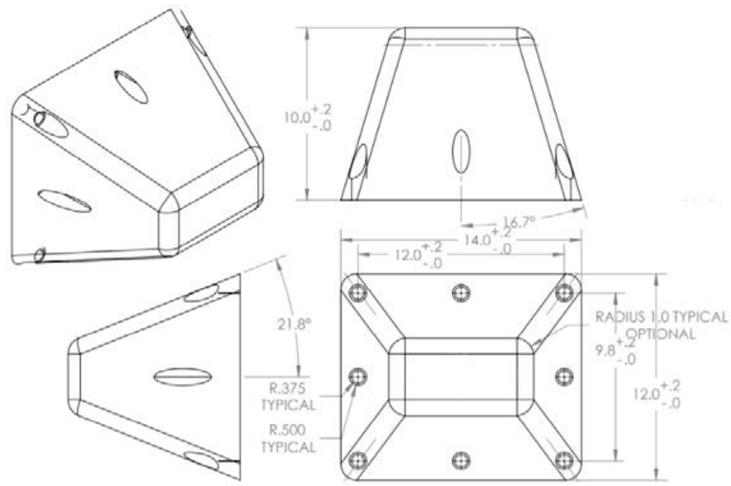

Figure 2.24 Standard FSAE impact attenuator design [1].

A 3-D model was created using the standard impact attenuator design as shown in figure 2.25. An Anti-intrusion plate is also designed as per the dimensions of the impact attenuator.

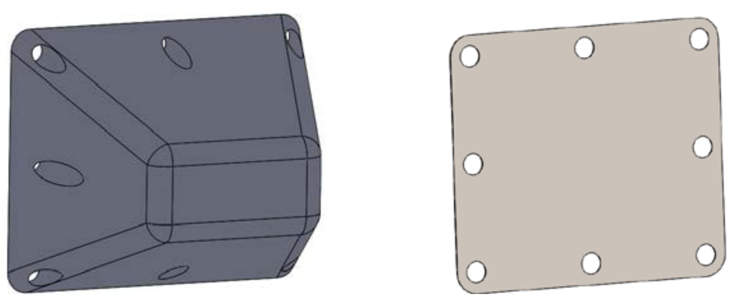
Figure 2.25 3-D models of impact attenuator and anti-intrusion plate.

3.4.3 Material selection and Testing

Once the model is created, the next objective is to select energy absorbing materials to be used in the construction. Since driver safety is one of the most important factors to be considered while designing a race car, teams have put considerable effort to learn about various impact attenuator materials. Energy absorbing foams are the most standard and basic material used by teams around the world. IMPAXX foams are one of the most commonly used materials and it is the material suggested in the standard impact attenuator design. This project will analyze the performance of IMPAXX 700, Rohacell-51WF and high-density polyurethane (PU) foams during drop tests.

Table 2.6 Material properties of selected impact absorbing foams.

Foam material	**Density (Kg/m3)**	**Poisson's ratio**	**Young's Modulus (MPa)**	**Yield Strength (MPa)**	**Reference**
IMPAXX 700	45	0	47	0.80	[15]
Rohacell-51WF	52	0	70	0.90	[16]
Polyurethane	96	0	36	0.95	[17]

Impact or crash analysis is a highly complex non-linear dynamic analysis and the analysis cost and time is considerably high. After learning about various methods adopted by the teams to test their impact attenuator designs, a very high majority depends on physical tests like drop tests or hydraulic impact tests. The analysis done using FEA are mainly limited to explicit FE codes such as LS-DYNA or ABACUS. Most efficient method to analyze time consuming problems like impact tests are done using explicit time integration methods. After searching about explicit codes available in the FEA tools already used in this project, it was found that SOLIDWORKS offers an explicit analysis module in the Drop Test simulation. A research was done on already available study reports of conducting an impact test using SOLIDWORKS Drop Test simulation module. It was found that there was barely any documented impact test analysis using SOLIDWORKS Drop Test. The main reason found by the author is that drop test is mainly intended for simulations involving dropping an object from a certain height and the object under study is the one which is dropped. But in actual physical drop test, the impact attenuator is placed on the ground and a calculated mass is dropped from a height and the object under study is the object placed on the ground. There is no option in SOLIDWORKS Drop Test for replacing the impact surface which is the ground by another object which needs to be studied. Hence the method of simulation had to be altered after learning about the physics behind a drop test. The point of study in a drop test starts once the mass starts to exert a certain force on the impact attenuator. In actual drop test, this is the point of time when the dropped mass contacts the impact attenuator. The analysis is done from this point of time till the velocity of the mass becomes zero. This event is simulated using SOLIDWORKS drop test by dropping the impact attenuator with the calculated mass attached to its back surface. At the point of contact with the ground, the mass starts to exert force on the impact attenuator and from this instance to till the velocity of mass becomes zero, the process will be exactly identical to the physical drop test and the two processes are shown in figure 2.26.

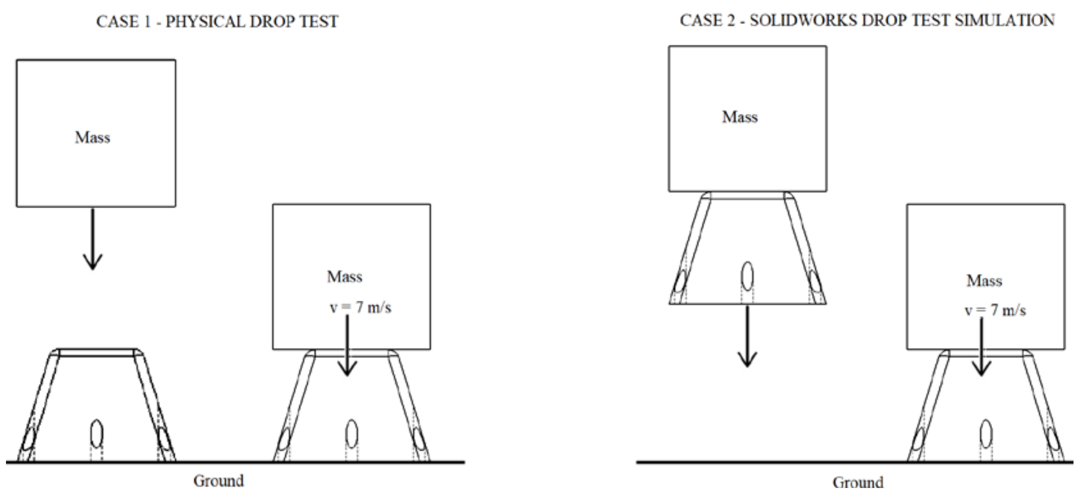

Figure 2.26 Representation of physical drop test and SOLIDWORKS drop text simulation.

In Drop Test simulation, the initial condition is given as the velocity at contact which is 7 m/s as per the rule. Also, the mass is modelled as with 300 Kg weight simulating the car weight. The time of impact will be different for different materials depending on the deceleration of the attenuator and was determined after few trial tests. The foam material should make the mass to decelerate at an average less than 20 g and peak of less than 40 g in order to use them in the competition. For measuring the transient variation of acceleration, velocity and displacement of the mass, transient sensors were created for all three cases with average values of all nodes in the mass. An overall average acceleration sensor was also created for the mass to measure the average deceleration of the mass during the entire impact time interval. The foam materials will undergo plastic deformation before failure during the impact. Hence a “Plasticity Von-mises model” was selected for the study. For drop test simulation, the material properties of none of the selected materials are available in SOLIDWORKS material database. The material details of each material were found from various reference documents since, failure of the impact attenuator is not happening before the yield points, stress-strain curves were imported to SOLIDWORKS before conducting the simulation. The stress-strain curves of the selected foams are shown in figure 2.27

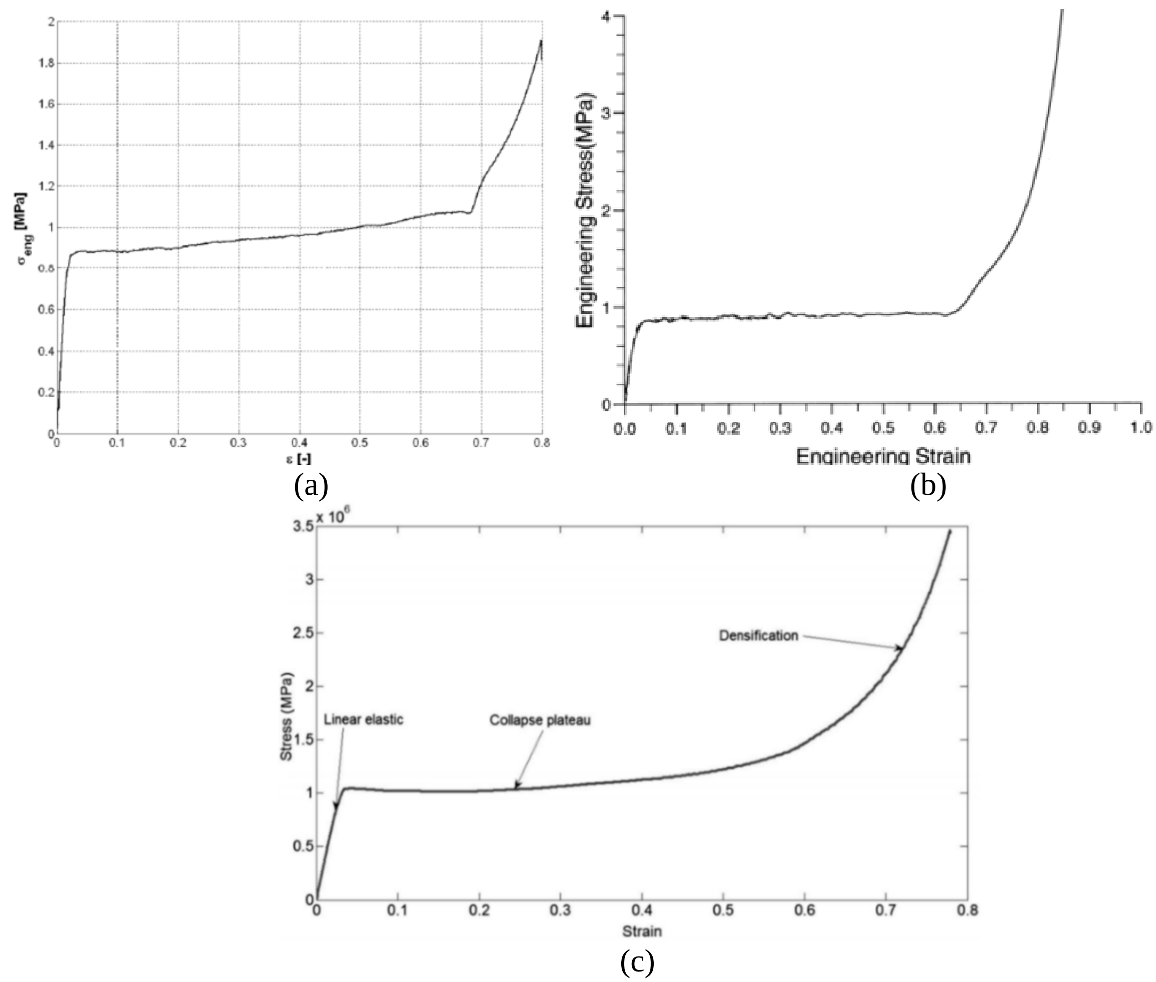

Figure 2.27 Stress -strain curves of selected foams (a) IMPAXX 700 [15]

(b) Rohacell-51WF [16] (c) High dense PU [17].

Simulation was conducted using each material to analyze the average and peak decelerations. The simulation results obtained for IMPAXX 700 foam are shown in figure 2.28 and figure 2.29

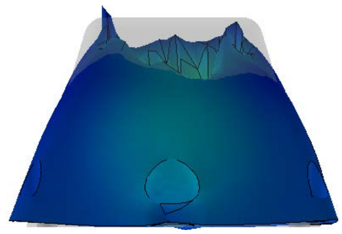

Figure 2.28 Deformation of IMPAXX 700 foam impact attenuator after drop test simulation.

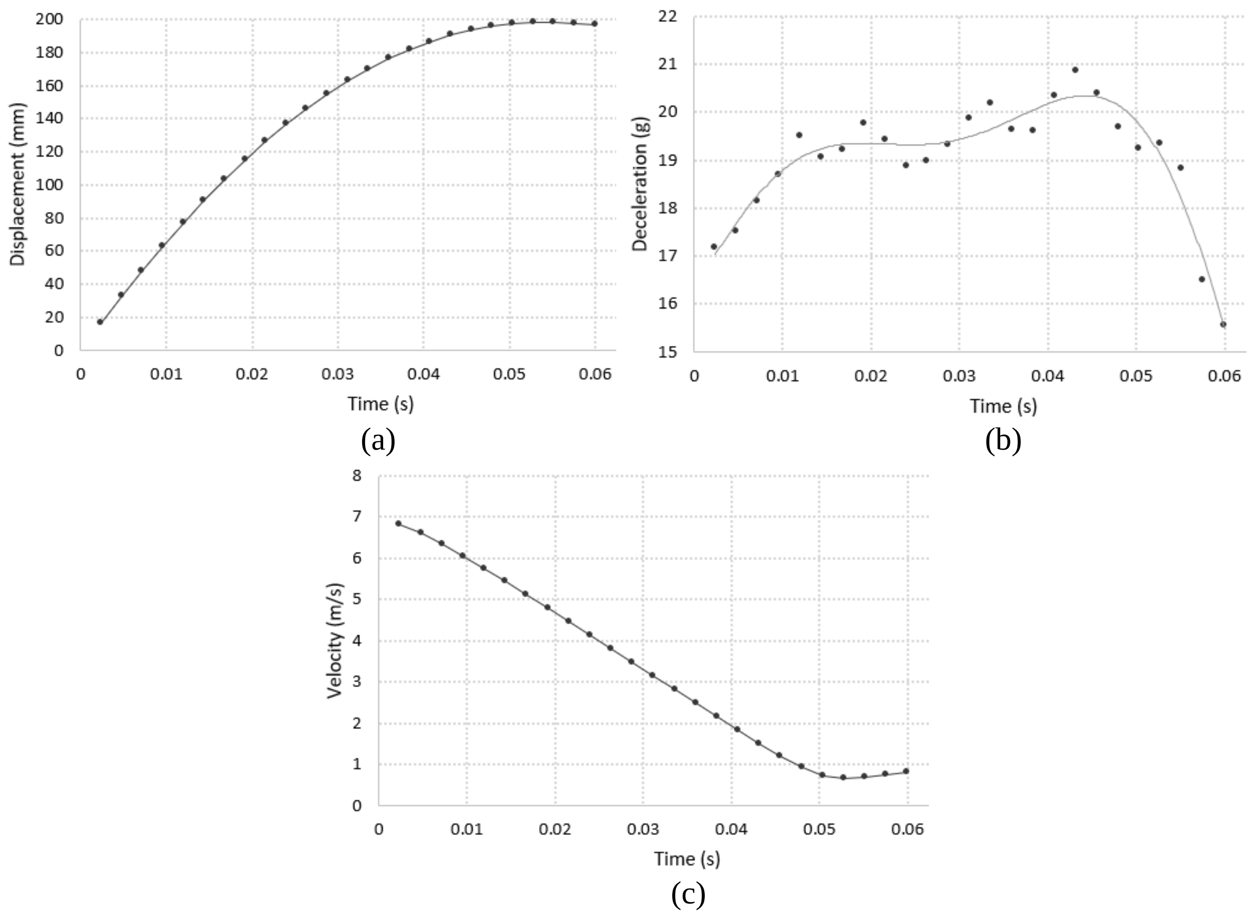

Figure 2.29 Drop Test simulation results of IMPAXX 700 foam impact attenuator (a) Resultant displacement vs Time (b) Resultant deceleration vs Time (c) Resultant velocity vs Time.

From the simulation, for impact attenuator with IMPAXX 700 foam, an average deceleration of 19 g and peak deceleration of 21 g was calculated. This satisfies both the required conditions for peak deceleration (<40 g) and maximum average deceleration (<20g).

The simulation results obtained for Rohacell-51WF foam are shown in figure 2.30 and figure 2.31

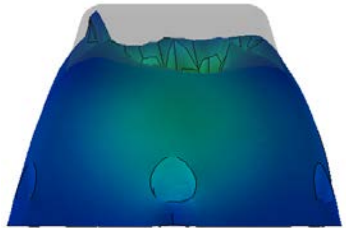

Figure 2.30 Deformation of Rohacell-51WF foam impact attenuator after drop test simulation.

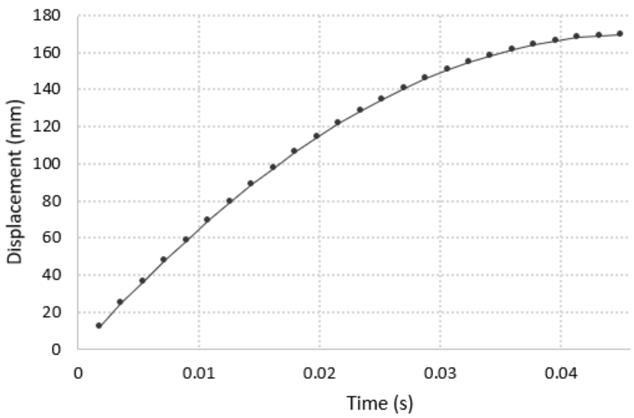

(a)

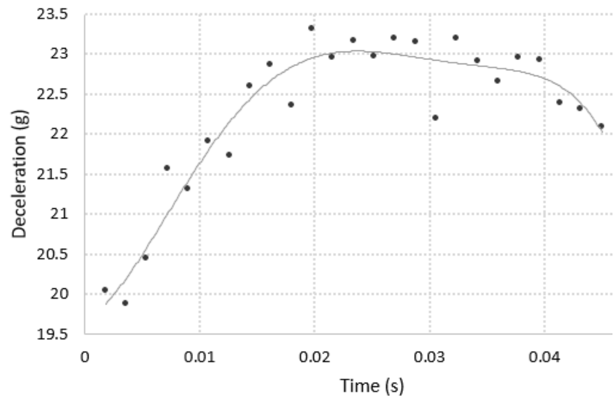

(b)

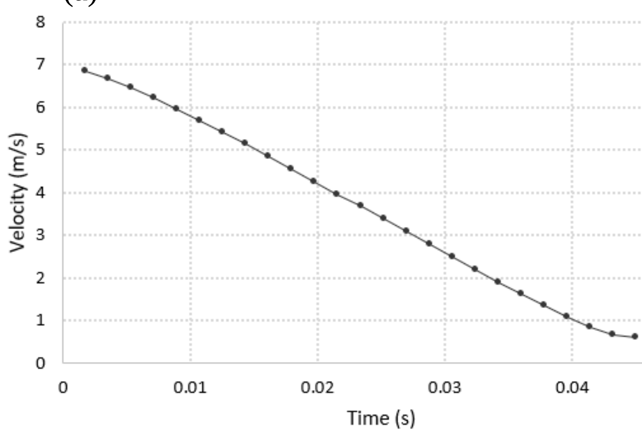

(c)

Figure 2.31 Drop Test simulation results of Rohacell-51WF foam impact attenuator (a) Resultant displacement vs Time (b) Resultant deceleration vs Time (c) Resultant velocity vs Time.

From the simulation, for impact attenuator with Rohacell-51WF foam, an average deceleration of 22.3 g and peak deceleration of 23.5 g was calculated. This satisfies the required conditions for peak deceleration (<40 g) but does not satisfy the condition for and maximum average deceleration (<20g).

The results obtained for high dense polyurethane foam are shown in figure 2.32 and figure 2.33.

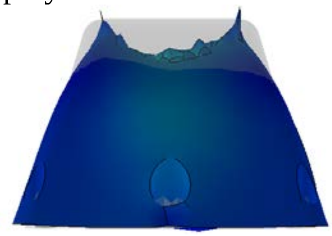

Figure 2.32 Deformation of high dense PU foam impact attenuator after drop test simulation.

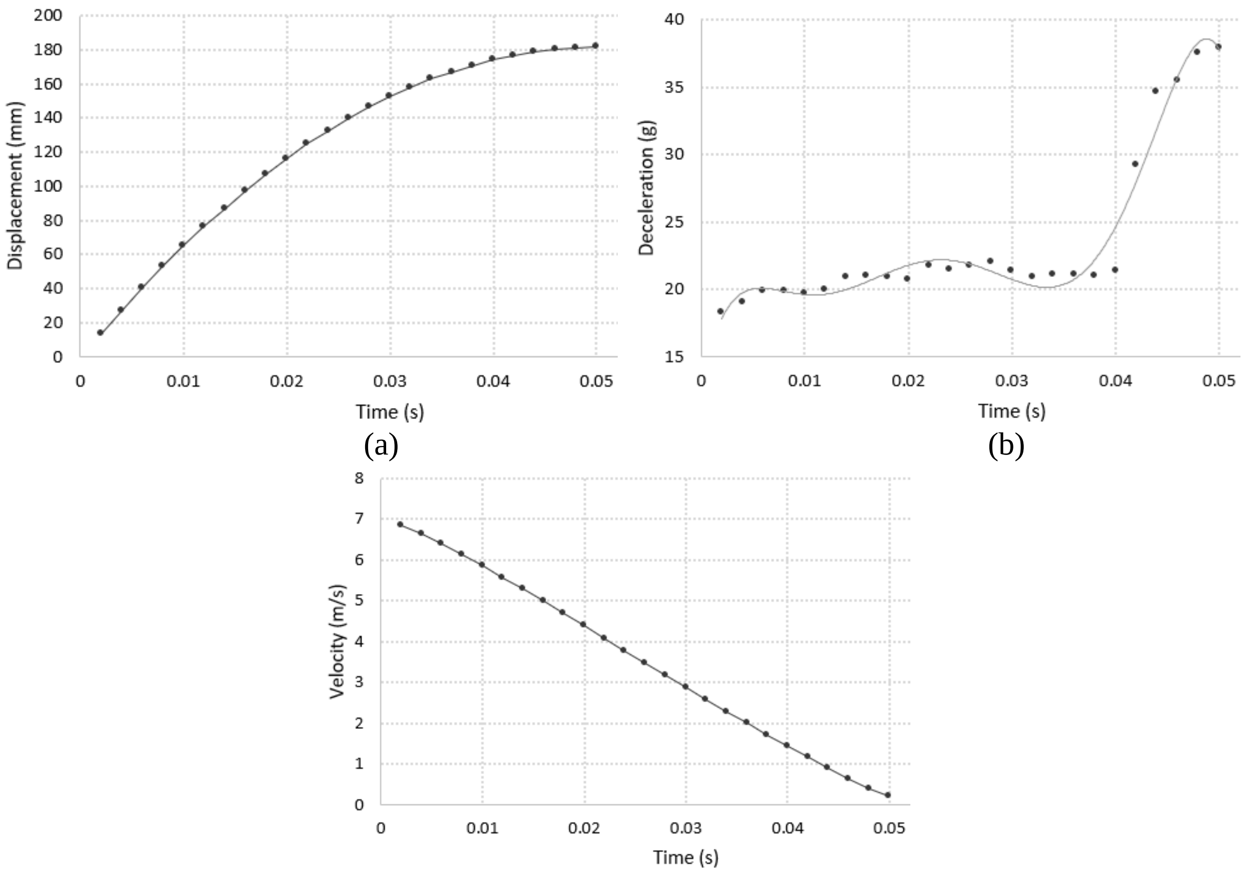

(c)

Figure 2.33 Drop Test simulation results of high dense PU foam impact attenuator (a) Resultant displacement vs Time (b) Resultant deceleration vs Time (c) Resultant velocity vs Time.

From the simulation, for impact attenuator with high dense PU foam, an average deceleration of 23.6 g and peak deceleration of 38 g was calculated. Comparing all three foams tested, even though all the foams satisfies the condition for maximum peak deceleration of 40g, only IMPAXX 700 foam was found to be satisfying the condition of maximum average deceleration of 20 g. Hence, IMPAXX 700 foam was selected as the material for impact attenuator.

3.5 Design of Aerodynamic Devices

3.5.1 Aerodynamics in FSAE

3.5.1.1 Wings and its working principle

The most commonly used and basic aerodynamic device in Formula SAE vehicles is wing. These are inverted airfoil cross sections extruded for a specific span length. Compared to the airfoil orientation of an airplane wing, race car wings are inverted. In fact, both works on the same principle, creating a vertical force when subjected to an airflow due to the pressure difference between the top and bottom surfaces. In the airfoil orientation for airplanes, it generated an upward force known as the lift force (or simply lift). Where as in race car wings, since it is inverted it generated a downward force known as negative lift or Downforce. While the purpose of wings in an airplane is to oppose its gravity forces and keep the airplane in the air while flying, downforce generated in race car wings are used to keep the tires firmly in the ground thereby generating more grip while cornering.

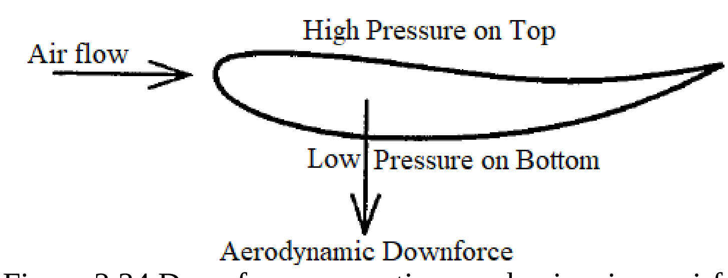

Figure 2.34 Downforce generating mechanism in an airfoil.

The downforce generating mechanism in an airfoil can be explained using Bernoulli’s equation. The simplified Bernoulli’s equation for a tube of stream lines around an airfoil can be written as,

$$p + \frac{1}{2}\rho v^2 = Constant$$

This is true for an air particle moving around an airfoil, outside its boundary layer, where the flow is predominantly nonviscous and incompressible. The density variation of air during subsonic flows in race car is negligible. Hence, whenever there is an increase in velocity, there will be a decrease in static pressure and vice versa. The air stream at inlet splits into two, one stream tube passing through the top surface and one through the bottom surface. In the above orientation of an airfoil, an air particle moving through the top surface must travel more distance due to more curvature on the top. This is in order to make sure that the amount of incoming air at inlet and the amount of air outgoing at the outlet should be equal. According to Bernoulli's equation, a reduction in air velocity at the top will result in an increase in static pressure at the top surface. Hence there exists a pressure difference between the top and bottom surface such that the pressure at the top is higher than that at the bottom. Hence, a force is acted on the airfoil due to the pressure difference along the downward direction, which will create the aerodynamic downforce.

The most important objective for race car aerodynamics is creating the downforce and the drag reduction is secondary [18]. So, the primary target would be to find the amount drag force that is acceptable in Formula SAE cars, and ensure that the drag caused is less than that value. Hence, during the wing design, it is necessary to calculate the sacrificial drag that is allowed for the vehicle and then during the CFD analysis, it should be ensured that the calculated maximum drag is less than the permissible limit.

3.5.1.2 Ground Effect

Ground effect is another phenomenon used in race cars for enhancing the available downforce. As discussed above, the top surface of the wing will be having higher pressure compared to the lower surface, which in turn generates the downforce. Amount of downforce generated is directly related to the pressure difference between the top and bottom surfaces. Downforce generated is the product of the pressure difference times the surface area upon which it is acted.

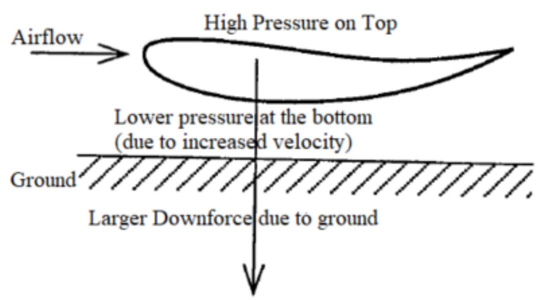

Figure 2.35 Downforce generating mechanism in an airfoil in ground effect.

When an airfoil is close to the ground, the air stream passing through the bottom surface will be having less space to travel due to the presence of the ground. This will increase the velocity of the stream in order to satisfy continuity equation, and hence further decreasing the pressure at the bottom surface as per Bernoulli's equation. Race car makes use of this phenomenon to enhance the downforce generated. The downforce generated will increase if the ground clearance is reduced to a certain point after which it will reduce the down force generated [19]. In Formula SAE, both front and side aerodynamic devices makes use of ground effects. Teams uses either an undertray or a set of side wings to make use of space available for aerodynamic devices at side. Undertrays are mainly are flat underbody device with an inlet and a diffuser. From literature reviews, undertrays are used in such competitions where rules specifically ask for flat underbody surfaces. Formula SAE rule book doesn't strictly ask for any flat underbody surfaces, hence usage of aerodynamic wings is a possibility at sides instead of undertrays, provided, it generates more downforce compared to undertrays with minimal drag.

3.5.3 Rear Wing Design

3.5.3.1 Airfoil Selection

First step in a race car wing design is identifying the best possible airfoil, that would give the required performance at the working conditions and with ease of manufacturability. Formula SAE competitions require airfoils that would generated high downforce at low velocities air stream. The average velocity expected in a Formula SAE race competition is around 11m/s or 25 mph. At the maximum expected chord length of less than 1m and at average velocity, chord Reynold's number will be less than 500,000, which is considered to be at low Reynold's number regime.

Airfoil selection is done after a thorough literature review of the performance details of various low Reynold's number airfoils. Department of Aeronautical and Astronautical Engineering at University of Illinois at Urbana-Champaign have published a five-volume report with Summary of Low-Speed Airfoil Data [20] [21] [22] [23] [24]. The book presents the results of wind-tunnel tests conducted at Princeton University on various Low-speed airfoils for model aircraft. This is one of the major references used in this document for obtaining performance data of various already existing Low-Speed Airfoils. Within the five volumes of the report, the authors have published test results of 149 Low-speed Airfoils that are used in various low-speed applications. After careful consideration of the lift coefficients of various Low-speed number airfoils, list for selection was reduced to five possible options. Maximum lift coefficients found experimentally for the selected five airfoils are shown in the table 2.7.

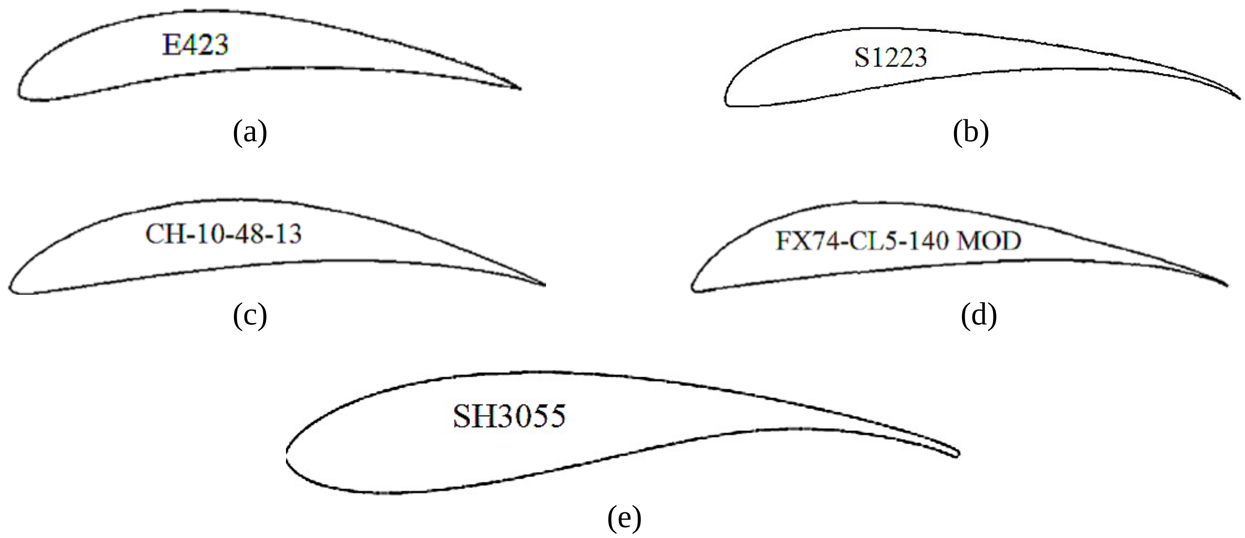

Figure 2.36 Profiles of selected airfoils (a) E423 [21] (b) S1223 [21] (c) CH-10-48-13 [20] (d) FX 74-CL5-140 MOD [20] (e) SH3055 [23].

Table 2.7 Maximum Lift coefficient of selected airfoils.

Airfoil	**C_{Lmax}**	**Re**	**Reference**
SH3055	1.91	2×10^5	[23]
CH-10-48-13	1.95	2×10^5	[20]
FX 74-CL5-140 MOD	2.00	2×10^5	[20]
E423	2.00	2×10^5	[21]
S1223	2.11	2×10^5	[20]

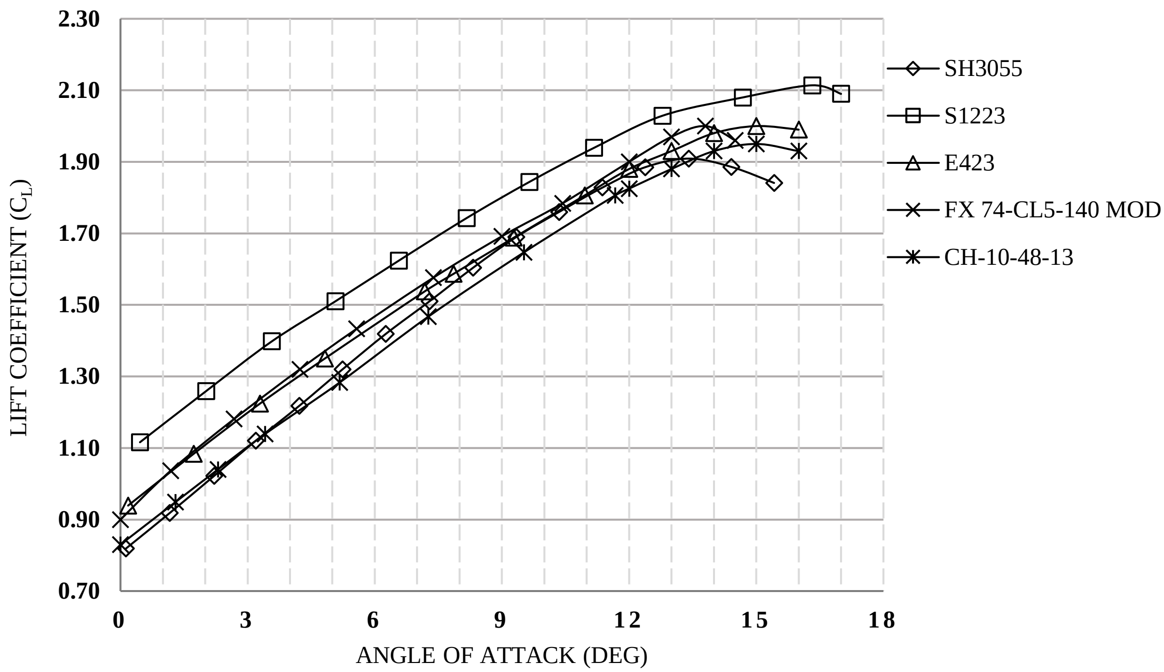

Figure 2.37 Comparison of C_L vs AOA for the selected airfoils.

Comparing the test results of the five airfoils selected, it is clear that S1223 is expected to generate maximum lift with similar working conditions compared to other airfoils. At a Reynolds number of around 2 x 10^5, the maximum lift coefficient is 2.11 at an angle of attack of approximately 16^0. The second most efficient airfoils are E423 and FX 74-CL5-140 MOD, both generating a lift coefficient of approximately 2.00 at angle of attacks 15^0 and 14^0 respectively. Other two airfoils generate lesser lift compared to these three. Hence S1223 would have been an obvious choice considering the lift coefficient numbers. But from the description of S1223 airfoil, it is specifically mentioned about it is very thin around its trailing edge. This is same with the case of FX 74-CL5-140 MOD too. These airfoils would be very difficult to manufacture with required accuracy considering the facilities available for a first-year team. Hence, the author has decided to use the Eppler E423 airfoil considering the reduced amount of aft camber and higher trailing edge thickness, which would make it easily manufacturable compared to the other considered airfoils.

3.5.3.2 Space Constraints

The size of the rear wing is mainly determined by the rules regarding the allowable space constraints in the rear end. The rules for rear mounted device states that the any part of the aerodynamic device should be within a distance of 250 mm from the rear point of the rear tires. The maximum height to which a rear wing can be mounted is also decided by the rule stating that and the top most point of any rear mounted device should not be higher than 1.2 m from the ground. The span of the rear wing should also lie between two vertical planes drawn from the inside of the inside of rear tires measured from the center of the wheel hub. Also, the front of the rear wing should not be further forward than the driven head restraint support. An allowable space to work with when developing a rear mounted device can be found out considering the above stated rules. Once thing to be noted here is that it won't be able to find the exact space constraints just by using the given rules if the position of wheels and design of the chassis is complete. This is the reason why the aerodynamic system's design for an FSAE vehicle is done after the chassis and suspension geometry design. Using these data, the available space for mounting rear wing can be found out and is shown in figure 2.38. The wing should fit inside an 800 mm x 600 mm rectangular space.

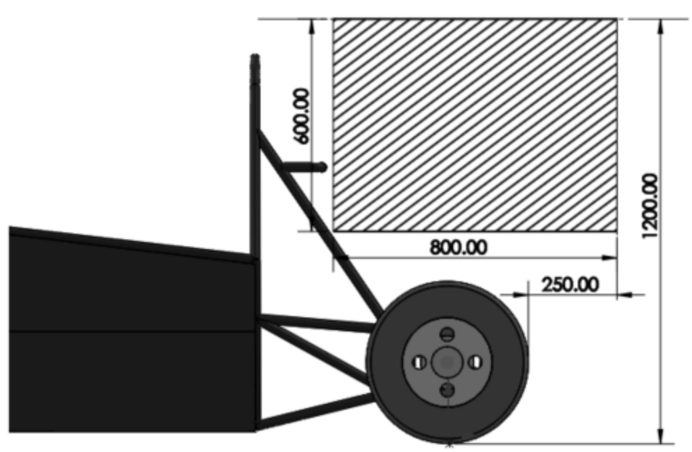

Figure 2.38 Space availability for rear mounted aerodynamic device.

3.5.3.3 CFD Model validation

Once the airfoil is selected and the space constraints is known, next step is to design the best wing configuration using the selected airfoil. Computational Fluid Dynamics (CFD) can be a great tool in the preliminary aerodynamics system design for a race car before a wind tunnel model developed [2]. CFD study using ANSYS Fluent module is used as a tool to analyze the lift and drag performance of different airfoil configurations. The ultimate aim of the study is to develop the best configuration of the airfoils to achieve the target performances. The studies have been limited to simplified 2-D profile configurations with the main aim to develop a configuration that meets the target lift performance identified from reference papers. The main input used from the CFD analysis for the overall car design in this project is the maximum theoretical downforce generated by the wings and ground devices. These force values along with other loads and weight transfers, is used to design the suspension components for the worse case loading. 3-D CFD studies will provide additional losses in lift due to the presence of components at proximity and other losses. Still, even a very well defined 3-D analysis cannot guarantee accurate results and the best ways to obtain accurate results are Wind Tunnel and on-track testing. A full 3-D CFD study can be performed in the future to find the reduced downforce values to fine tune the overall balance and suspension components to generate maximum lateral force. Hence, this project will rely on 2-D analysis to obtain the best airfoil configuration with the theoretical maximum downforce values. Fine tuning can be done for the overall balance of the car using on-track testing results which is more accurate than 3-D analysis. The first step in the CFD analysis is the CFD model validation. Since CFD, unlike structural analysis (FEA), can be very challenging due to the dynamic and difficult to predict behavior of fluid motions. Hence validation of the CFD model selected is very important. Model Validation was done against the results of wind tunnel testing conducted on E423 airfoil at Princeton University [21]. Test was conducted with airfoils of around 0.3 m chord length, at various Reynolds numbers. Average vehicle speed seen in FSAE competition is around 10-15 m/s. Hence, the lift values of wind tunnel results with chord Reynolds number of 300,000 was selected for validation. Combination of chord length 0.32 m and 14 m/s was selected which gives a chord Reynolds number just above 300,000. The airfoil was tested using different CFD models available in ANSYS Fluent to compare the numerical results to the experimental results obtained from the reference. Analysis was done with angle of attack varying from 0^0 to 16^0 and percentage deviation of the numerical results and the experimental results was analyzed. The first turbulence model used for the analysis was a standard two equation k-ε model. Two equation models are computationally simpler and usually produces acceptable results. Even though the model was able to predict the lift values with acceptable accuracy at low angles of attack, but it was found ineffective to predict performance at higher angles. The same phenomenon was identified with another two equation model, called k-ω model available in Fluent. The further research was focused on three equation model available in Fluent which is Transition k-kl-ω. Three equation model is computationally more demanding and is difficult to achieve convergence unless having a good quality mesh. Still this model predicted the performance of the airfoils with acceptable accuracy both at lower and higher angle of attacks. This can be understood by the theory behind low Reynolds number airfoils at low turbulence intensity, which is similar to the case seen in FSAE conditions. The low Reynolds number aerodynamics at angle of attack near the stall region is predominantly governed by the laminar boundary layer and transition to turbulent flow. Airfoils working in a range of Reynolds number from 100,000 to 500,000 is affected by a phenomenon called laminar separation bubbles [25]. A Transition k-kl-ω model is capable of effectively addressing the laminar to turbulent transition phenomenon and is found to produce best results for low Reynolds number low turbulent intensity scenarios [26]. It required a very refined mesh with parameters as shown in table 2.8 to achieve convergence of the results with a Transition k-kl-ω model. A comparison of results obtained from the numerical analysis and the experimental results from the reference paper is presented using table 2.9

Table 2.8 Mesh parameters used for CFD model validation.

Mesh Type		Unstructured- linear triangular elements
Max face Size		0.30 m
Face Sizing	Geometry	Fluid domain
	Type	Element Size
	Element Size	2×10^{-3} m
	Size Function	Uniform
	Behavior	Hard
Edge sizing 1	Geometry	Airfoil edges
	Type	Element Size
	Element Size	1×10^{-3} m
	Size Function	Uniform
	Behavior	Hard
Edge Sizing 2	Geometry	Airfoil edges
	Type	Sphere of Influence
	Sphere radius	0.5 m
	Element Size	7×10^{-3} m

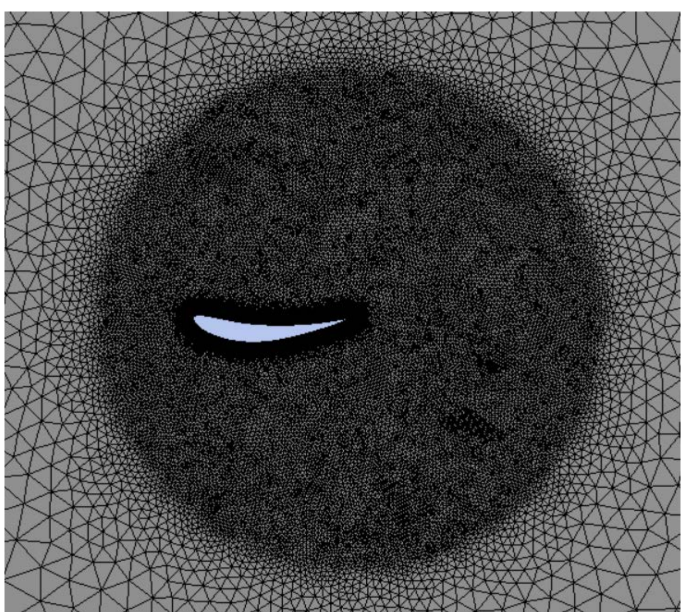

Figure 2.39 Mesh used for CFD model validation.

Table 2.9 Comparison of lift coefficients results from numerical analysis and reference.

AOA (Deg)	C_L (Reference)	C_L (Numerical)	% Deviation
0	0.95	1.00	-5.3
2	1.1	1.22	-10.9
4	1.3	1.44	-10.8
6	1.45	1.59	-9.7
8	1.60	1.70	-6.2
10	1.8	1.81	-0.6
12	1.9	1.84	3.2
13	1.95	1.85	5.1
14	1.92	1.81	5.7
15	1.91	1.81	5.2
16	1.90	1.80	5.3

Velocity profiles of the model validation study for different angle of attacks are shown in figure 2.40 and pressure profiles are shown in figure 2.41

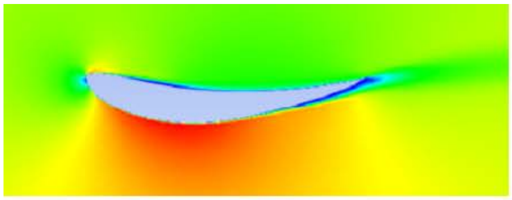

AOA – 0^0

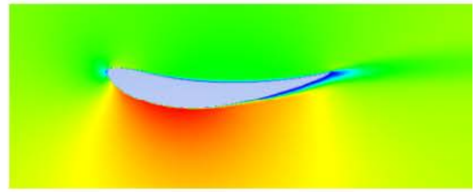

AOA – 2^0

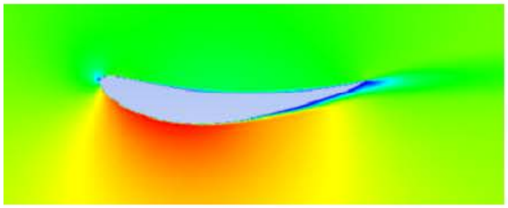

AOA – 4^0

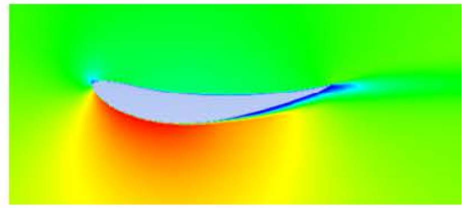

AOA – 6^0

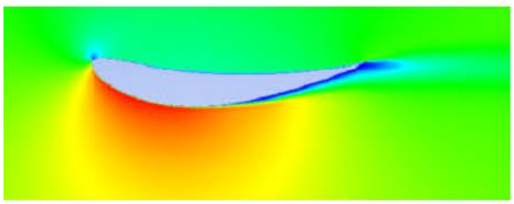

AOA – 8^0

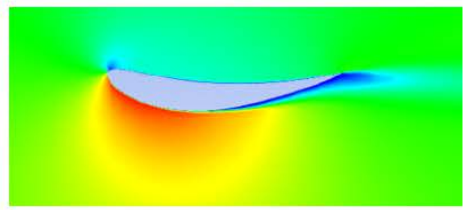

AOA – 10^0

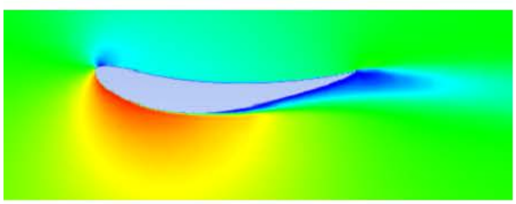

AOA – 12^0

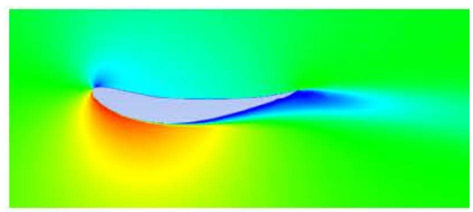

AOA – 13^0

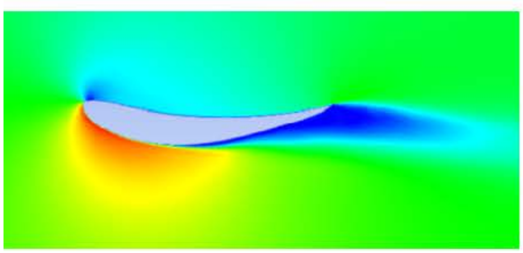

AOA – 14^0

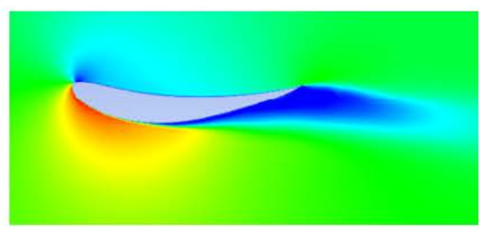

AOA – 15^0

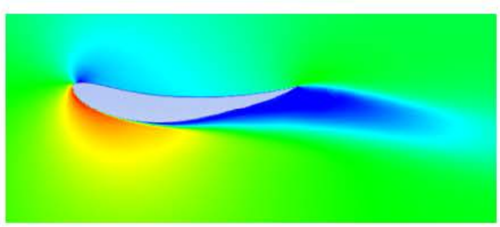

AOA – 16^0

Figure 2.40 Velocity plots of E423 airfoil at AOA from 0^0 to 16^0.

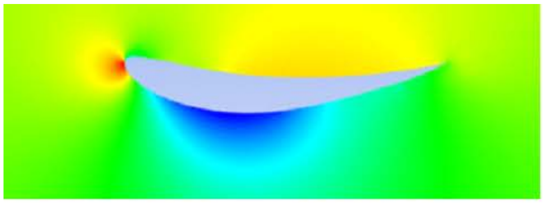

AOA – 0^0

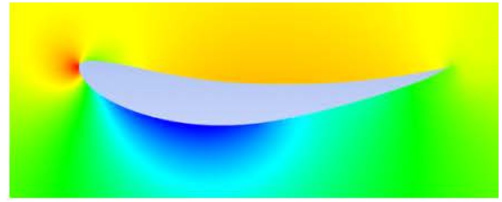

AOA – 2^0

AOA – 4^0

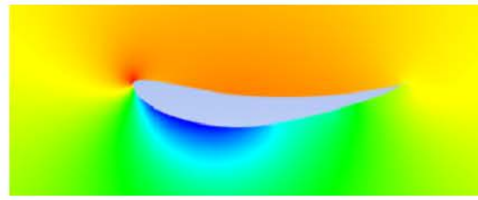

AOA – 6^0

AOA – 8^0

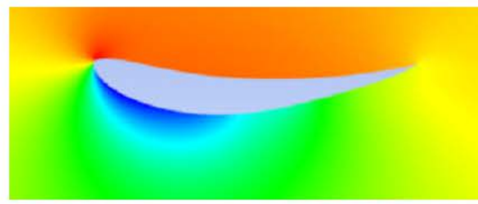

AOA – 10^0

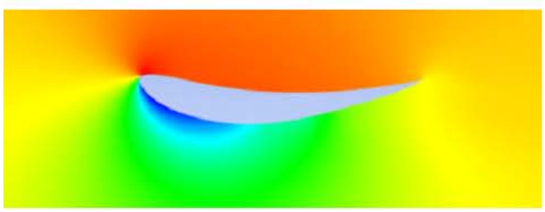

AOA – 12^0

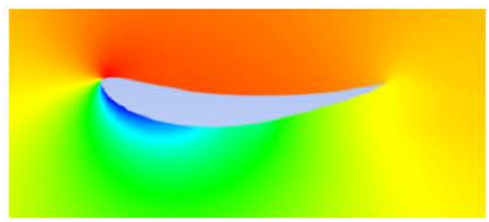

AOA – 13^0

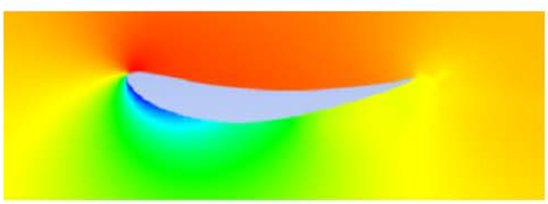

AOA – 14^0

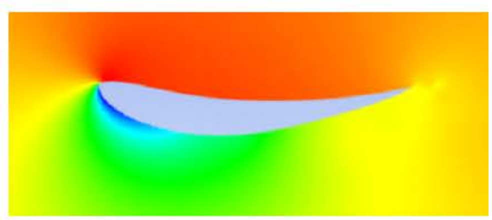

AOA – 15^0

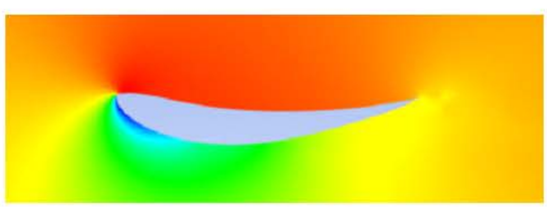

AOA – 16^0

Figure 2.41 Pressure plots of E423 airfoil at AOA from 0^0 to 16^0.

3.5.3.4 Rear Wing Configurations and Testing

Once the CFD model is validated, analysis can be done to find the best airfoil configuration possible to achieve target lift coefficient with a drag value less the permissible limits. Hence a target lift and permissible drag values should be identified. Target lift values are identified from literature reviews. A lift coefficient target of 4.0 at a speed of 40 km/hr or 11 m/s identified by Monash university is decided to be target lift coefficient for this project [27]. The process used to find the drag value according to the vehicle conditions is done as per McBeath [28]. The first step in this process is to identify the sacrificial brake engine power that can be used to overcome the vehicle drag. This can be found as shown below which assumes that the aerodynamic drag forces consume the maximum brake engine power.

$$Brake\ power\ absorbed\ in\ kW = \frac{C_D \times A \times v^3}{1{,}633}$$

C_D is the drag coefficient of the car without wings, which is considered as 0.83 which is the value corresponding to 2003 Monash FSAE car [27]. Also, the brake engine power of the selected Honda CBR600RR engine is 78 kW. Frontal area of a single seater car without wings for the same Monash 2003 car is around 0.9 m^2. Solving the equation using these values will yield the maximum velocity the car can achieve as approximately 55.5 m/s or 200 km/h when the engine with 78 kW brake engine power is affected with a drag coefficient of 0.83. This is higher than the usual top speed achieved by FSAE cars which is around 30 m/s. So, calculating the power required to overcome the drag produced by the base car at 30 m/s,

$$kW\ required\ to\ overcome\ drag\ at\ 30\,m/s = \frac{0.83 \times 0.9 \times 30^3}{1{,}633} = 13\ kW$$

This means that the remaining 65 kW of brake horse power is available for the drag induced by incorporating additional wings. Using this value, the maximum drag coefficient possible for the wing can be calculated using the same equation. Also it is reported that the drag in a single seater car is predominantly affected by rear wing and the other devices contributes very little to it [28]. This assumption is validated using wind tunnel testing by Monash FSAE team[27]. Hence while calculating the drag coefficient, the maximum allowable plan area is calculated according to the rear wing geometry. From the allowable space for rear wing from figure 2.38, a maximum chord length of the final wing configuration is assumed to be 0.9 m (little less than the diagonal of the rectangle demonstrating the available space). Also, since the rules mandates that the wing should fit inside two vertical planes drawn from inside of the rear wheels, a maximum span length is approximately 1 m. This gives the frontal area 0.9 m^2.

Solving equation for maximum allowable drag coefficient,

$$C_D = \frac{Available\ kW\ \times 1{,}633}{A \times v^3}$$

$$= \frac{65\ \times 1{,}633}{0.9 \times 30^3} = 4.4$$

This is indeed a very high value for expected drag coefficient and hence the drag is not expected to play a big role in a FSAE car. Hence drag reduction is not considered as a primary objective in this work. Now, from the CFD model validation, the maximum lift coefficient value achieved before stall is 1.85 at an angle of 13^0 and the target value is greater than 4.0. Hence multi-element configuration should be used where an arrangement of more than one airfoil is used. Since the validation is done based on a velocity of 14 m/s, the same is used for the analysis of multi-element configuration to learn and compare the variation in lift values with different configurations.

The concept used for the analysis of multi element configuration is the same as that for the single element analysis. As the angle of attack increases, the lift value also increases till stall point and then decreases. Hence in the first multi-element configuration with two wings, the main wing is set at 13^0, which is the stall angle for the first airfoil, and the angle of the second wing will be increased in different steps to find the stall angle for the second airfoil. Further that point, lift will start to decrease. Now when a third or subsequent element is used, the previous airfoil will be kept at its stall angle and the angle of the newly added airfoil is gradually increased. This method is followed throughout this design even for other wings. The results of the 2- element configuration is shown in table 2.10. The velocity profiles are shown in figure 2.42 pressure profiles in figure 2.43.

Table 2.10 Lift coefficients obtained for two element rear wing configuration.

AOA (Deg)	**C_L**
23.31	3.2
23.74	3.25
24.79	3.39
25.20	3.19

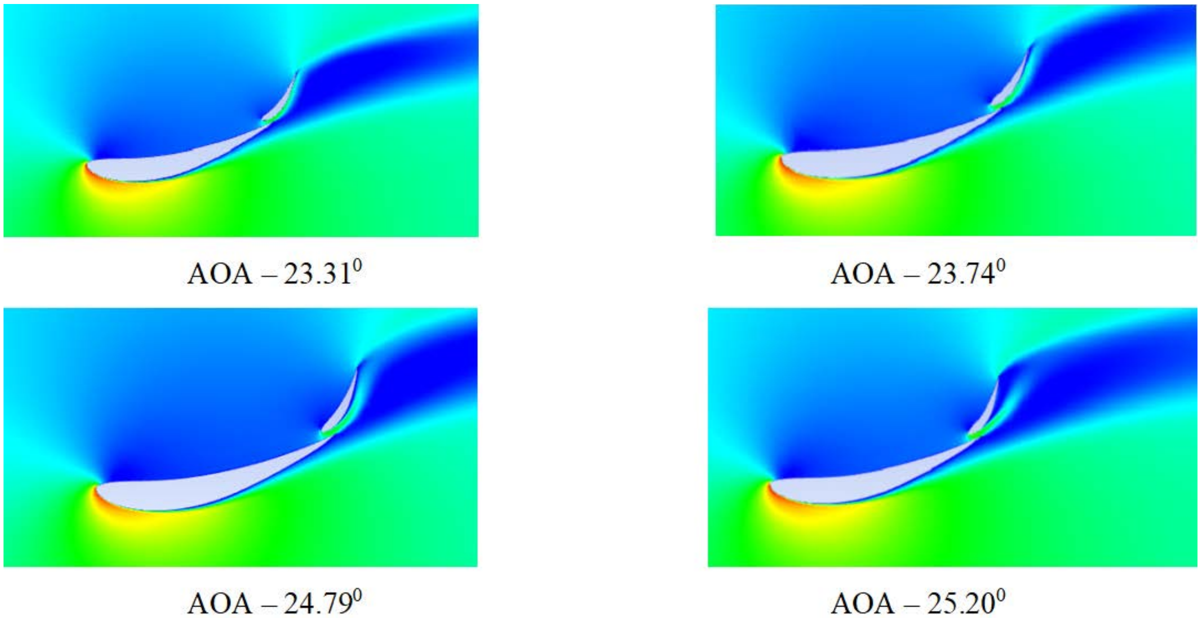

Figure 2.42 Velocity plots of 2 element configuration at AOA from 23.31^0 to 25.20^0.

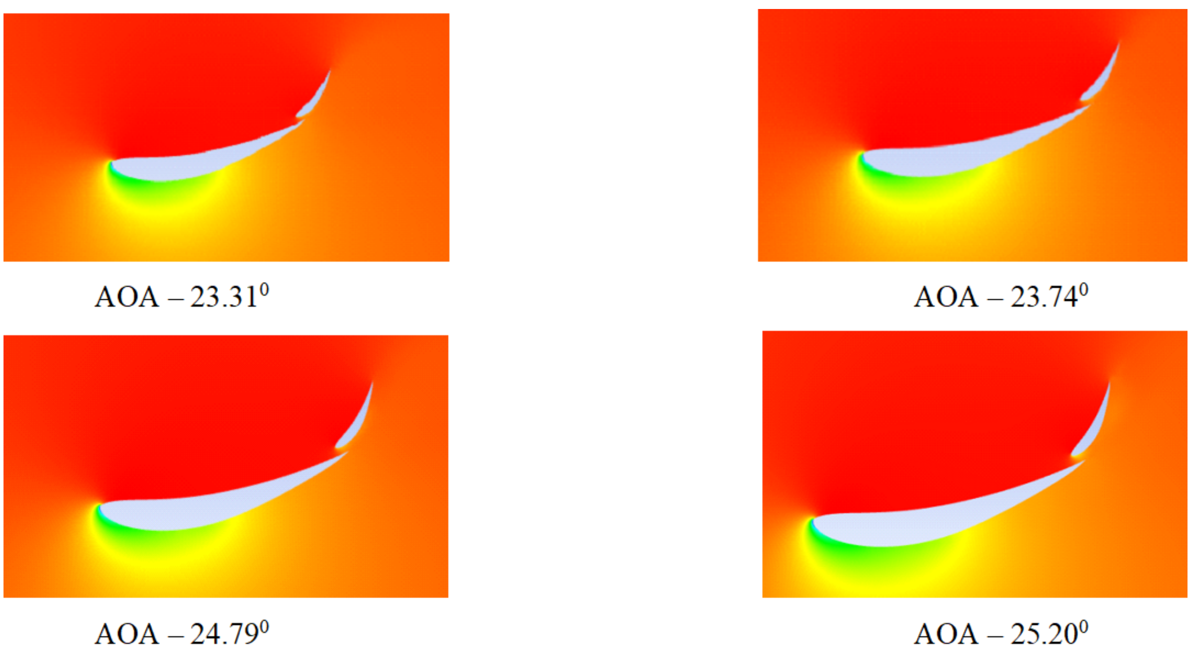

Figure 2.43 Pressure plots of 2 element configuration at AOA from 23.31^0 to 25.20^0.

The maximum lift coefficient achieved is 3.39 at an angle of attack of 24.79^0. This means that more elements should be added to the configuration to achieve lift coefficient above 4.0.

But before adding the third airfoil it was decided to alter the current confiuration to obtain better results. As can be seen from the velocity profile of the study with 2 elements, it can be seen that there is some considerable amount of boundary layer separation at the end, which causes negative pressure at the bottom and of the airfoils. Hence the possiblity of a slotted design as shown in figure 2.44 was explored which could bypass some air from the top surface to the bottom surface.

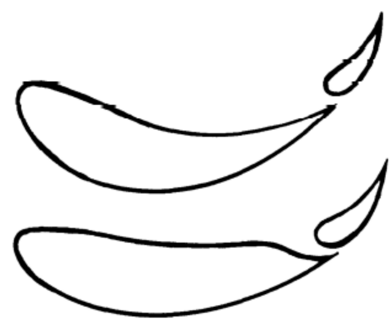

Figure 2.44 Slotted design for multi element airfoil configuration [29].

This could reenergize the flow at the bottom surface of the airfoils which could reduce the negetive pressure developed at the bottom surface. Hence it is expected to generate more lift since it would be able to push the angle of attack to a higher value. Also, it was found easier of obtain solution convergence when a slotted design was used since it highly reduced the flow irregularities. The results obtained are shown in table 2.11. The corresponding velocity plots are shown in figure 2.45, and the pressure plots are shown in figure 2.46.

Table 2.11 Lift coefficients obtained for slotted two element rear wing configuration.

AOA (Deg)	**C_L**
27.76	3.05
28.19	3.48
28.40	3.53
28.61	3.49

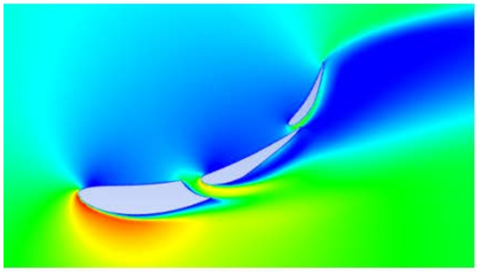

AOA – 27.76^0

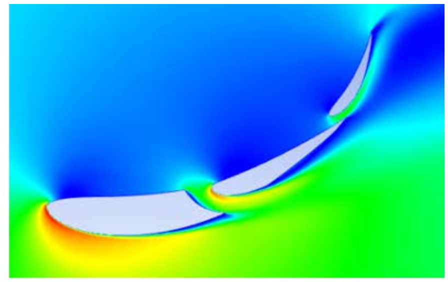

AOA – 28.19^0

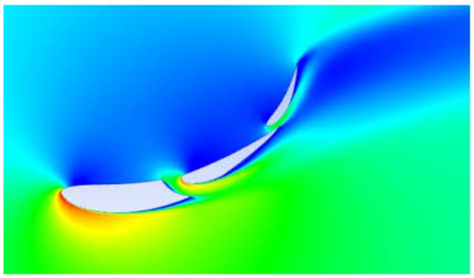

AOA – 28.40^0

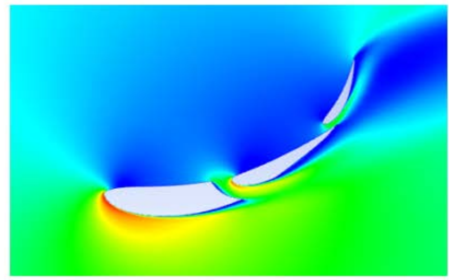

AOA – 28.61^0

Figure 2.45 Velocity plots of slotted 2 element configuration at AOA from 27.76^0 to 28.61^0.

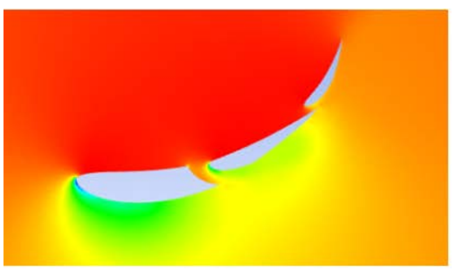

AOA – 27.76^0

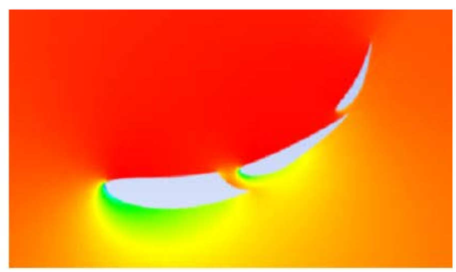

AOA – 28.19^0

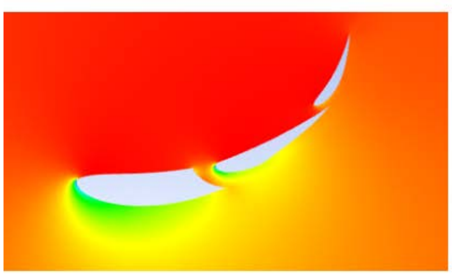

AOA – 28.40^0

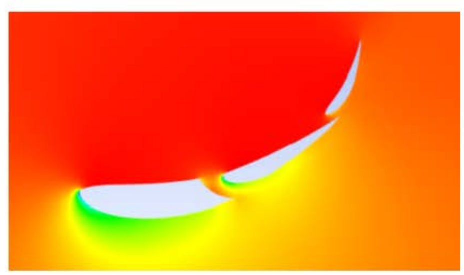

AOA – 28.61^0

Figure 2.46 Pressure plots of slotted 2 element configuration at AOA from 27.76^0 to 28.61^0.

Hence, by using a slotted design, the maximum lift coefficient was increased from 3.39 to 3.53 and the stall angle was pushed higher from 24.79^0 to 28.40^0. Hence the slotted design was found helpful in delaying stall and thereby increasing the lift coefficient. Now since, the lift value achieved is still not above the target value, the next airfoil was added. The results obtained are shown in table 2.12. The corresponding velocity plots are shown in figure 2.47, and the pressure plots are shown in figure 2.48.

Table 2.12 Lift coefficients obtained for slotted three element rear wing configuration.

AOA (Deg)	**C_L**
32.47	3.95
32.54	3.94
32.60	4.19
32.73	4.13
32.86	4.13
33.17	4.05

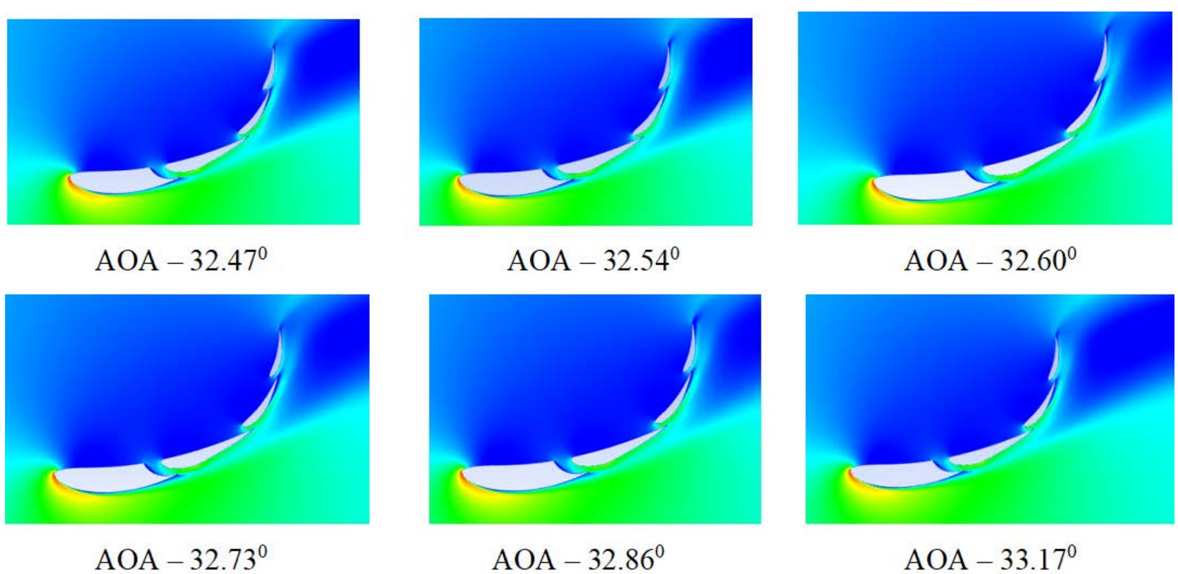

Figure 2.47 Velocity plots of slotted 3 element configuration at AOA from 32.47^0 to 33.17^0.

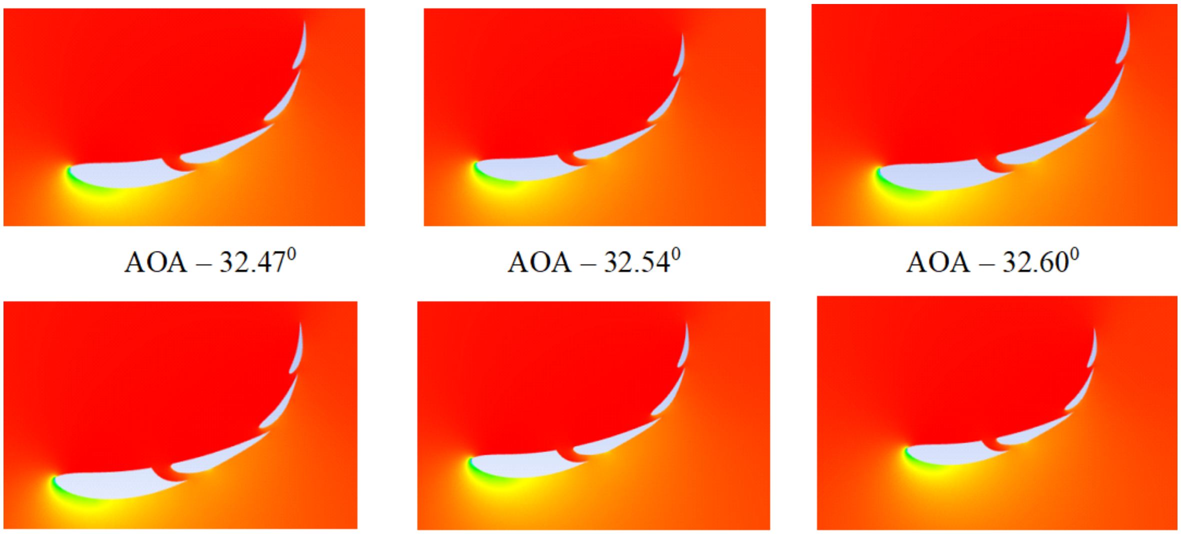

AOA – 32.47^0 AOA – 32.54^0 AOA – 32.60^0

AOA – 32.73^0 AOA – 32.86^0 AOA – 33.17^0

Figure 2.48 Pressure plots of slotted 3 element configuration at AOA from 32.47^0 to 33.17^0.

The results obtained here is for a velocity of 14 m/s. Typical skid pad speed at FSAE is around 11 m/s [4]. Also, the target lift coefficient of 4.0 should be calculated at a velocity of 11 m/s. Hence the analysis of the final configuration is done at 11 m/s to find the lift coefficient. At 11 m/s, the selected multi element geometry has a lift of 4.09 at a chord length of about 0.65 m. Comparing this value to the initial target of lift coefficient over 4.0 at 11 m/s and 0.65 m chord, it achieved the target and the geometry is finalized for the maximum lift arrangement. From the available space limits, the selected arrangement was scaled to obtain the maximum chord length permissible within the available space constraints and it was found to be 0.9 m. Hence the final multi element arrangement was scaled to be having 0.9 m chord length.

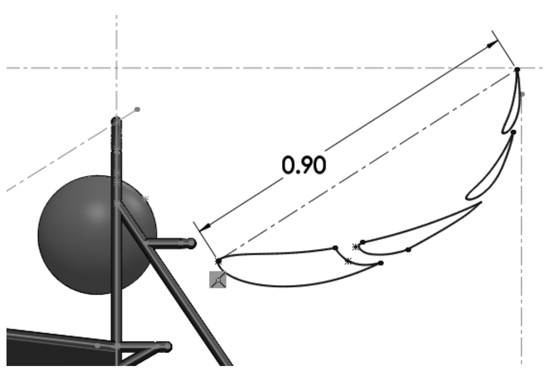

Figure 2.49 Maximum chord length possible in available space for rear wing.

Competition rules limits the span of the wing to be within the inside of the rear tires and hence the maximum allowable span is 1 m. Corresponding lift and drag values are found out and are shown in table 2.13. The analysis was also done at the maximum speed of 30 m/s found in FSAE competitions. This was used to find the theoretical maximum downforce created at maximum speed and this is taken as a reference to do the structural analysis of the wings. Usually, there speeds are achieved at acceleration events where the wings will be adjusted to produce no downforce to avoid the drag penalty. Hence in normal cases these higher downforces won't be generated at all.

Table 2.13 Rear wing aerodynamic performance at 11 m/s and 30 m/s.

	Rear Wing at 11 m/s	**Rear Wing at 30 m/s**
C_L	4.61	3.77
ρ (kg/m^3)	1.225	1.225
A (m^2)	0.90	0.90
Downforce (N)	307.5	1350.8
C_D	0.43	0.47
Drag (N)	28.7	168.4

3.5.4 Side/Underbody Aerodynamic Devices Design

3.5.4.1 Space Constraints

Considering the vehicle is equipped with a rear and front wing, the further available space for mounting an aerodynamic device is between the front and rear wheels. Rules state that any aerodynamic device mounted between front and rear wheels should not span out of vertical plains drawn through lines connecting outer surface of front and rear tires at both sides. This leaves the available space to mount a device both at below the vehicle body and at both sides of the car. Also, the height of the maximum point in any aerodynamic device mounted between the wheels should be less than 500 mm. The side view of maximum available space (in mm) is shown in figure 2.50.

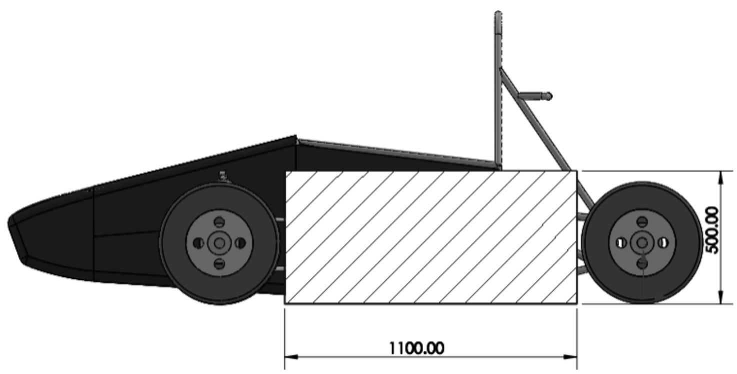

Figure 2.50 Space availability for side/underbody aerodynamic device.

3.5.4.3 Side/Underbody Devices Configurations and Testing

Two most common types of aerodynamic devices used between the wheels in FSAE competitions are undertray with diffusers and side wings.

(a) © University of Michigan

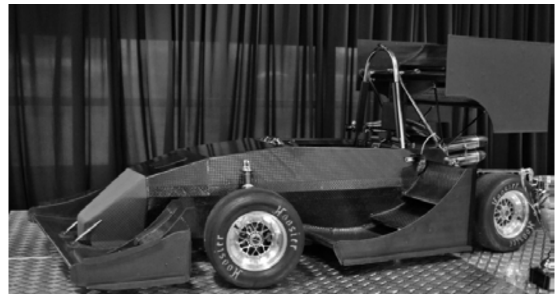

(b) © Oregon University

Figure 2.51 Side/Underbody Device in FSAE (a) Undertray diffuser (b) Side wings.

Undertrays used in race cars have an inlet section where the air is entered, a throat section where the air velocity increases due to the decreased cross section area and a diffuser where the air velocity id gradually decreased and exited. The increased velocity in the throat section decreases the pressure of the air stream and the decreased velocity in the diffuser section increases the air pressure gradually and is exited through the diffuser outlet with atmospheric pressure. The pressure difference between the top and bottom of the undertray generates the downforce. The downforce generated is closely related to the height between the ground and the bottom of undertray. When this height decreases, the downforce increases until a certain height after which the downforce starts to decrease, which is usually (ground clearance : undertray length) ratio of 0.01 – 0.05 [30].

Side wings are similar to the rear wings, but it will have enhanced lift values due to the proximity to the ground as explained in section 3.5.1.2. Similar to undertrays, wings with ground proximity will also have increased lift till a certain ground clearance and then will start to decrease. A comparison study was done on a 2-D undertray model with various configurations and with side wings to find which one performs the better in FSAE conditions. It is assumed that a 2-D analysis of both undertray and side wings will provide the maximum possible downforce values neglecting 3-D losses.

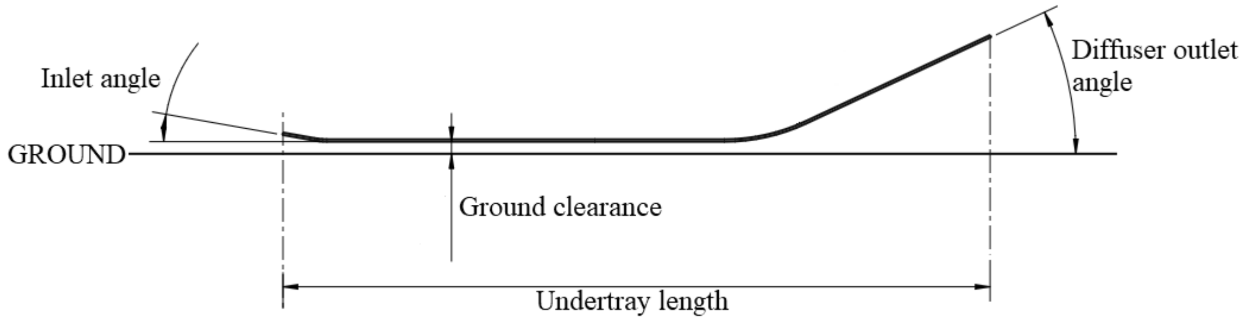

Figure 2.52 Undertray 2-D model used for finding maximum downforce configuration.

The undertray geometry shown in figure 2.52 is used to analyze different undertray configurations. Studies were conducted by varying the diffuser outlet angle and locations. Studies were conducted separately for the undertray portion coming under the car body and that coming on the sides. Undertray length at the side were decided by rule stated for devices between the wheels as shown in figure 2.50. The undertray length of section at the bottom of the car is decided by the rule for rear mounted device as shown in figure 2.38 since the diffuser end will locate near the rear end of the car. Lift coefficients were calculated separately for the bottom and side sections for all the configurations. Once the maximum lift values were found out, study was conducted with ground clearance varying from ground clearance to length ratio of 0.01 – 0.05. The result obtained for both bottom and side sections were combined to get the total downforce result and are shown in table 2.14. The 3-D model of the undertray which generated maximum possible downforce is shown in figure 2.53.

Table 2.14 Undertray aerodynamic performance at 11 m/s.

	Side sections	**Bottom Section**
C_L	1.89	0.44
ρ (Kg/m³)	1.225	1.225
A (m²)	0.78	1.425
v (m/s)	11	11
Downforce (N)	109.3	46.5
Total Downforce (N)	155.7	
C_D	0.241	0.06
Drag (N)	13.9	6.3
Total Drag (N)	20.3	

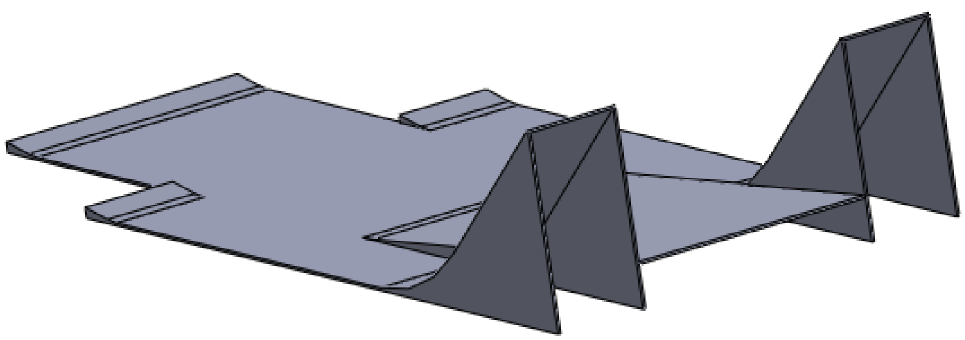

Figure 2.53 3-D model of undertray configuration with maximum possible downforce.

Once the maximum possible downforce values of the undertray configuration obtained, the best possible side wing configuration is designed. The wing configuration for the rear wing is taken as the starting point for simplicity. The size the wing is governed by the space constraints as shown in figure 2.50. But the available wing configuration should be altered further to achieve maximum lift since many researches has shown that the stall angle will decrease when an airfoil is subjected to ground effect [31]. Hence it is expected to have higher lift values at little lower Angle of Attack compared to the rear wing arrangement. The results obtained are shown in table 2.15. Velocity plots are shown in figure 2.54 and pressure plots are shown in figure 2.55.

Table 2.15 Lift coefficients obtained for side wing configuration.

AOA (Deg)	C_L
32.60	8.31
30.60	8.19
27.95	10.04
27.33	10.71
26.68	10.19

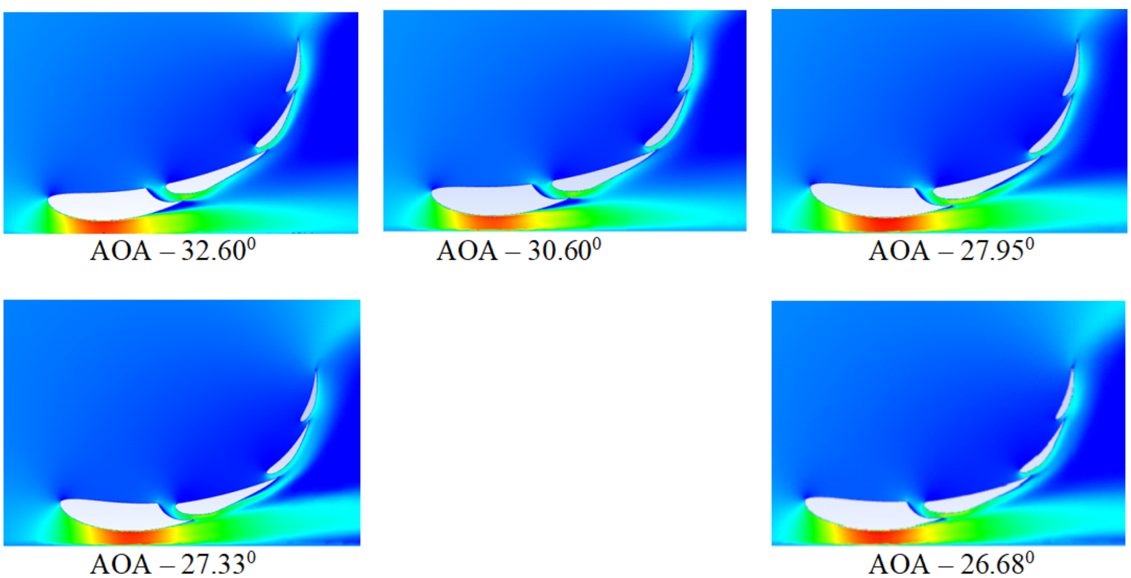

Figure 2.54 Velocity plots of side wing configuration at AOA from 32.60^0 to 26.68^0.

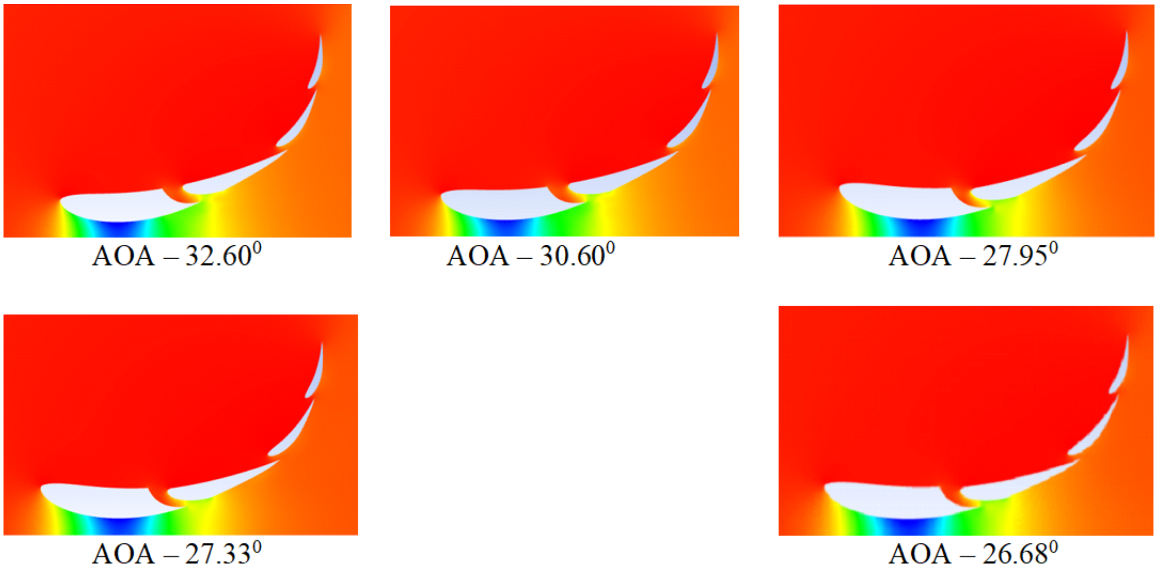

Figure 2.55 Pressure plots of side wing configuration at AOA from 32.60^0 to 26.68^0.

The analysis confirmed the expected change in stall angle for the wing configuration due to ground effect. The same configuration used for rear wing had its maximum lift value at an angle of attack of 32.60^0. When the same configuration was used for side wing which works with ground effect, the maximum lift value was achieved at an angle of attack of 27.33^0 which is less than the angle of attack for wing tested without ground effect. This means that the wing stall occurred at a lower angle of attack after which the lift generated reduced. The results obtained for the side wings at velocity of 11 m/s and 30 m/s are shown in table 2.16.

Table 2.16 Side wing aerodynamic performance at 11 m/s and 30 m/s.

	Side Wing at 11 m/s	**Side Wing at 30 m/s**
C_L	10.71	8.07
ρ (kg/m^3)	1.225	1.225
A (m^2)	0.42	0.42
Downforce (N)	333.4	1868.4
C_D	1.16	1.21
Drag (N)	36.1	280.1

In comparison, a side wing option is found better since it generated a maximum downforce of 333.4 N whereas undertray generated a maximum downforce of 155.7 N.

3.5.5 Front Wing Design

3.5.5.1 Space Constraints

According to rules, the front point of any aerodynamic device mounted at the front should not be further forward than 700 mm from the front point of the front tires. Regarding the mounting height of the wings, it is stated that the front mounted device should not obstruct viewing the parts of front tires above a height of 250 mm from the ground. This effectively makes the maximum possible height at which the top most point of the wing to be less than 250 mm from the ground. The span of the wing is decided by the rule stating that the front mounted device should be within a space between two normal planes drawn from the outside of the tires. The final allowable space for mounting a front wing is shown in figure 2.56. The wing should be able to be inscribed into a 700 mm x 250 mm rectangle positioned as shown.

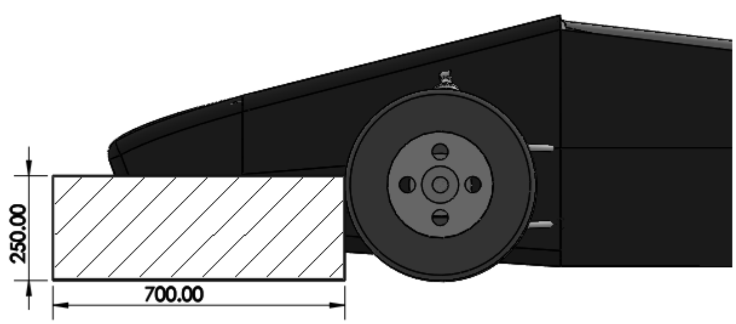

Figure 2.56 Space availability for front mounted aerodynamic device.

3.5.5.2 Front Wing Configurations and Testing

The primary purpose of the front wing is to generate the amount of lift force required to balance the moments caused by the downforce generated by the rear and side wings. Since the downforces are transferred to the road through the tires, the aerodynamic balance is done with respect to the half wheel base [27]. Hence the front wing should have a lift force that can produce an opposite moment produced by the rear wing and side wing. It is decided to place the side wings as rear as possible to the rear tires so that it will also generate a moment with respect to the half wheel base. There by more lift can be afforded at the front wing and the moments will be balanced out. The center of pressures of the rear and side wings are obtained from the CFD analysis. Now, these wings are placed at the desired locations and the total moment created due to the downforces are calculated and the required as shown in figure 2.57. From the space constraints and a few trials, it is decided to select the distance from the half wheel base to front wing center of pressure to be 1560 mm.

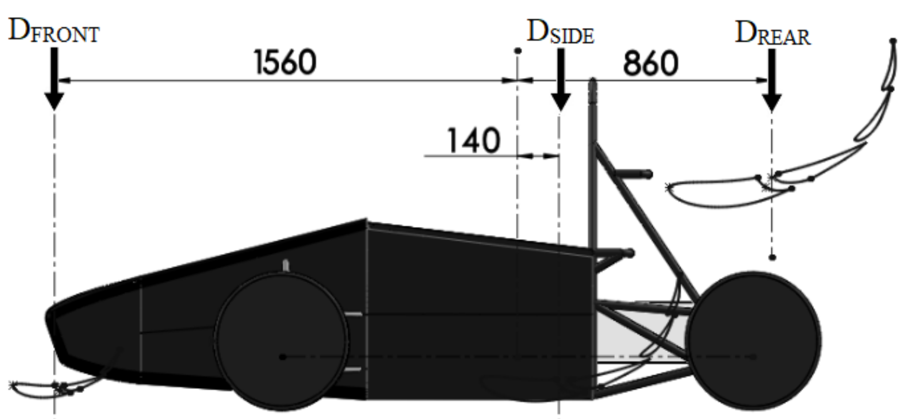

Figure 2.57 Aerodynamic downforce balancing of front, rear and side wings.

$$(D_{REAR} \times 860) + (D_{SIDE} \times 140) = D_{FRONT} \times 1560$$

$$(308 \times 860) + (334 \times 140) = D_{FRONT} \times 1560$$

$$\text{Hence } D_{FRONT} = 200 \text{ N}$$

The lift coefficient should be able to generate 200 N on that corresponding area.

Lift coefficient and the downforce are related by the equation below.

$$C_L = \frac{2 \times D}{\rho \times v^2 \times A}$$

Where area is the product of effective chord length and the span. The maximum possible span for the front wing from the existing design is 1 m. Now, knowing a downforce that should be generated, and the density and velocity known, it is possible to calculate the various combinations of chord length and lift coefficient needed to generate 200 N of downforce at the front wing and are listed in table 2.17. Any of the combination can generate 200 N of downforce, but the small chord lengths are preferred due to possible weight reduction. Various 3 element and 4 element configurations with listed chord length are tested and 3 element wing configurations with a chord length 0.38 m and angle of attack of 18.21^0 yielded the required lift coefficient required in that corresponding chord length.

Table 2.17 Lift coefficients needed at different chord lengths for 200 N downforce.

Chord length	**Target C_L**
0.35	8.02
0.36	7.8
0.37	7.59
0.38	7.39
0.39	7.2
0.4	6.98

The final results obtained for the front wing for both at 11 m/ and 30 m/s are listed in table 2.18. The velocity profile for the selected configuration is shown in figure 2.58 and pressure plot is shown in figure 2.59.

Table 2.18 Front wing aerodynamic performance at 11 m/s and 30 m/s.

	Front Wing at 11 m/s	**Front Wing at 30 m/s**
C_L	7.38	9.15
ρ (kg/m^3)	1.225	1.225
A (m^2)	0.365	0.365
Downforce (N)	200	1841
C_D	0.47	0.41
Drag (N)	13	82

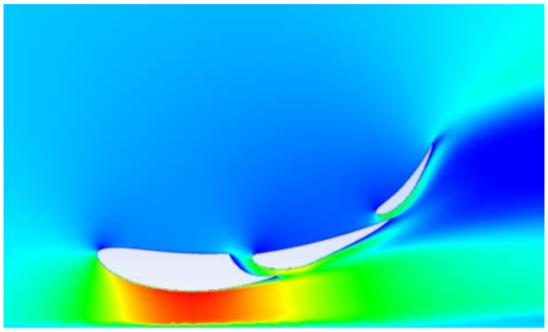

Figure 2.58 Velocity plot of front wing configuration for 200 N downforce.

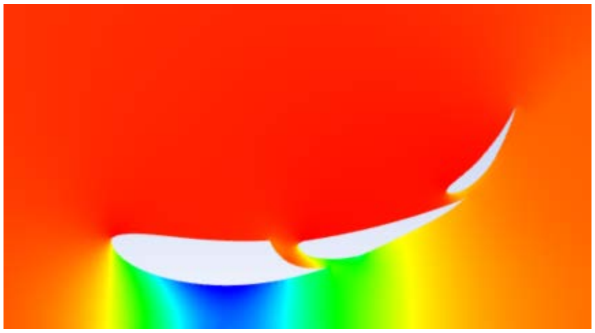

Figure 2.59 Pressure plot of front wing configuration for 200 N downforce.

3.5.5 Structural Analysis of Wings

The main objective of performing a structural analysis for the wings in this project is to determine to determine approximate weights of the wings to performs load analysis of the suspension. A thorough research was done on the methods of conducting a structural analysis of a race car wing due to aerodynamic loads. The best and most accurate method found for conducting these types of analysis is by conducting a Multiphysics simulation. An accurate estimate of the stress and strain caused by the pressure force due to air flow can be determined by conducting a Multiphysics simulation for Fluid Structural interaction using Multiphysics simulation software such as ANSYS AIM. Fluid Structural interaction simulations combines both CFD and Structural analysis. Aerodynamic forces created due to pressure differences on wing surfaces is calculated by a CFD solver and the forces are fed into structural analysis which is used to calculate nodal displacements and stresses. In this project, CFD analysis has already been using ANSYS fluent 2-D simulations and the approximate downloads were calculated for all three wings. A three-equation turbulence model called Transition k-kl-ω model was used for the validation and analysis. This is a complex model in terms of mesh quality required and solution time needed. Hence, for Multiphysics simulation the same Transition k-kl-ω model should be used to get a solution that can be compared to the CFD results obtained from 2-D studies. Also, since the study should be done in 3-D, the amount of time and resource required to generate a mesh similar to the one used in 2-D studies along with the solution time will be very large. Hence, a literature review was done on other simplified methods used previously to carry out the structural analysis with reasonable accuracy for determining the weight of the wings. Stroud et al (1972) used plate theory for structural analysis of a aircraft wing by assuming a uniform normal loading on the wings [32]. Blondeau et al (2003) conducted structural analysis on aircraft wing with a uniform loading and quadratic loading, the latter being more realistic to the downforce distribution and the maximum stress results were found very close. [33]. Marisarla et al (2003) used the downforce results obtained from separate CFD analysis as an input force for structural analysis using ANSYS [34]. Considering the above methods, a simplified method to consider the downforce values at maximum speed of 30 m/s from the CFD analysis already conducted as a uniformly distributed normal load on the designed wing configurations was selected for structural analysis using SOLIDWORKS. A considerable assumption made here is that the downforce is equally distributed over the whole wing surface, which is a simplified assumption. But, considering the lesser amount of time and resource needed to conduct such an analysis and the moderate accuracy level that can be achieved for finding the weights of the wings, this method is found to be reasonable.

Before conducting the analysis, the material to be used for the wing construction should be decided. Most common materials used for wing construction by various FSAE teams were investigated. FSAE teams uses composite materials such as CFRP or Glass Fiber with a stiffening core to construct the wings. As discussed in section 2.2.4 for Carbon Fiber monocoques, they have high cost and hence Glass Fiber (S class for high strength) is selected. Also, the core is decided to be made of Polyurethane foam. Structural analysis was performed with different thickness of glass Fiber outside the Polyurethane foam core. The thickness of Fiberglass was incremented on an order of 0.25 mm since it is the minimum commercially available fiberglass thickness [35]. The properties of S-Glass Fiber and Polyurethane foam (PU64) for analysis are given in table 2.19.

Table 2.19 Mechanical properties of S-Glass Fiber and Polyurethane foam.

Material	**Density (Kg/m3)**	**Yield Strength (MPa)**	**Young's modulus (MPa)**	**Reference**
PU64	64	0.6	30	[36]
S-Glass Fiber	2490	210	90000	[37, 38]

3.5.5.1 Rear Wing Structural Analysis

The rear wing was tested with a downforce of 1350 N obtained from the CFD analysis of rear wing at 30 m/s from section 3.5.2.4. For all analyses, fixed constraint is applied for both left and right surfaces of the all elements in the wing, which are attached to the end plates. The maximum downforce is applied to the all the surfaces of the wing as a uniformly distributed load. The constraints and forces are shown in figure 2.60. A curvature-based mesh with a maximum element size of 0.008 m was used for the analysis. The results obtained from FEA are shown from figure 2.61 to 2.63.

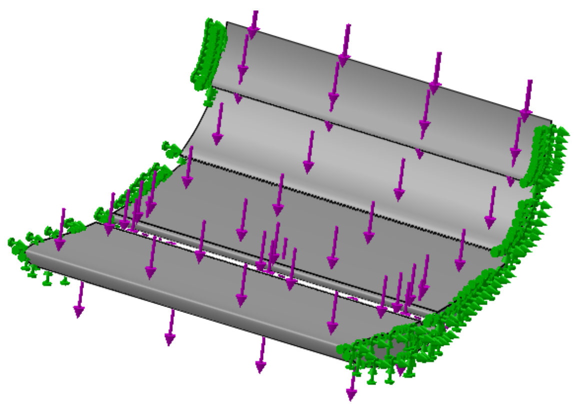

Figure 2.60 Rear wing FEA model with load and constraints.

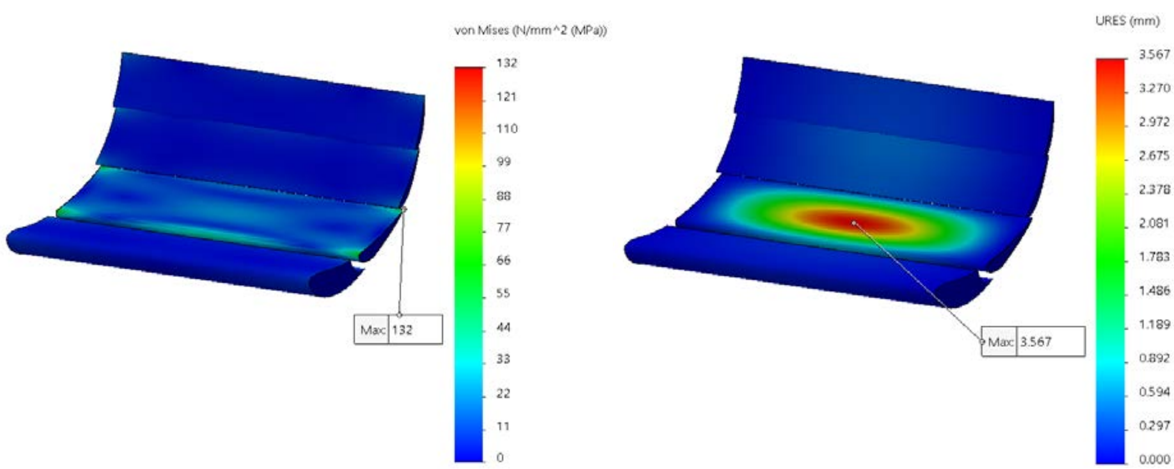

Figure 2.61 FEA results of rear wing with 1.5 mm Fiberglass thickness.

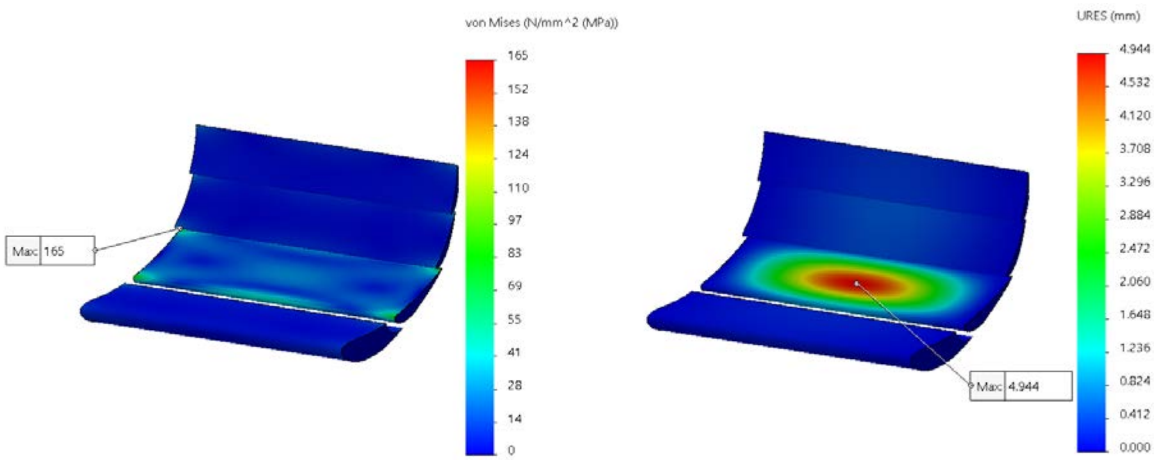

Figure 2.62 FEA results of rear wing with 1.25 mm Fiberglass thickness.

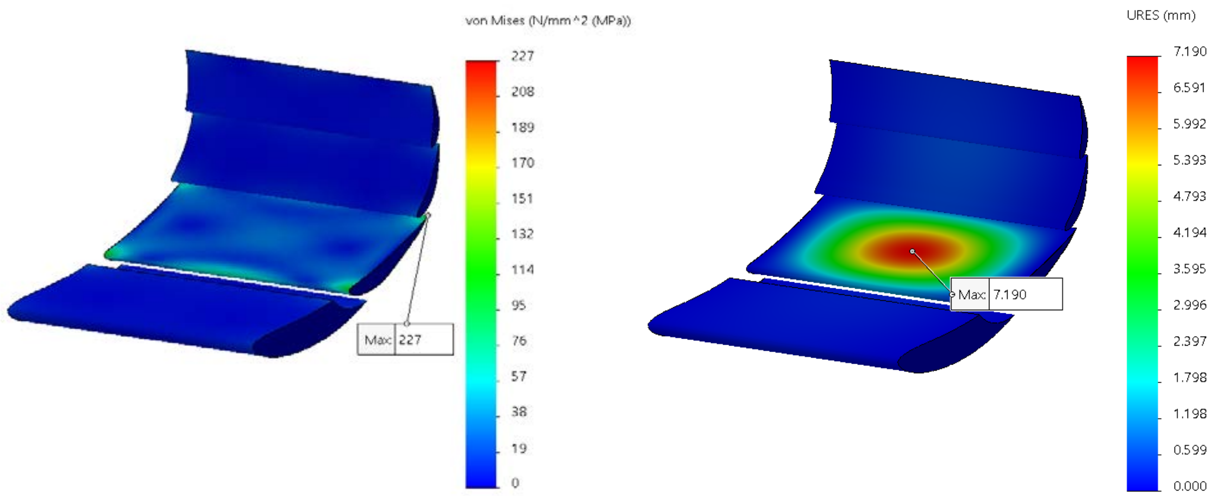

Figure 2.63 FEA results of rear wing with 1 mm Fiberglass thickness.

Table 2.20 FEA results for rear wing with varying fiberglass thickness.

Fiberglass thickness (mm)	**Max. Von Mises (MPa)**	**Max. Displacement (mm)**	**FOS**	**Weight (Kg)**
1.5	132	3.567	1.59	10.59
1.25	165	4.944	1.27	9.66
1	227	7.19	0.93	8.26

From the analysis, the model having Fiberglass thickness of 1.25 having FOS 1.27 is selected as the final design. It will require 5 layers of Fiberglass with thickness 0.25 mm and the approximate weight calculated for the wing is 8.26 Kg.

3.5.5.2 Side Wing Structural Analysis

The side wing was tested with a downforce of 1868 N obtained from the CFD analysis of side wing at 30 m/s from section 3.5.4.3. Constraints and forces for analysis are similar to the rear wing analysis and is shown in figure 2.64. A curvature-based mesh with a maximum element size of 0.008 m was used for the analysis. The results are shown from figure 2.65 to 2.67

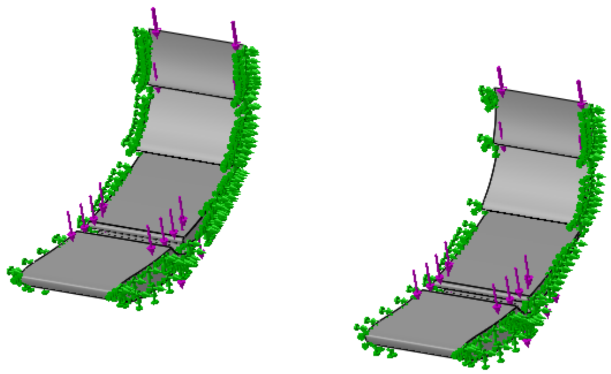

Figure 2.64 Side wing FEA model with load and constraints.

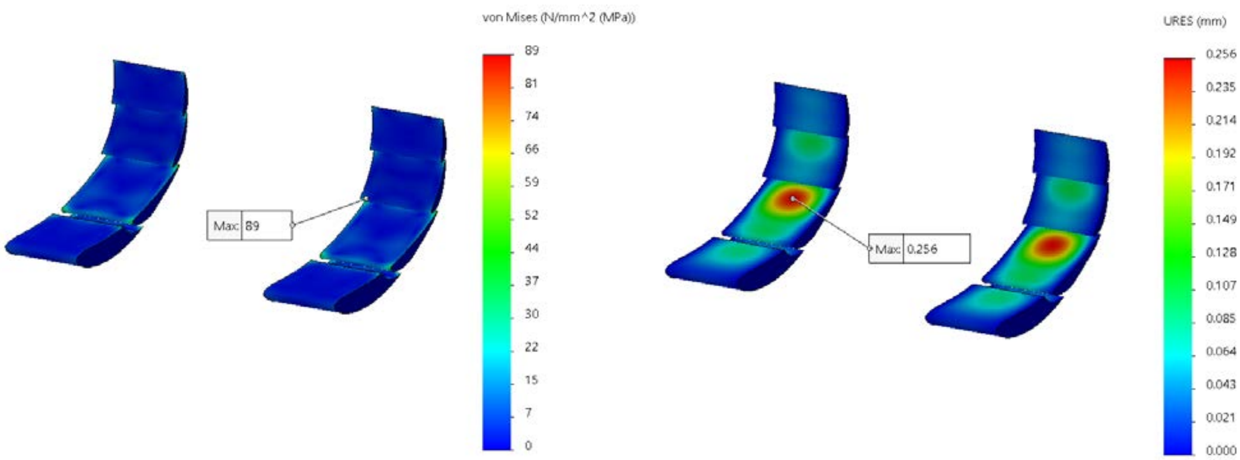

Figure 2.65 FEA results of side wing with 1.5 mm Fiberglass thickness.

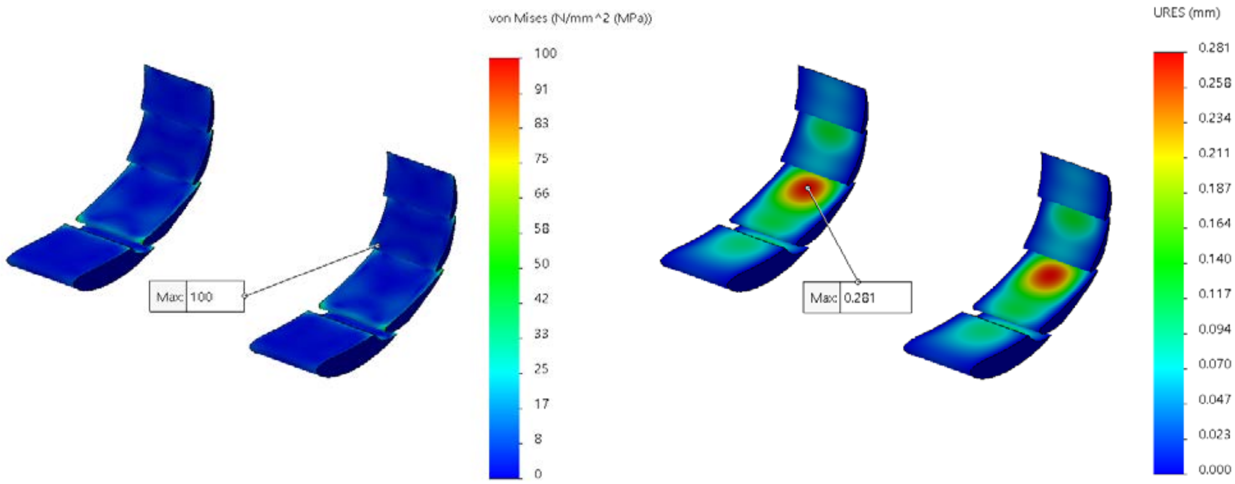

Figure 2.66 FEA results of side wing with 1.25 mm Fiberglass thickness.

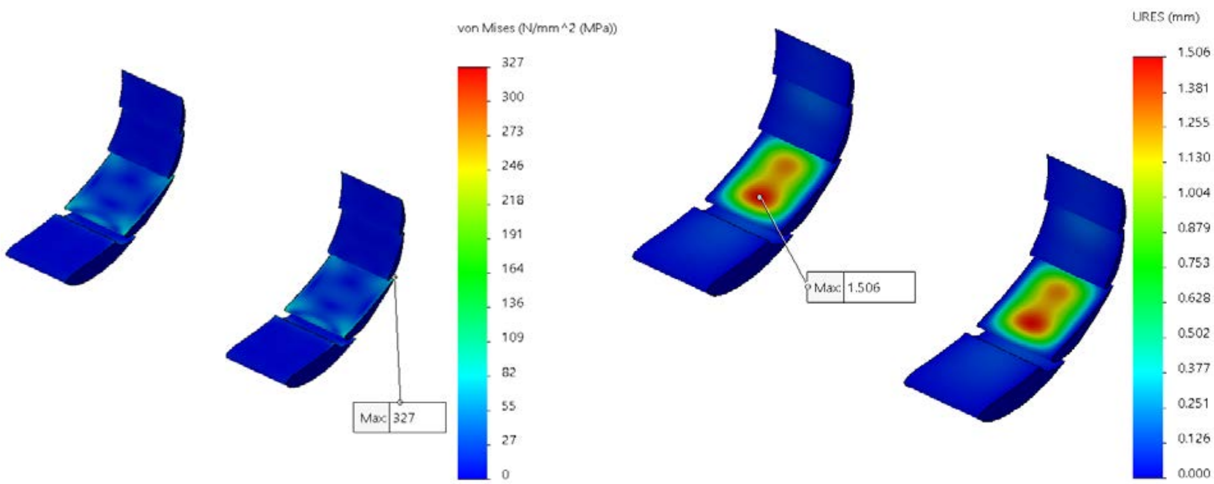

Figure 2.67 FEA results of side wing with 1 mm Fiberglass thickness.

Table 2.21 FEA results for side wing with varying fiberglass thickness.

Fiberglass thickness (mm)	Max. Von Mises (MPa)	Max. Displacement (mm)	FOS	Weight (Kg)
1.5	89	0.256	2.36	5.05
1.25	100	0.281	2.10	4.68
1	327	1.506	0.64	3.71

From the analysis, the model having Fiberglass thickness of 1.25 having FOS 2.10 is selected as the final design. It will require 5 layers of Fiberglass with thickness 0.25 mm and the approximate weight calculated for the wing is 4.68 Kg.

3.5.5.3 Front Wing Structural Analysis

The front wing was tested with a downforce of 1841 N obtained from the CFD analysis of front wing at 30 m/s from section 3.5.4.2. Constraints and forces for analysis are similar to the rear wing analysis and is shown in figure 2.68. A curvature-based mesh with a maximum element size of 0.006 m was used for the analysis. The results are shown from figure 2.69 to 2.71

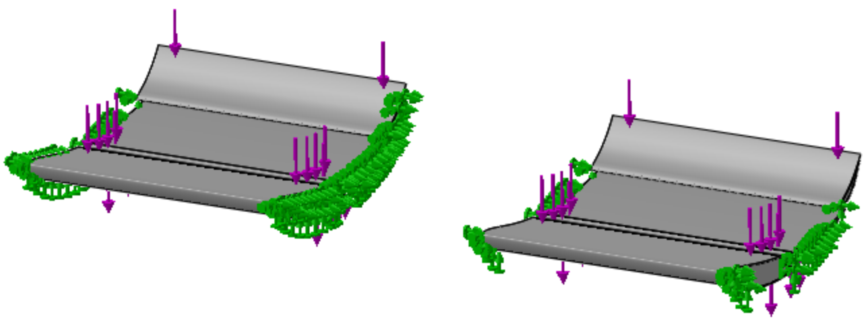

Figure 2.68 Front wing FEA model with load and constraints.

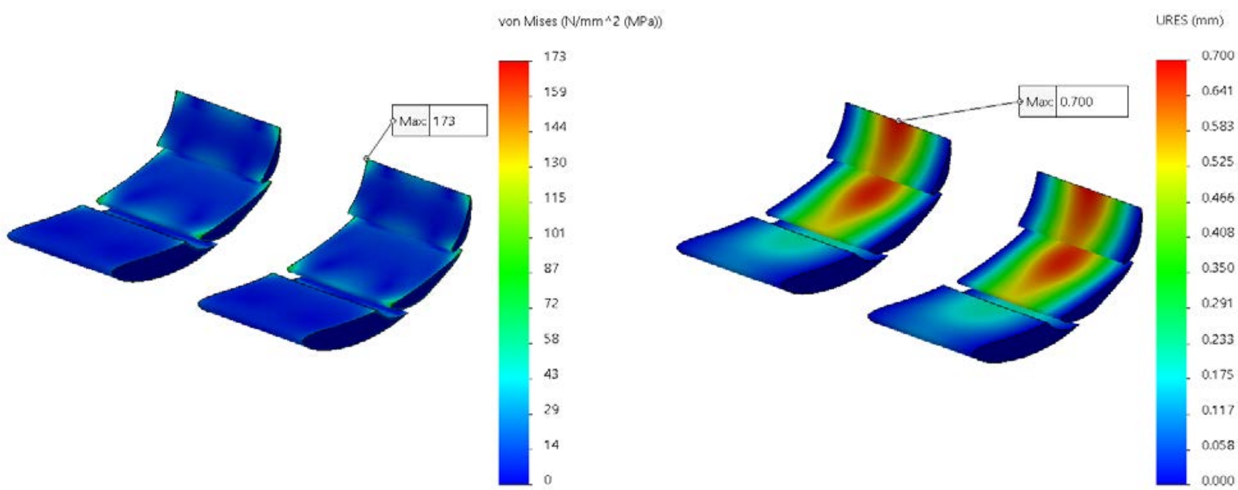

Figure 2.69 FEA results of front wing with 2 mm Fiberglass thickness.

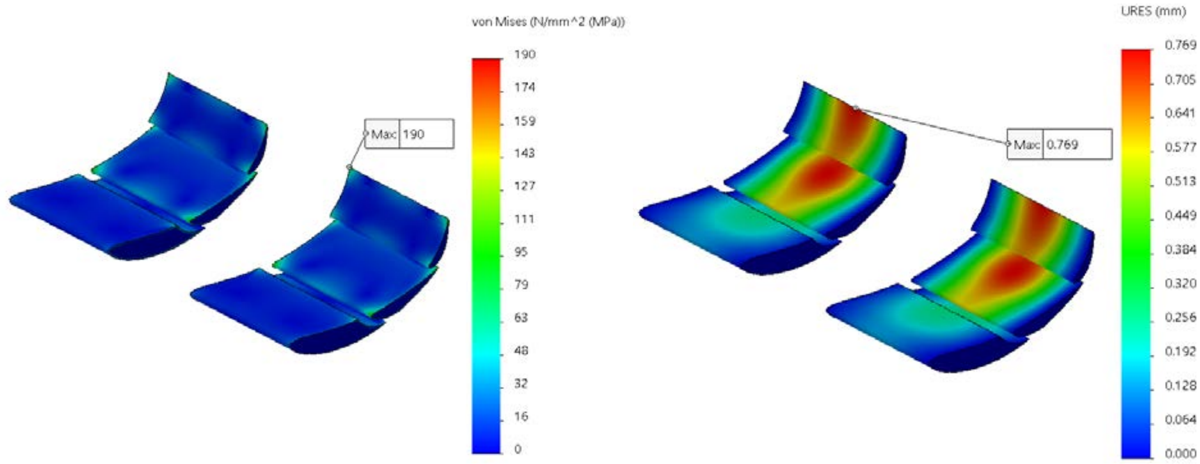

Figure 2.70 FEA results of front wing with 1.75mm Fiberglass thickness.

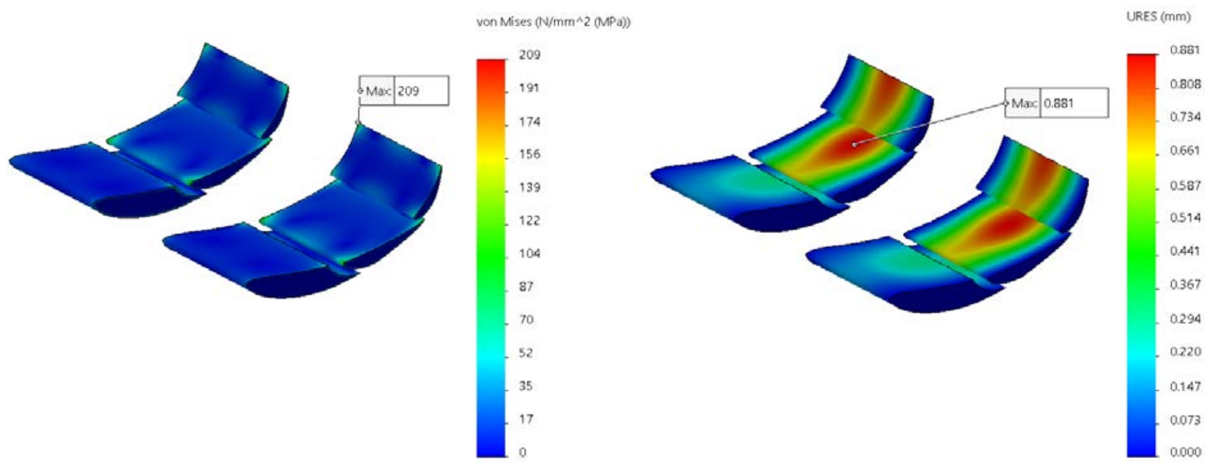

Figure 2.71 FEA results of front wing with 1.5 mm Fiberglass thickness.

Table 2.22 FEA results for front wing with varying fiberglass thickness.

Fiberglass thickness (mm)	Max. Von Mises (MPa)	Max. Displacement (mm)	FOS	Weight (Kg)
2	173	0.7	1.21	4.65
1.75	190	0.769	1.11	4.30
1.5	209	0.881	1	3.70

From the analysis, the model having Fiberglass thickness of 1.75 having FOS 1.11 is selected as the final design. It will require 7 layers of Fiberglass with thickness 0.25 mm and the approximate weight calculated for the wing is 4.30 Kg.

3.6 Suspension System Analysis

During the previous sections, a finalized chassis, suspension geometry, impact attenuator, and aerodynamic devices were designed. In order to perform suspension system kinematic and dynamic analysis, the major input parameters required are the position of CG of the vehicle, expected weight, aerodynamic downforces, suspension geometry and other miscellaneous parameters. Among these, all other parameters except the CG and expected weight of the vehicle are already determined. To find the position of CG and weight of the vehicle, the already designed components were assembled in SOLIDWORKS. Sample 3-D models of other components of the vehicle which are not designed as a part of this project such as the engine, differential and axles, pedal box, seat, spring-damper units, steering unit, battery etc. were downloaded from various CAD forums for FSAE. These were used only as masses representing the components to find the overall CG of the vehicle and also to check if the components would fit well inside the space allocated for them while designing chassis and other devices. The resulting assembly is shown in figure 2.72 and 2.73. The results of CG location and weight are listed in table 2.22.

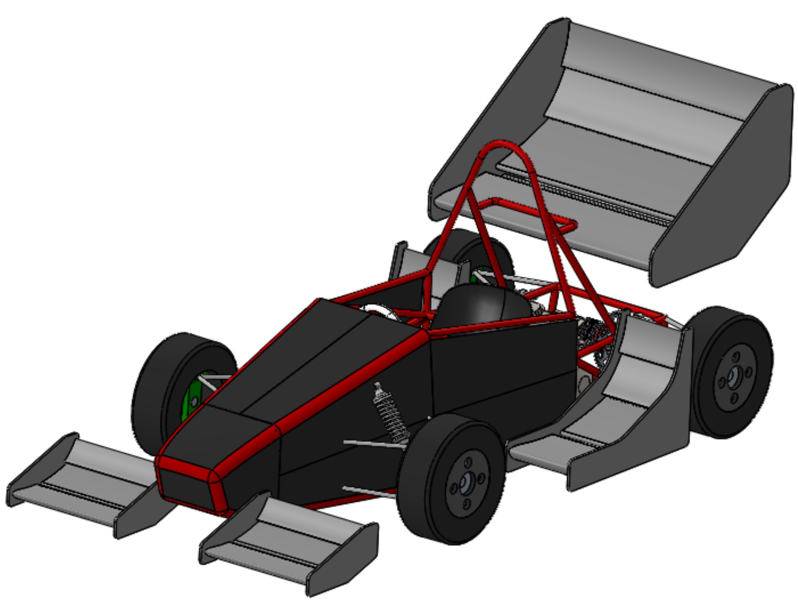

Figure 2.72 Isometric view of Final Assembly of all the components of the car.

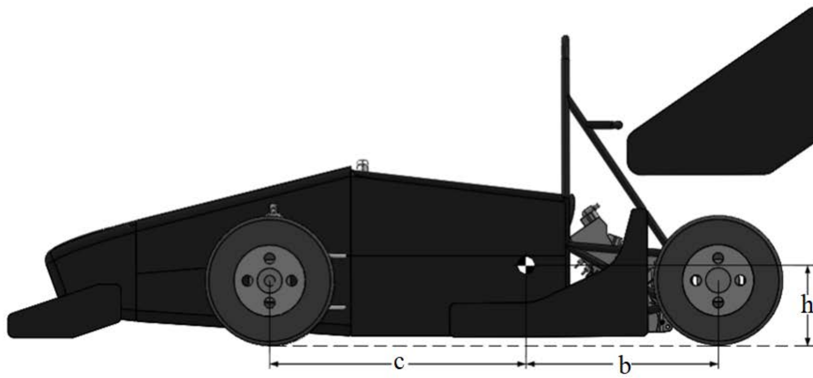

Figure 2.73 Side view of Final Assembly of the car with CG location.

Table 2.23 Approximate CG location and weight of final car assembly.

		Without Driver	With 170 lbs Driver
CG location	c (in)	35.32	33.53
	b (in)	27.68	29.47
	h (in)	11.06	10.40
Weight Kg (lbs)		180 (397)	257 (567)

The vehicle test conditions during inspections are specified for a driver weighing 170 lbs. Hence the total weight of the car including the driver is found to be 257 Kg or 567 lbs.

The stability of the car will be tested in the competition using a tilt test during technical inspection. During the test the vehicle will be tilted to an angle of 60^0 to the horizontal which corresponds to a lateral acceleration of 1.7 g and the vehicle should not roll over. Knowing the width of the vehicle, it is now possible to find the highest possible CG height for the vehicle which will still keep the vehicle without rolling during the tilt test. This maximum value can be compared with the CG height value obtained from the assembly to find if the CG height would be enough during the tilt test. The static stability of a vehicle at a certain tilt angle is defined by a property called static stability factor (SSF) defined by the equation below [39]. SSF connects the roll angle to the track width of the vehicle and the center of gravity height.

$$SSF = \frac{T}{2 \times h} = \tan \emptyset = A_y$$

where $\emptyset$ is the tilt angle.

Substituting the values of average track width, tilt angle or lateral acceleration, an approximate value of CG height to be needed to prevent rollover can be calculated.

$$\frac{1200}{2 \times h} = \tan 60° = 1.7\ g$$

$$h = 353\ mm\ or\ 13.89\ in$$

Comparing the CG height of 10.40 in obtained from the SOLIDWORKS assembly, which is less than the maximum CG height obtained from the above calculation, it can be inferred that the car will pass the tilt test without rollover. Using the same calculation for SSF, it can also be learned that with a CG height of 10.40 in with a track width of 1200 mm, it can withstand a maximum lateral acceleration of 2.27g which is way higher than any peak lateral acceleration observed in FSAE competitions and hence there is no rollover probability during the competition.

3.6.1 Front and Rear suspension Kinematics

It is necessary to analyze both the suspension Kinematics and Dynamics to understand about the performance of the designed suspension geometry during various vehicle maneuvers. One thing to be kept in mind while analyzing the suspension system is that the main function of the suspension system is to ensure the proper contact of the tires with the ground during all expected vehicle motions. Also, all the suspension design text books and documents state that there is no one best suspension design for any vehicle. The design is considered to be a good one if it performs its intended functions within acceptable limits of target parameters. Suspension kinematics of the designed suspension geometry should be analyzed during vehicle roll during cornering and bump and droops due to road surface irregularities. The most important condition for an FSAE car among those is the vehicle roll during cornering and road irregularities are negligible. The suspension design in FSAE competitions is mainly concentrated on its performance during corners and a good suspension design should enable maximum tire grip which will enable the car to travel the corners faster. Hence, optimization of the suspension design is done by considering vehicle roll as the main criteria. The objective of optimization during vehicle roll is by ensuring proper tire contact during the maximum expected vehicle roll, which is when the vehicle will be travelling the corner at maximum speed. Hence, the first step in the suspension kinematic study is to determine the expected vehicle roll for the already designed vehicle at expected FSAE track conditions.

If the torsional stiffness of the chassis is very high, the roll angle at front and rear axle will be identical during cornering[6]. The torsional stiffness of the chassis is already found to be reasonably high for an FSAE car. Hence, it is assumed that the roll angle will be same for front and rear axles. For finding the roll angle, the first thing to be determined is the target roll stiffness needed the suspension system. Stiffer the suspension is for rolling, less roll angle will be there. Although vehicle roll is undesirable for a race car, it is not possible to eliminate it completely since the suspension cannot be too stiff since it will adversely affect the handling and smooth ride of the car. Usually, the chassis torsional stiffness and suspension roll stiffness are related such that the chassis is 3-5 times stiffer than the suspension for racecars and 7-40 times stiffer for passenger cars [40]. Hence a suspension roll stiffness was decided based on the chassis torsional stiffness data available from section 3.3.3.

Calculated chassis torsional stiffness is 2300 lbs-ft / deg. Since the chassis is very stiff for an FSAE car and getting a very high roll stiffness would affect the ride, suspension roll stiffness is decided to be 1/5th of the chassis torsional stiffness.

Hence roll stiffness = 2300/ 5 = 460 lbs ft / deg = 63 Kg m / deg

Now, roll angle can be calculated using the equations below [6]

$$\varphi = \frac{-W \times H}{K_{\varphi F} + K_{\varphi R}} \times A_Y$$

where,

$$A_Y = A_\alpha \cos \alpha + \sin \alpha$$

In FSAE, banking angle $\alpha = 0^0$, hence

$$A_Y = A_\alpha = \frac{v^2}{R \times g}$$

Velocity considered for the suspension is the average cornering velocity in FSAE competitions, 11 m/s. It can be seen from the equation that maximum lateral acceleration A_Y for a fixed cornering velocity of 11 m/s is achieved at lowest turning radius. Minimum radius of turn varies according to different dynamic events which are Autocross and Skidpad events. Radius of turn in Autocross event varies from 11.5 m to 22.5 m and that for Skid Pad event is 9 m. Hence the maximum lateral acceleration for roll stiffness calculation is obtained with a turning radius of 9 m at Skid Pad event.

$$A_Y = \frac{11^2}{9^2 \times 9.81} = 1.37\ g$$

Normal load acting on the vehicle constitute of car weight and total aerodynamic downforce at 11 m/s. From previous calculations, expected weight of the car is calculated to be 257 Kg and approximate aerodynamic downforce is calculated to be 84 Kg.

Hence, $W = 257 + 84 = 341\ Kg$

$H = 0.2066\ m$

Total Roll stiffness $K_\varphi = K_{\varphi F} + K_{\varphi R} = 63\ Kg\ m/deg$

Hence maximum roll angle at a lateral acceleration of 1.37 g is calculated to be

$$\varphi = \frac{-341 \times 0.2066}{63} \times 1.37 = -1.53°$$

Maximum roll predicted is -1.53 deg considering a target suspension roll stiffness of 63 Kg m/deg. While designing the suspension spring- damper and/or anti-roll bar, the target roll stiffness of the vehicle should be considered as 63 Kg m/deg.

Now, since the expected roll angle while cornering is known, the suspension kinematics was analyzed for this roll angle and the optimization of the required parameters should also be done. The most economical way of doing a suspension kinematics study was found to be by using a specialized suspension kinematic modelling tool. There are many such tools available with varying limits of capabilities such as ADAMS CAR, OptimumKinematics, SusProg3D, Lotus Shark etc. The main advantage of these software is that they have built-in suspension templates, and studies which means the user don't have to create 3-D CAD models for the analysis and instead they can import the co-ordinates of the designed suspension geometry and the software will generate a suspension model. In this project a tool called Lotus Shark is used for the suspension kinematics study. As stated above, it has built-in suspension templates and the user can import the co-ordinates of the suspension geometry. For Lotus Shark, while inputting the suspension hard point co-ordinates, all the data should be consistent based on the co-ordinate system as shown in figure 2.74. The origin can be placed anywhere in front of the vehicle such that the X-Z plane passes through the center of the vehicle. A double wishbone suspension model was selected from the built-in templates and the required suspension hardpoint co-ordinates were inputted by measuring them from the suspension geometry designed in SOLIDWORKS and the entered co-ordinate details for front suspension are shown in figure 2.75.

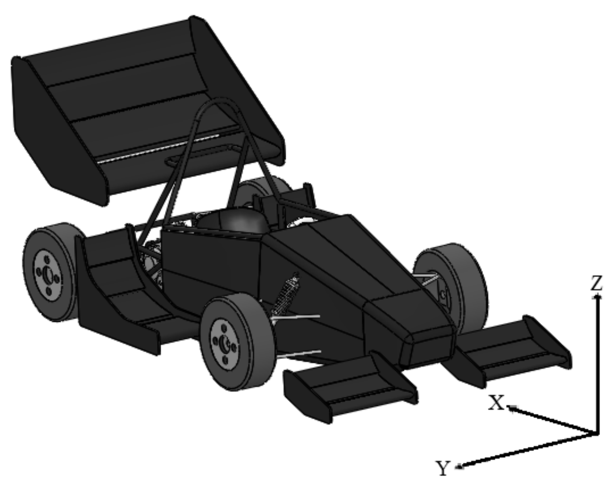

Figure 2.74 Lotus Shark suspension analysis co-ordinate system.

Using the co-ordinates entered, the software generated front suspension models as shown in figure 2.76. The initial design didn't have any static camber, and the kinematics were analyzed firstly for 1.53^0 roll calculated. The objective was to study about the camber gain for the tires at 1.53^0 roll. Once the change in camber was determined, the objective was to make the camber at 1.53^0 roll to be approximately 0^0 in order to make sure that maximum contact area is available between the tire and the ground, hence generating maximum grip. A considerable assumption made here is that the tire stiffness is infinitely high and hence the camber angle depends only on the roll angle. It was not possible to incorporate the tire deformations during the calculations due to lack of availability of TTC or similar tire data. Once these data are available for the future teams, they can be incorporated during the calculations to get more accurate results.

	X (mm)	Y (mm)	Z (mm)
Point 1: Lower wishbone front pivot	317.5000	205.0000	139.5900
Point 2: Lower wishbone rear pivot	762.0000	268.2500	137.4500
Point 3: Lower wishbone outer ball joint	469.9000	577.8500	127.0000
Point 5: Upper wishbone front pivot	317.5000	210.8800	313.7300
Point 6: Upper wishbone rear pivot	762.0000	274.3100	316.7500
Point 7: Upper wishbone outer ball joint	469.9000	556.4900	330.2000
Point 8: Damper wishbone end	469.9000	501.8100	129.5700
Point 9: Damper body end	469.9000	198.2100	536.6500
Point 11: Outer track rod ball joint	452.2500	577.8500	127.0000
Point 12: Inner track rod ball joint	469.9000	231.0600	138.7100
Point 16: Upper spring pivot point	469.9000	198.2100	536.6500
Point 17: Lower spring pivot point	469.9000	501.8100	129.5700
Point 18: Wheel spindle point	469.9000	567.1700	228.1266
Point 19: Wheel centre point	469.9000	590.5500	228.6000

Figure 2.75 Front suspension hard point co-ordinates for Lotus Shark suspension analysis.

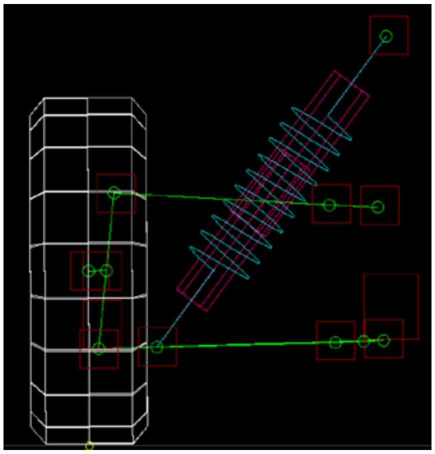

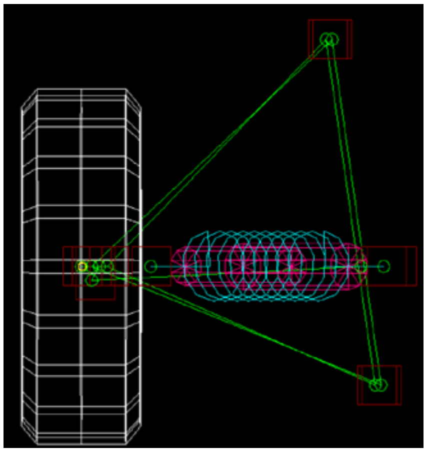

Figure 2.76 Front and top views of front suspension model in Lotus Shark.

The results for camber change during the vehicle roll of 1.53^0 obtained from the software is plotted in figure 2.77. This shows that the tire with 0^0 camber initially, will have a maximum positive camber of around 1.2^0 at the maximum roll angle of 1.53^0. Since the objective is to obtain maximum tire contact during maximum roll angle, the camber at maximum roll should be made 0^0. Hence, it is decided to add a static negative camber of around 1.2^0 to the design which will make the camber at maximum roll around 0^0. The results obtained for the roll analysis after adding a static negative camber of around 1.2^0 is shown in figure 2.77.

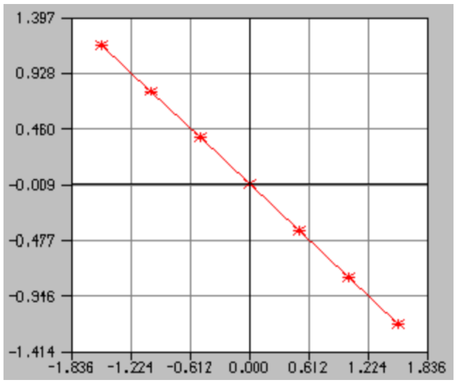

(a)

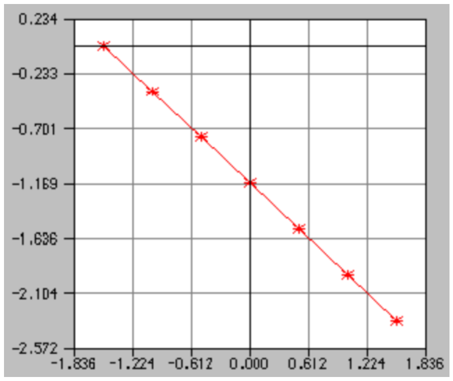

(b)

Figure 2.77 Front Camber variation till maximum roll (a) at 0^0 static camber (b) at 1.2^0 static camber.

Variation of roll center height is also analyzed for vehicle roll and is shown in figure 2.78. Variation of roll center height should be minimum in order to have better handling of the vehicle [8].

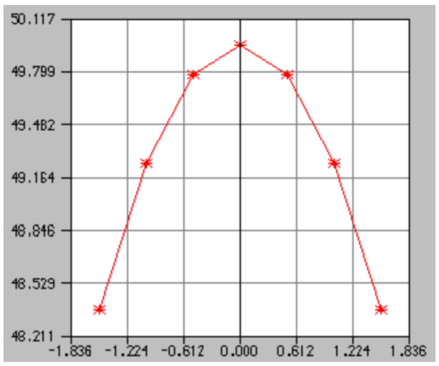

Figure 2.78 Front Roll center variation till maximum roll with 1.2^0 static camber.

The Results show that the roll center migration is less than 3 mm which is considered to be very small and is very predictable also.

Similar to the analysis done for the front suspension, the rear suspension co-ordinates were also inputted into the software as shown in figure 2.79.

	X (mm)	Y (mm)	Z (mm)
Point 1: Lower wishbone front pivot	134.3800	259.4500	144.2100
Point 2: Lower wishbone rear pivot	338.3800	259.4500	144.2100
Point 3: Lower wishbone outer ball joint	223.2500	558.8000	127.0000
Point 5: Upper wishbone front pivot	112.1400	247.8800	322.7200
Point 6: Upper wishbone rear pivot	386.6300	247.8800	322.7200
Point 7: Upper wishbone outer ball joint	223.2500	537.5600	329.0900
Point 8: Damper wishbone end	194.7200	462.7100	132.6400
Point 9: Damper body end	162.1400	247.8800	322.7200
Point 11: Outer track rod ball joint	220.0000	558.8000	127.0000
Point 12: Inner track rod ball joint	223.2500	259.4500	144.2100
Point 16: Upper spring pivot point	162.1400	247.8800	322.7200
Point 17: Lower spring pivot point	194.7200	462.7100	132.6400
Point 18: Wheel spindle point	222.6400	548.1800	227.7125
Point 19: Wheel centre point	222.6400	590.5500	228.6000

Figure 2.79 Rear suspension hard point co-ordinates for Lotus Shark suspension analysis.

Th resultant rear suspension model generated by the software is shown in figure 2.80. The analysis was done to learn about the camber variation and roll center migration for the maximum roll angle of 1.53^0.

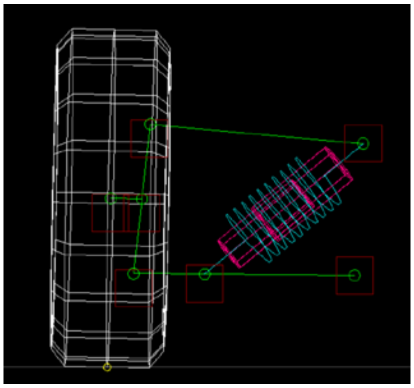

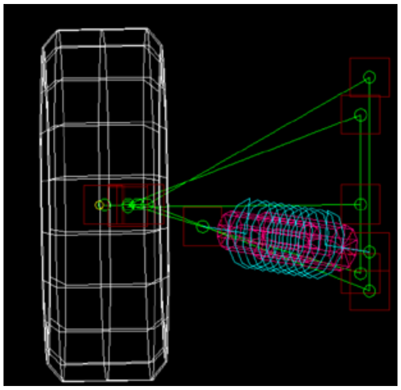

Figure 2.80 Front and top views of rear suspension model in Lotus Shark.

Similar to the analysis done for front suspension, the first analysis is done with a static camber of 0^0. The camber variation during vehicle roll is shown in figure 2.81.

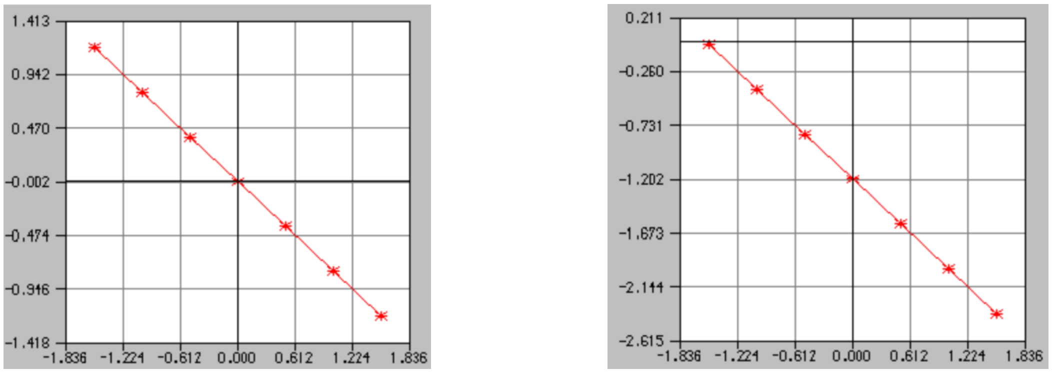

(a) (b)

Figure 2.81 Rear Camber variation till maximum roll (a) at 0^0 static camber
(b) at 1.2^0 static camber.

It can be seen that at -1.53^0 roll angle, a positive camber of 1.2^0 is found on the outside tire. Hence a negative static camber of 1.2^0 is assigned to the rear tires and the analysis as shown in figure 2.81 prove that at maximum roll angle, the camber will be around 0^0 thereby ensuring maximum tire contact and traction. Analysis was done also for the roll center migration and it shows that the roll center variation is around 3 mm which is very small compared to the rear roll center height of around 63 mm or 2 inches as shown in figure 2.82.

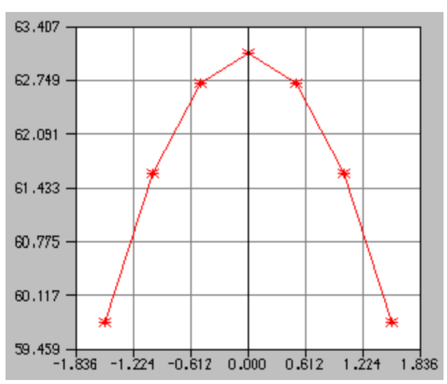

Figure 2.82 Rear Roll center variation till maximum roll angle with 1.2^0 static camber.

3.6.2 Lateral Load Transfer while Cornering

Load transfer while cornering (lateral load transfer), braking and acceleration (longitudinal load transfer) should be calculated in order to find the maximum expected load on each tire at front and rear. These loads will be utilized to identify the worst case load acting on each wheel which will be used to conduct FEA on the suspension components. The equations used for the load transfer calculations are from "Race car vehicle dynamics" by Milliken [6].

The normal load acting on each wheel while the vehicle moves at 11 m/s is due to both weight of the vehicle (W_C) and aerodynamic downforce D. The distribution of normal load on front and rear axle are given by,

$$W_F = \frac{\left[\left(W_C \times \frac{c}{L}\right) + \frac{D}{2}\right]}{2}$$

$$W_R = \frac{\left[\left(W_C \times \frac{b}{L}\right) + \frac{D}{2}\right]}{2}$$

Center of gravity is located at a distance of 33.5 inches from the front wheels towards the rear with a wheel base of 63 inches. Hence static load on each front and rear tire are

$$W_F = \frac{\left[\left(257 \times \frac{29.5}{63}\right) + \frac{84}{2}\right]}{2} = 81.17\ Kg$$

$$W_R = \frac{\left[\left(257 \times \frac{33.5}{63}\right) + \frac{84}{2}\right]}{2} = 89.33\ Kg$$

Hence the overall static load is distributed among front and rear tires at a ratio of $48 : 52$ percentage. The next step is to find the maximum conditions of lateral load transfer during cornering and longitudinal load transfer during acceleration and braking.

Firstly, the lateral load transfer during cornering at a lateral acceleration of 1.37g is considered.

Lateral load transfer in front and rear wheels are given by,

$$\Delta W_F = A_Y \times \frac{W}{t_F} \times [\frac{H \times K_{\varphi F}}{K_{\varphi F} + K_{\varphi R}} + \frac{b \times Z_{RF}}{L}]$$

$$\Delta W_R = A_Y \times \frac{W}{t_R} \times [\frac{H \times K_{\varphi R}}{K_{\varphi F} + K_{\varphi R}} + \frac{c \times Z_{RR}}{L}]$$

To find the weight transfer at front and rear while cornering, we need to know the distribution of total roll stiffness among the front and rear wheels. Roll stiffness distribution will affect the amount of load transferred from the inside to outside wheel while cornering. Since we are using same type of tires in front and rear, the lateral force acting on front and rear tires will solely depend on the normal load acting on them, which is a result of the amount of load transferred to the outside tires. The lateral force on front and rear outside tires will decide whether the vehicle will have understeer, neutral steer or oversteer while cornering. If the lateral force on the front outside tire is higher than the rear outside tire, the vehicle will have understeer. Similarly, if the lateral force on the rear outside tire is higher than front outside tire, the vehicle will have oversteer. Designers sometimes provide a small amount of understeer or oversteer according to the driving conditions or the driver feedback. As a first-time car, this vehicle will be designed to have neutral steer for better control in corners. To achieve neutral steer, the lateral force (normal load also) on front and rear outside tires should be similar. Calculating the weight transfer using equations, it is found that a roll stiffness distribution of 57:43 percentage on front and rear will produce similar amount of normal load on front and rear outside tires.

Roll stiffness on front and rear with a roll stiffness distribution of 57:43 percentage are,

$$K_{\varphi F} = K_{\varphi} \times 0.57 = 63 \times 0.57 = 35.9\ Kg.m/deg$$

$$K_{\varphi R} = K_{\varphi} \times 0.43 = 63 \times 0.43 = 27.1\ Kg.m/deg$$

Hence, lateral load transfer on front is

$$\Delta W_{CF} = 1.37 \times \frac{341}{1.22} \times \left[\frac{0.2066 \times 35.9}{63} + \frac{0.85 \times 0.05}{1.6}\right] = 55.42\ Kg$$

This means that the normal load on front outside tire due to lateral load transfer is

$$W_{FCo} = W_{FS} + \Delta W_F = 81.17 + 55.42 = 136.59\ Kg$$

Similarly, the normal load on front inside tire due to lateral load transfer is

$$W_{FCi} = W_{FS} - \Delta W_F = 81.17 - 55.42 = 25.75\ Kg$$

Similarly, lateral load transfer on rear is

$$\Delta W_{CR} = 1.37 \times \frac{341}{1.18} \times \left[\frac{0.2066 \times 27.1}{63} + \frac{0.75 \times 0.0635}{1.6}\right] = 47.06\ Kg$$

This means that the normal load on front outside tire due to lateral load transfer is

$$W_{RCo} = W_{RS} + \Delta W_R = 89.33 + 47.06 = 136.39\ Kg$$

Similarly, the normal load on front inside tire due to lateral load transfer is

$$W_{RCi} = W_{RS} - \Delta W_R = 89.33 - 47.06 = 42.27\ Kg$$

Normal load on front and rear outsides tires are similar, both around 136 Kg, and hence the vehicle is designed to have neutral steer at corners with lateral acceleration of 1.37g.

3.6.3 Longitudinal Load Transfer

Longitudinal load transfer is analyzed during conditions of 1 g braking and 1 g acceleration.

Longitudinal load transfer from the rear axle to the front axle while braking is given by,

$$\Delta W_B = \frac{A_B \times W_C \times h}{L}$$

$$= \frac{1 \times 257 \times 0.264}{1.6} = 42.4\ Kg$$

Normal load on front axle due to longitudinal weight transfer while braking

= Static load + Downforce + Weight transfer

Normal load on each front tire due to longitudinal weight transfer while braking

$$W_{FB} = \frac{162.34 + 42.4}{2} = 102.37\ Kg$$

Normal load on each rear tire due to longitudinal weight transfer while braking

$$W_{RB} = \frac{178.66 - 42.4}{2} = 68.13\ Kg$$

Similarly, longitudinal load transfer from the front axle to the rear axle while braking is given by,

$$\Delta W_A = \frac{A_A \times W_C \times h}{L}$$

$$= \frac{1 \times 257 \times 0.264}{1.6} = 42.4\ Kg$$

Normal load on rear axle due to longitudinal weight transfer while acceleration

= Static load + Downforce + Weight transfer

Normal load on each rear tire due to longitudinal weight transfer while acceleration

$$W_{RA} = \frac{178.66 + 42.4}{2} = 110.53\ Kg$$

Normal load on each front tire due to longitudinal weight transfer while acceleration

$$W_{FA} = \frac{162.34 - 63.6}{2} = 59.97\ Kg$$

The maximum normal load on each tire during conditions of combined cornering and braking, and cornering and acceleration can be found out using the individual normal loads calculated.

$$W_{CBFo} = W_{BF} + \Delta W_{CFo} = 102.37 + 55.42 = 157.79\ Kg$$

$$W_{CBFi} = W_{BF} + \Delta W_{CFi} = 102.37 - 55.42 = 46.95\ Kg$$

$$W_{CAFo} = W_{AF} + \Delta W_{CFo} = 59.97 + 55.42 = 115.39\ Kg$$

$$W_{CAFi} = W_{AF} + \Delta W_{CFi} = 59.97 - 55.42 = 4.55\ Kg$$

$$W_{CBRo} = W_{BR} + \Delta W_{CRo} = 102.37 + 55.42 = 157.79\ Kg$$

$$W_{CBRi} = W_{BR} + \Delta W_{CRi} = 102.37 - 55.42 = 46.95\ Kg$$

$$W_{CARo} = W_{AR} + \Delta W_{CRo} = 59.97 + 55.42 = 115.39\ Kg$$

$$W_{CARi} = W_{AR} + \Delta W_{CRi} = 59.97 - 55.42 = 4.55\ Kg$$

Table 2.24 Normal tire loads during cornering, braking and acceleration.

TIRE	**W_S (Kg)**	**ΔW_C (Kg)**	**W_C (Kg)**	**ΔW_B (Kg)**	**W_B (Kg)**	**ΔW_A (Kg)**	**W_A (Kg)**	**W_{CB} (Kg)**	**W_{CA} (Kg)**
Front Outside	81.17	55.42	136.59	42.4	102.37	-42.4	59.97	157.79	115.39
Front Inside	81.17	-55.42	25.75	42.4	102.37	-42.4	59.97	46.95	4.55
Rear Outside	89.33	47.06	136.39	-42.4	68.13	42.4	110.53	115.19	157.59
Rear Inside	89.33	-47.06	42.27	-42.4	68.13	42.4	110.53	21.07	63.47

From table 2.23, it can be seen that the maximum load condition at front tires is 157.79 Kg and rear tires is 157.59 Kg, both can be rounded off to 158 Kg or approximately 1580 N. This load will be used as the worst-case load while doing FEA on the suspension arms to determine the minimum required tube dimensions.

3.6.4 Spring and Damping Coefficients' Determination

Ride frequency is given by,

$$\omega = \frac{1}{2\pi}\sqrt{\frac{K_R \times 9.81}{W}}$$

A ride frequency of 2 Hz is selected at the front and 1.8 Hz at the rear.

From equation Ride rate at front and rear for the selected ride frequencies at front and rear are,

$$K_{RF} = \frac{(\omega_F \times 2\pi)^2 \times W_{FS}}{9.81} = \frac{(2 \times 2\pi)^2 \times 81.17}{9.81} = 1307\ Kg/m$$

$$K_{RR} = \frac{(\omega_R \times 2\pi)^2 \times W_{RS}}{9.81} = \frac{(1.8 \times 2\pi)^2 \times 89.33}{9.81} = 1165\ Kg/m$$

Wheel center rate is given by,

$$K_W = \frac{K_R \times K_T}{K_T - K_R}$$

Approximate tire stiffness K_T is considered to be 700 lbs/in or 12,500 Kg/m [4]. This is not an exact value since it is not available at the moment due to not having access to TTC data. This is selected as an approximate value after studying tire stiffness of some other FSAE tires from the reference document. Once TTC data is available, the exact value of tire stiffness can be used in the equation.

Hence, front wheel center rate is

$$K_{WF} = \frac{K_{RF} \times K_T}{K_T - K_{RF}} = \frac{1307 \times 12500}{12500 - 1307} = 1460\ Kg/m$$

Similarly, rear wheel center rate is

$$K_{WR} = \frac{K_{RR} \times K_T}{K_T - K_{RR}} = \frac{1165 \times 12500}{12500 - 1165} = 1285\ Kg/m$$

Now, we need to find the spring roll stiffness in front and rear. Spring roll stiffness is given by,

$$K_{\varphi S} = \frac{K_R \times t^2}{2}$$

Hence, front spring roll stiffness is given by,

$$K_{\varphi SF} = \frac{K_{RF} \times {t_F}^2}{2} = \frac{1307 \times 1.22^2}{2} = 973\ Kg.m/rad = 17\ Kg.m/deg$$

Similarly, rear spring roll stiffness is given by,

$$K_{\varphi SR} = \frac{K_{RR} \times {t_R}^2}{2} = \frac{1165 \times 1.18^2}{2} = 811\ Kg.m/rad = 14.16\ Kg.m/deg$$

Initially, the total roll stiffness calculated at the front and rear were 35.9 $Kg.m/deg$ and 27.1 $Kg.m/deg$ respectively. From the above calculation, it can be seen how much of the required roll stiffness can be provided by using springs while maintaining the expected ride frequencies of 2 Hz and 1.8 Hz at the front and rear axle respectively. Hence, it is clear that additional roll stiffness should be provided by means of anti-roll bars at the front and rear to attain roll stiffness of 35.9 $Kg.m/deg$ at front and 27.1 $Kg.m/deg$ at rear.

Additional roll stiffness that must be provided by anti-roll bar is given by,

$$K_{\varphi A} = \frac{\left[K_\varphi \times \frac{180}{\pi} \times K_T \times \frac{t^2}{2}\right]}{\left[K_T \times \frac{t^2}{2} - \left(K_\varphi \times \frac{180}{\pi}\right)\right]} - K_W \times \frac{t^2}{2}$$

Hence, anti- roll bar stiffness needed at front axle is,

$$K_{\varphi AF} = \frac{\left[K_{\varphi F} \times \frac{180}{\pi} \times K_T \times \frac{{t_F}^2}{2}\right]}{\left[K_T \times \frac{{t_F}^2}{2} - \left(K_{\varphi F} \times \frac{180}{\pi}\right)\right]} - K_{WF} \times \frac{{t_F}^2}{2}$$

$$= \frac{\left[35.9 \times \frac{180}{\pi} \times 12500 \times \frac{1.22^2}{2}\right]}{\left[12500 \times \frac{1.22^2}{2} - \left(35.9 \times \frac{180}{\pi}\right)\right]} - 1460 \times \frac{1.22^2}{2}$$

$$= 1544.3\ Kg.m/deg = 27.13 Kg.m/deg$$

Similarly, anti- roll bar stiffness needed at rear axle is,

$$K_{\varphi AR} = \frac{\left[K_{\varphi R} \times \frac{180}{\pi} \times K_T \times \frac{{t_R}^2}{2}\right]}{\left[K_T \times \frac{{t_R}^2}{2} - \left(K_{\varphi R} \times \frac{180}{\pi}\right)\right]} - K_{WR} \times \frac{{t_R}^2}{2}$$

$$= \frac{\left[27.1 \times \frac{180}{\pi} \times 12500 \times \frac{1.18^2}{2}\right]}{\left[12500 \times \frac{1.18^2}{2} - \left(27.1 \times \frac{180}{\pi}\right)\right]} - 1285 \times \frac{1.18^2}{2}$$

$$= 995.3\ Kg.m/deg = 17.37 Kg.m/deg$$

Now, we will find the amount of wheel displacement during the weight transfer while cornering at the front and rear.

$$Front\ wheel\ displacement = \frac{55.42}{1460} = 38\ mm$$

$$Rear\ wheel\ displacement = \frac{47.06}{1285} = 37\ mm$$

Motion ratio is the ratio between amount of spring/damper displacement to the amount of wheel displacement. It can also be defined as the ratio between the distance B and A in figure 2.83

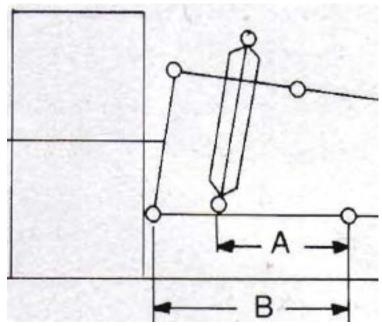

Figure 2.83 Spring-damper mounting location and motion ratio relationship [8].

$$MR = \frac{B}{A}$$

As B moves close to A, motion ratio approaches 1 and when B is at A, motion ratio will be 1. But it is difficult to mount the spring/damper near the lower ball joint.

In this case, wheel moves 38 mm at front and 37 mm at rear. This means that if the motion ratio is 1, then spring/damper will also move by 38 mm and 37 mm at front and rear respectively.

Here a motion of 25 mm is selected for the spring/damper at front and rear in order to achieve an achievable mounting distance of the spring/damper.

Hence the motion ratio at the front and rear are given by,

$$MR_F = \frac{25}{38} = 0.66$$

$$MR_R = \frac{25}{37} = 0.68$$

Now it is possible to adjust the spring/damper mounting point to achieve the above motion ratios. At front the distance B from the suspension geometry is 347 mm, this gives distance A as 229 mm. Similarly, at rear distance B is 300 mm, giving the value of A as 204 mm.

Now, with the wheel rates and motion rations know, it is possible to calculate the spring rates at front and rear as shown in the equation below

$$K_{SF} = \frac{K_{WF}}{{MR_F}^2} = \frac{1460}{0.66^2} = 3352\ Kg/m$$

$$K_{SR} = \frac{K_{WR}}{{MR_R}^2} = \frac{1285}{0.68^2} = 2779\ Kg/m$$

Now, in order to find the damping coefficient required, the critical damping coefficient should be determined first which is given by

$$C_{CR} = 2\sqrt{(K_S \times M)}$$

Critical damping coefficient at front and rear are calculated as follows

$$C_{CRF} = 2\sqrt{(1460 \times 68.75)} = 200.4\ Kg\ s/m = 2004\ N\ s/m$$

$$C_{CRR} = 2\sqrt{(1285 \times 75)} = 196.3\ Kg\ s/m = 1963\ N\ s/m$$

Then the required damping coefficient is the product of critical damping coefficient and the damping ratio. A damping ratio of 0.7 is selected from literature reviews. Hence the required damping coefficients at front and rear are,

$$C_F = 2004 \times 0.7 = 1403\ N\ s/m$$

$$C_R = 1963 \times 0.7 = 1374\ N\ s/m$$

Now, knowing the spring stiffness and damping coefficient required, selection can be done to recommend the best spring-damper unit. From research, it was found that a very large majority of good performing teams use Öhlins TTX25 MkII spring damper unit. Hence the same is recommended for this suspension design also. Since the calculated maximum spring-damper motion is 25 mm, the selected Öhlins spring-damper with a stroke length of 57 mm will be enough for the suspension and the technical details are shown in Appendix A. Also, regarding the anti-roll bar, it is recommended to purchase or design an adjustable anti-roll bar which will help to fine tune the car balance by varying the roll distribution among front and rear axles.

3.6.5 FEA of Suspension Arms at Worst Case Loads

The maximum normal load acting on front and rear wheels are calculated in section 3.6.3. Using these forces, and the lateral force generated due to that, it is possible to find the forces acting on upper and lower arms of the front and rear suspensions by force – moment equilibrium equations as shown in figure 2.84. A lateral acceleration of 1.37 g was used in the calculation of suspension design and the same will be used to find the lateral force generated.

$$F_{lateral} = 1.37 \times F_{normal} = 1.37 \times 1580 = 2165\ N$$

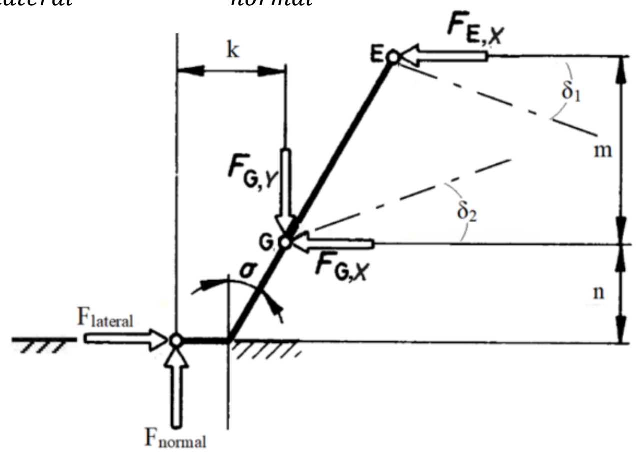

Figure 2.84 Forces acting on double A-arm suspension and tire contact patch [41].

Knowing F_{normal}, $F_{lateral}$ and the distances k, l, m and n, it is possible to determine the force components acting at the suspension outer ball center locations using force – moment equilibrium equations. Also, δ_1 and δ_2 are the angle made by the upper and lower arms with the horizontal. Since the spring-damper is mounted to the lower arm in all cases, a vertical reaction force will be generated in the lower arms.

From force equilibrium in vertical direction,

$$F_{normal} = F_{G,Y} = 1580\ N$$

from force equilibrium in horizontal direction,

$$F_{lateral} = F_{G,X} + F_{E,X}$$

Now, considering moment equilibrium about G,

$$(F_{lateral} \times n) + (F_{E,X} \times m) = (F_{normal} \times k)$$

From suspension geometry, values of k, m and n are determined

$$k = 32\, mm \qquad m = 203\, mm \qquad n = 127\, mm$$

Hence,

$$F_{E,X} = \frac{(F_{normal} \times k) - (F_{lateral} \times n)}{m}$$

$$F_{E,X} = \frac{(1580 \times 32) - (2165 \times 127)}{203} = -1105\, N$$

Hence,

$$F_{G,X} = F_{lateral} - F_{E,X}$$

$$F_{G,X} = 2165\, N + 1105 = 3270\, N$$

The chassis ends of both the upper and lower control arms are connected to the chassis using ball joints, which has 3 translational degrees of freedom. The lower control arms have one more constraint due to the ball joint connection to the spring-damper system. Hence, when the wheel moves upward, bending and axial stresses will be generated in the lower control arms due to forces $F_{G,X}$ and $F_{G,Y}$. The upper arms will be free to move about the ball joints at the chassis end and hence it will not generate any stress. Hence the FEA will be conducted on the front and rear lower control arms where the stresses will be generated. 4130 chromoly steel which is decided for the chassis will be used for the suspension arms as well. Tube sizing is determined from the standard tube sizes available [13] and a FOS of 1.6 is selected from literature reviews [42]. Also, angle δ_2 is measured for both front and rear suspensions, to find the angle at which the forces should be applied to the lower control arm.

$$\delta_{2,\,front} = 3.33^0 \qquad \delta_{2,\,rear} = 1.93^0$$

The FEA is done using SOLIDWORKS and beam elements are used which is the best option due to the uniform cross section thin tubes. Different available tube sizes are tested considering the required FOS with minimum possible outside dimeter due to packaging benefits. From the analysis, it was found that 4130 Chromoly steel tube with 5/8 inches outer diameter and 5/32 inches thickness have a FOS of 1.6 for front and 1.7 for rear lower control arms and the results are shown in figure 2.88. The upper control arms can be constructed with the same tube or with same outside diameter and minimum possible thickness since it doesn't generate any stresses.

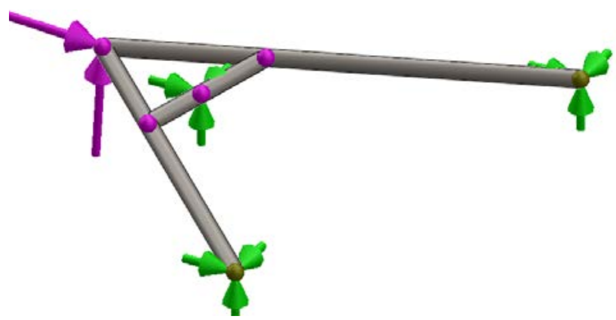

Figure 2.85 Lower suspension arm FEA model with load and constraints.

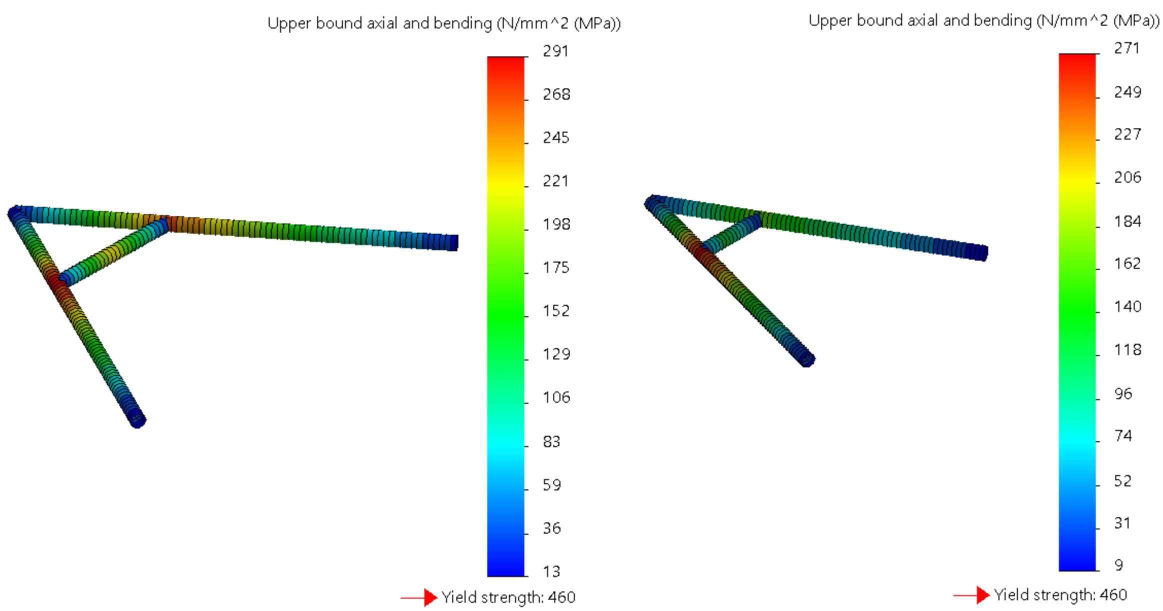

(a) (b)

Figure 2.86 Suspension arm Upper bound axial and bending stress plots (a) Front lower arm (b) Rear lower arm.

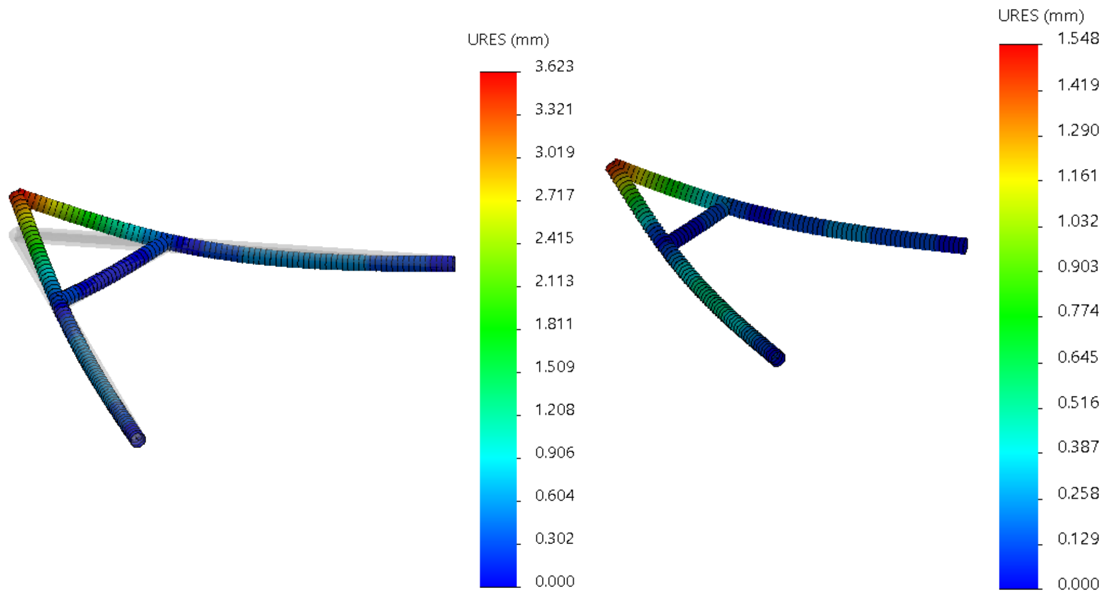

(a) (b)

Figure 2.87 Suspension arm Displacement plots (a) Front lower arm (b) Rear lower arm.

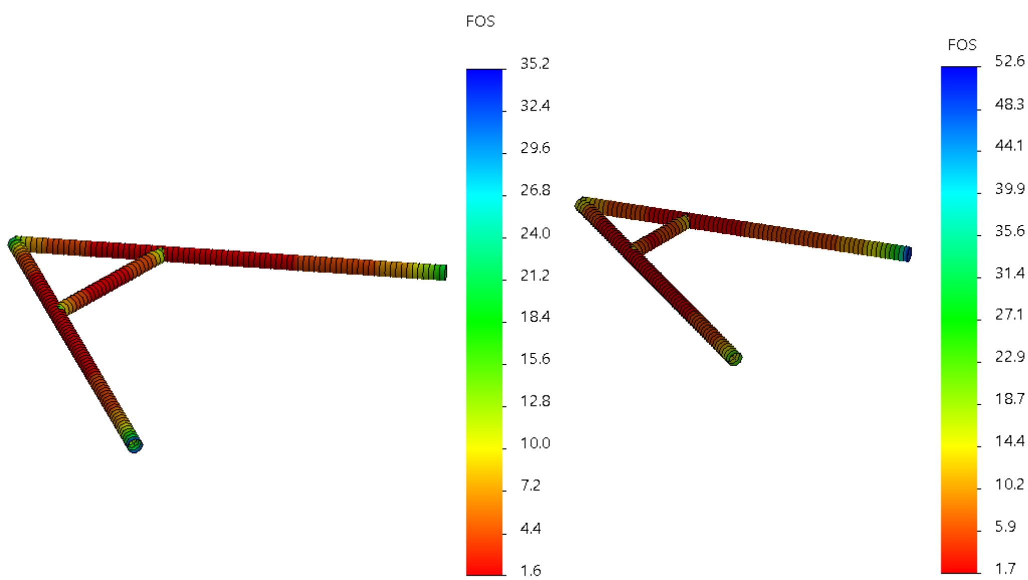

(a) (b)

Figure 2.88 Suspension arm FOS plots (a) Front lower arm (b) Rear lower arm.

CHAPTER 4: Future Works

This project is intended to learn and design the basics of the chassis, suspension, impact attenuator and aerodynamic components of a first-time FSAE car. There were so many challenges while designing all the components together due to lack of input parameters while designing a system which was supposed to be obtained from the performance analysis of another system, which was non-existent. Also, since FSAE is a competition sport, there is very few published documents for learning about the methods and technologies used by the well performing teams. This thesis puts together the design of chassis, suspension, impact attenuator and aerodynamic systems with a proper description of how each system are interconnected. Since designing all the systems together, which involves various fields of mechanical engineering, there are possibilities for detailed studies with the designs presented here for the development of the individual systems. Some of the areas that can be focused in the future for each individual system are described below.

a) *Chassis*

Once a proper manufacturing facility is established, research can be conducted on the possibility of manufacturing a composite monocoque using CFRP or other composites in place of a steel space chassis. Composite monocoques provide very high torsional stiffness along with the reduction of weight which is very beneficial to race cars. The monocoque designs can be optimized for drag reduction and also can be used to generate downforce utilizing ground effects if properly designed. Driver ergonomics can also be considered while designing the future chassis. many teams utilized engines as a structural member as it has very high stiffness. This option can be examined for increasing the overall chassis stiffness and can also help to reduce weight since it can eliminate many chassis members and still generating high torsional stiffness.

b) *Impact Attenuator*

A standard impact attenuator design is used for the analysis described in this document. Even though the design with IMPAXX 700 foam as the construction material satisfies all the requirements specified in the rule book further studies can be done to test various materials like honeycomb structures, CFRP, or other impact absorbing materials and the shape can be optimized according to the material selected. Physical drop tests can also be conducted to compare the numerical results and the experimental results to validate the numerical models.

c) *Aerodynamics*

A full body 3-D CFD study can be conducted to learn about the effects caused by the neighboring components on the performance on each wing. Also, the nosecone design can be further optimized to reduce drag. On-track testing will give the best results if a wind tunnel facility is not available. The CFD results should be compared with the on-track test results to validate the numerical results. Since, weight optimization of aerodynamic components are also important, an accurate structural analysis of the wings can be very beneficial. Fluid-structural interaction analysis using a Multi-physics software (ANSYS AIM) is the best possible option to obtain better structural results due to the aerodynamic pressure loads on the wings. Also, 3-D CFD studies can be conducted on each wing models to analyze the effect of the end plate shape and thickness in the downforce generation.

d) *Suspension*

The major work to be done is to consider the tire data while tuning the suspension design. Since optimizing the tire performance to generate maximum lateral force is one of the main requirements of a good suspension system, tire test data is very important. The suspension design presented here has provided details on how the tire data could be used to further improve design. Once a proper FSAE team is formed, Tire data from FSAE TTC should be acquired for using in the suspension design. TTC tire test data can be used to identify the nature of lateral force generation of different race tires in different test conditions. While suspension design, these data can be used to utilize the tire to the maximum and to achieve the required conditions for large lateral force generation. Full vehicle dynamics can be carried out using specialized tools such as ADAMS CAR to optimize the overall car by actual on-track simulations. During the research done for the thesis, it was found that designing the suspension system considering the steering system is very beneficial in the performance optimization of the suspension by learning about the effects of caster, toe angles and analysis of bump-steer during wheel travel.

REFERENCES

1. *Formula SAE Rules 2019*, SAE International, 2018.
2. Katz, J., *Aerodynamics Of Race Cars*. 2006. **38**(1): p. 27-63.
3. *2018 Formula SAE Michigan Event Guide*. 2018, SAE International.
4. Kasprzak, E.M. and D. Gentz, *The Formula SAE Tire Test Consortium-Tire Testing and Data Handling*. 2006, SAE International.
5. Gaffney, E.F. and A.R. Salinas, *Introduction to Formula SAE® Suspension and Frame Design*. 1997, SAE International.
6. Milliken, W.F. and D.L. Milliken, *Race car vehicle dynamics*. Vol. 400. 1995: Society of Automotive Engineers Warrendale.
7. Genta, G. and L. Morello, *The automotive chassis*. Vol. 1. 2009: Springer.
8. Adams, H., *Chassis engineering : chassis design building & tuning for high performance handling*. 1993, New York: HPBooks. 142.
9. Nair, V., *Determination Of Factors To Improve Effectiveness Of Triangulation Members For A Formula Sae Race Car Frame*, In *Mechanical Engineering*. 2012, The University Of Texas At Arlington: Arlington. p. 89.
10. Eurenius, C.A., et al., *Analysis of Composite Chassis*. 2013.
11. Christensen, J., *Carbon Fibre Monocoque Chassis Feasibility and Manufacturability for FSAE*. 2015, SAE International.
12. Riley, W.B. and A.R. George, *Design, Analysis and Testing of a Formula SAE Car Chassis*. 2002, SAE International.
13. *Tubing and Pipe*, in *The EMJ Stock List and Reference Book*. 2007.
14. Heisler, H., *Advanced Vehicle Technology*. Second ed. 1989, Oxford: Butterworth-Heinemann.
15. De Vries, D.J.E.U.o.T., *Characterization of polymeric foams*. 2009.
16. Li, Q.M., R.A.W. Mines, and R.S. Birch, *The crush behaviour of Rohacell-51WF structural foam*. International Journal of Solids and Structures, 2000. **37**(43): p. 6321-6341.
17. Mohamed, M., et al., *Manufacturing and characterization of polyurethane based sandwich composite structures*. 2015. **123**: p. 169-179.
18. Katz, J., *Race car aerodynamics : designing for speed*. 2006, Cambridge, MA, USA: R. Bentley.
19. Zerihan, J. and X.J.J.o.a. Zhang, *Aerodynamics of a single element wing in ground effect*. 2000. **37**(6): p. 1058-1064.
20. Michael S. Selig, J.J.G., Andy P. Broeren, Philippe Giguere, *Summary of Low-Speed Airfoil Data*. Vol. 1. 1995, Virginia: SoarTech Publications.
21. Michael S. Selig, C.A.L., Philippe Giguere, Cameron P. Ninham, James J. Guglielmo, *Summary of Low-Speed Airfoil Data*. Vol. 2. 1996, Virginia: SoarTech Publications.
22. Christopher A. Lyon, A.P.B., Philippe Giguere, Ashok Gopalarathnam, Michael S. Selig, *Summary of Low-Speed Airfoil Data*. Vol. 3. 1997, Virginia: SoarTech Publications.
23. Michael S. Selig, B.D.M., *Summary of Low-Speed Airfoil Data*. 2004, National Renewable Energy Laboratory.
24. Gregory A. Williamson, B.D.M., Benjamin A. Broughton, Robert W. Deters, John B. Brandt, Michael S. Selig, *Summary of Low-Speed Airfoil Data*. Vol. 5. 2012.

25. Williamson, G.A., *Experimental Wind Tunnel Study Of Airfoils With Large Flap Deflections At Low Reynolds Numbers*, in *Aerospace Engineering*. 2012, University of Illinois at Urbana-Champaign: Urbana, Illinois.
26. Amanullah Choudhry, M.A., Richard Kelso, *A study of long separation bubble on thick airfoils and its consequent effects.* International Journal of Heat and Fluid Flow, 2015. **52**: p. 84-96.
27. Wordley, S. and J. Saunders, *Aerodynamics for Formula SAE: Initial Design and Performance Prediction*. 2006, SAE International.
28. McBeath, S., *Competition Car Downforce*. 1998, Somerset: Haynes Publishers.
29. Smith, C., *Tune to win*. 1978, Fallbrook: Aero Publishers.
30. Cooper, K.R., et al., *The Aerodynamic Performance of Automotive Underbody Diffusers*. 1998, SAE International.
31. Yang, W. and Z.J.C.j.o.c.p. Yang, *Aerodynamic investigation of a 2D wing and flows in ground effect.* 2009. **26**(02).
32. Stroud, W.J., C.B. Dexter, and M. Stein, *Automated preliminary design of simplified wing structures to satisfy strength and flutter requirements.* 1972.
33. Blondeau, J., J. Richeson, and D. Pines. *Design of a morphing aspect ratio wing using an inflatable telescoping spar*. in *44th AIAA/ASME/ASCE/AHS/ASC Structures, Structural Dynamics, and Materials Conference*. 2003.
34. Marisarla, S., et al. *Prediction of Structural Behavior of Joined-Wing Configuration of High-Altitude Long Endurance (HALE) Aircraft*. in *41st AIAA Aerospace Science Meeting & Exhibit, January, Reno, NV, AIAA*. 2003. Citeseer.
35. *Carolina Technical Fabrics Product Handbook.*
36. LL Sparks, J.A., *Thermal and Mechanical Properties of Polyurethane Foams and a Survey of Insulating Concretes at Cryogenic Temperatures*. 1984, National Bureau of Standards: Colorado.
37. *Fiberglass and Composite Material Design Guide*. Available from: http://www.performancecomposites.com/about-composites-technical-info/122-designing-with-fiberglass.html.
38. Wallenberger, F.T., J.C. Watson, and H.J.M.P. Li, OH: ASM International, . *Glass fibers.* 2001: p. 27-34.
39. Winkler, C., et al., *Heavy vehicle size and weight: test procedures for minimum safety performance standards.* 1992.
40. Danielsson, O. and A.G. Cocana, *Influence of body stiffness on vehicle Dynamics characteristics in passenger cars*, in *Chalmers University of Technology*. 2015.
41. Reimpell, J., H. Stoll, and J. Betzler, *The automotive chassis: engineering principles*. 2001: Elsevier.
42. Seward, D., *Race car design*. 2014: Macmillan International Higher Education.
43. *Keizer 10i wheel manufacturer drawing*. Available from: http://keizerwheels.com/product_cat/formula-sae-racing-wheels/

APPENDIX A: Manufacturer data of selected components

I. Öhlins TTX25 MkII Damper unit

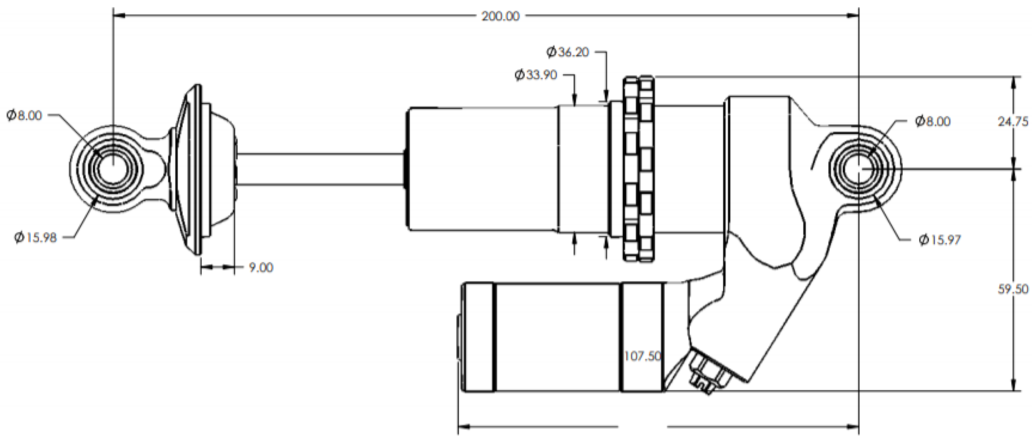

II. ISR-22-048-0A Brake Rotor

ISR

PART NUMBER : 22-048-OA

22-048-0A

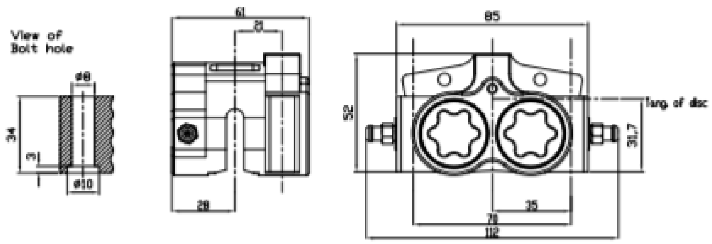

Technical data:

Piston diameter:	25mm (x4)
Piston material:	Tufram coated aluminium alloy
Pad type:	ISR 29-002 (x4)
Pad area:	$14cm^2$
Swept height of disc:	27mm
Disc size:	150-250mm
Disc thickness:	4.6-5.0mm
Hydrualic threads:	M10x1.25
Weight incl. pads:	0.46kg
Surface finish:	Clear anodised

ISR-MC AB, DROTTNINGV. 15, S-147 31 TUMBA, SWEDEN TEL:+46853037671, FAX:+46853033296